HIGH SHEAR ARTERIAL THROMBOSIS: MICROFLUIDIC DIAGNOSTICS AND NANOTHERAPUETICS

A Dissertation
Presented to
The Academic Faculty

by

Michael T. Griffin

In Partial Fulfillment
of the Requirements for the Degree
Doctor of Philosophy in Bioengineering

Georgia Institute of Technology

May 2020

HIGH SHEAR ARTERIAL THROMBOSIS: MICROFLUIDIC DIAGNOSTICS AND NANOTHERAPEUTICS

Approved by:

Dr. David N. Ku, Advisor
Department of Mechanical Engineering
Georgia Institute of Technology

Dr. Shannon L. Meeks
Department of Pediatrics
Emory University School of Medicine

Dr. Cyrus K. Aidun
Department of Mechanical Engineering
Georgia Institute of Technology

Dr. Susan N. Thomas
Department of Mechanical Engineering
Georgia Institute of Technology

Dr. C. Ross Ethier
Department of Biomedical Engineering
Georgia Institute of Technology

Date Approved: December 19th, 2019

This thesis is dedicated to all the people in my life who have been a mentor to me along the way, beginning with my very first mentors: Mom and Dad.

ACKNOWLEDGEMENTS

I have many people to thank for helping me complete this thesis project. First and foremost to my advisor, Dr. David Ku, who provided incredible guidance and expertise throughout this project. His mentoring and advising methods pushed me to develop my thesis questions and hypotheses on my own, and through my many discussions with him we were able to fine tune them. I am incredibly grateful for his mentoring and everything that he has done for me during graduate school. Thank you to Dr. Cyrus Aidun, whom I had the pleasure to work with closely during most of my time at Georgia Tech and in many ways has helped guide a large portion of this thesis. Next, thank you to Dr. Ross Ethier and Dr. Susan Thomas, both of whom I have gotten to know through my course work and several interactions in IBB. Their examples of research and education excellence have inspired me throughout graduate school and will continue to do so throughout my career. Finally, thank you to Dr. Shannon Meeks, who has provided quick and thoughtful feedback from the context of a clinical researcher, which has been very valuable for this thesis.

Thanks to all of the members of the Biofluids and Medical Device Research Group, both past and present. I was very fortunate to be able to work with some amazing researchers and friends (listed in order of appearance): Susan Shea, Joav Birjiniuk, Sumit Khetarpal, Tyler Harden, Sean Mihm, Cassidy Wang, Dongjune Kim, Jonathan Schwartz, Chris Bresette, Zixiang (Leo) Liu, Qing Han, Trent Callcott, Patricia Yang, Britt Van Rooij, and Gian Rivera Crespo. A special thanks to Susan who was my first mentor in the lab and provided a lot of guidance along the way. I would also like to thank the undergraduate students who helped me at various points with this research: Nate Hill,

Jaydra von Behren, and Courtney Smith. Collaborators Yuanzheng Zhu and Katrina Bark were also instrumental in driving this work, and both a joy to work with over the years. Finally, thank you to all of the people of IBB 2A in the Sulchek, Forest, and Ethier labs whom I have gotten to know and have enjoyed sharing lab and office space with, along with lunches and coffee breaks.

Thank you also to the members of both the Stamps Health Lab (Lisa Carr, Jana Kendrick Griffin, Evodie Epane, Tabarrion Stoves, and Helen Ukoh) and the Grady Memorial Hospital Cath Lab (Dr. Michael McDaniel, Dr. Rajesh Sachdeva, and all of the techs and nurses). I have greatly enjoyed working with all of you and our conversations. Thanks also to the Georgia Tech BioE community that has provided so much support over the past 4.5 years. Dr. Andres Garcia, Dr. Hang Lu, and Dr. Manu Platt have created an incredible program and have been excellent leaders and mentors to us graduate students. Of course, this program would not be as successful as it is without the wonderful Laura Paige, who has always been there for me throughout the graduate process and has been a constant source of support.

Thank you to my friends and family. To all of the friends I have made in Atlanta through the GT BioE program and the GT Catholic Center, thank you for being sources of support and good times over the past 4 years. Thank you to my parents, sisters, and in-laws for being constant supporters of me during this thesis. Finally, thank you to my wife, Megan. You have been my rock during this journey that we were on together, and have supported me incredibly over the last few months as I've worked to finish this project. Your example of your own thesis defense earlier this year was inspiring, and I will forever

appreciate your support as I tried to achieve the same goal. I love you and am looking forward to this next chapter together.

TABLE OF CONTENTS

LIST OF TABLES

LIST OF FIGURES

LIST OF SYMBOLS AND ABBREVIATIONS

ACS	Acute Coronary Syndrome
ADP	Adenosine Diphosphate
ANOVA	Analysis of Variance
ARRIVE	Aspirin to Reduce Risk of Initial Vascular Events
ARU	Aspirin Response Units
ASA	Acetylsalicylic Acid
ASCEND	A Study of Cardiovascular Events in Diabetes
ASPREE	Aspirin in Reducing Events in the Elderly
AUC	Area Under the Curve
AuNP	Gold nanoparticle
CAPRIE	Clopidogrel versus Aspirin in Patients at Risk of Ischemic Events
CBC	Complete Blood Count
CFD	Computational Fluid Dynamics
CHARISMA	Clopidogrel for High Atherothrombotic Risk and Ischemic Stabilization, Management and Avoidance
CNC	Computer Numerical Control
CNP	Charged Nanoparticles
COX-1	Cyclooxygenase-1
COMMIT	Clopidogrel and Metoprolol in Myocardial Infarction Trial
CT	Closure Time (for PFA-100)
CTF	Collagen Thin Film
CYP	Cytochrome P450
DAPT	Dual Antiplatelet Therapy

DNS	Direct Numerical Simulation
DOE	Design of Experiments
EDTA	Ethylenediaminetetraacetic acid
EPI	Epinephrine
FENE	Finitely Extensible Nonlinear Elastic
GLL	Grayscale laser lithography
GP	Glycoprotein
GRAVITAS	Gauging Responsiveness With a VerifyNow Assay-Impact on Thrombosis and Safety
GTT	Global Thrombosis Test
kDa	Kilodalton
LB	Lattice-Boltzmann
LJ	Lennard-Jones
LT	Lysis Time
LTA	Light transmission aggregometry
MACE	Major Adverse Cardiovascular Event
MI	Myocardial Infarction
MTA	Microfluidic Thrombosis Assay
NSAIDS	Non-steroidal Anti-inflammatory Drugs
OT	Occlusion Time
P2Y12	Chemoreceptor for ADP on platelet membrances
PAR-1	Protease Activated Receptor 1
PBS	Phosphate Buffered Saline
PCI	Percutaneous Coronary Intervention
PDMS	Polydimethylsiloxane

PEG	Polyethylene Glycol
PFA-100	Platelet Function Analyzer 100
PFT	Platelet Function Test
PGG2	Prostaglandin G2
PGH2	Prostaglandin H2
PLGA	Polylactic co-glycolic acid
PPP	Platelet Poor Plasma
PRP	Platelet Rich Plasma
PRU	P2Y12 Reactivity Units
PS	Polystyrene
PSA	Polystyrene-Amine
PSC	Polystyrene-Carboxyl
PURSUIT	Platelet Glycoprotein IIb/IIIa in Unstable Angina: Receptor Suppression Using Integrillin Therapy)
PVA	Polyvinyl Alcohol
RGB	Red Green Blue
RPA	Rapid Platelet Accumulation
SIPA	Shear Induced Platelet Accumulation
T-TAS	Total Thrombus-formation Analysis System
TXA2	Thromboxane A2
VN	VerifyNow
vWF	von Willebrand Factor
WPB	Weibel-Palade bodies

SUMMARY

Atherothrombosis is the causal event in acute myocardial infarction and stroke. These occlusive arterial thrombi require the confluence of high shear rates from a stenosis, exposure of mural collagen from a ruptured plaque cap, and the aggregation of platelets on elongated vWF. A functional assay of thrombotic occlusion would be able to diagnose the propensity of individual patients to occlude and determine patient-specific drug regimens. Current platelet function tests do not have the relevant fluid mechanics, collagen surface, or proper anticoagulant to mimic arterial thrombotic occlusion. I have created an improved microfluidic assay that includes all the above factors, uses a small amount of whole blood, and is validated against clinical thrombosis over two orders of magnitude in size.

Antiplatelet therapies, such as aspirin and clopidogrel, have been developed to irreversibly inhibit platelet activation or binding. However, they do not work as intended for a large percentage of the population, as up to 60% of patients exhibit resistance to therapy per current non-specific platelet assays. Resistance persists even with dual antiplatelet therapy (DAPT). The poor therapeutic efficacy of current anti-platelet agents with their associated major bleeding risks indicate the need for both a functional thrombosis assay and improved antithrombotic agents.

The overall goal of this thesis is to develop a low variability device for clinical diagnostics and arterial thrombosis research. I hypothesize that the main sources of variability observed in previous microfluidic assays of thrombosis are due to three fundamental design factors of high relevance to arterial thrombosis. Secondly, I

hypothesize that the endpoint of occlusion time in the improved assay will be sensitive to antiplatelet responsiveness. Finally, I hypothesize that such a device can be utilized to develop and evaluate new antithrombotic nanoparticle therapies. Both in vitro and in vivo models of thrombosis will be utilized to investigate the hypotheses in this thesis.

CHAPTER 1. INTRODUCTION

1.1 Myocardial Infarction and Ischemic Stroke

Arterial thrombosis is the condition where a platelet aggregate forms at the site of an atherosclerotic injury and occludes blood flow to major organs such as the heart and brain, leading to a heart attack or ischemic stroke. Heart attacks, also known as myocardial infarctions, and ischemic strokes are major adverse cardiovascular events (MACE) that are the leading causes of death in the United States. Myocardial infarction, where a blood clot develops in the coronary arteries and restricts blood flow to heart muscle, is the largest contributor to this percentage. It is estimated that approximately 720,000 Americans will have a first-time myocardial infarction this year, with approximately 335,000 having a recurring event [1]. Ischemic stroke occurs when a thrombotic embolus becomes lodged in the cerebrovasculature and prevents blood flow. There are approximately 610,000 new cases of ischemic stroke each year in the United States, with approximately 185,000 recurrent events [1]. While these cardiovascular complications accounted for 23.6% of all deaths in 2018, they also can impose life-long complications on survivors, such as paralysis, weakness, and the need for daily medications [1].

The annual financial burden resulting from these conditions is enormous, with the combination of direct and indirect costs for heart disease and stroke related conditions being $244.9B in 2014 [1]. This number is projected to grow to a staggering $500B by 2035. The costs associated with cardiovascular diseases significantly outpace the costs of all other pathological and disease categories.

To reduce these costs (or at least the rate of growth) continued research into improved diagnostics and therapies is needed. The current initial therapy of choice for patients at risk of myocardial infarction or stroke is daily low-dose aspirin to prevent the formation of platelet aggregates, or thrombi. This may be combined with another therapy as a dual antiplatelet therapy (DAPT) approach, but the cardiologist must weigh in factors such as the patient's relative risk for MACE and their risk for a bleeding event, which is enhanced through the usage of antithrombotic or antiplatelet therapies. Typically, this choice is made through the cardiologist's judgment of risk factor (i.e. medical history and age) rather than through quantifiable means with a diagnostic test. If a patient experiences either myocardial infarction or stroke while on therapy, a new therapeutic plan must be initiated to overcome this "antiplatelet resistance" and prevent a subsequent event.

Therefore, the remaining sections of this thesis chapter will go into more detail about the pathology of arterial thrombosis, as well as current therapies to prevent the formation of arterial thrombi and diagnostics to determine the efficacies of those therapies. The aims of this thesis to progress the field of thrombotic therapies and diagnostics will then be specified.

1.2 The Role of Platelets and von Willebrand Factor

The critical common factor in myocardial infarction and ischemic stroke is thrombosis occurring in an atherosclerotic artery. Initiated by plaque-cap rupture of an atherosclerotic artery due to pathophysiological high shear blood flow, a platelet-rich, white clot forms. This phenomenon diverges from the classical Virchow's Triad for coagulation, as arterial thrombosis requires: 1) high shear blood flow, 2) a pro-thrombotic

surface, and 3) platelets and von Willebrand Factor (vWF) [2, 3]. While the development of atherosclerosis is responsible for the narrowing of the artery to create high shear and eventually disrupting the endothelial cell layer, the blood components platelets and vWF are always in the flow.

Platelets are anuclear cell fragments in the blood circulation that make up just 1% of the blood volume. Originating from bone marrow, they are known for playing a major role in blood clot formation and wound healing [4]. Platelets will adhere to the site of vascular injury and begin to form what is commonly termed as the "platelet plug" to block off the injury site from circulation. This is mediated by platelet membrane glycoproteins GPIb and GPIIb/IIIa. GPIb allows for the initial adhesion of platelets to clotting proteins at the injury site, while GPIIb/IIIa allows for clot strengthening interactions [5-7]. In addition, platelets have internal stores of many important molecules and proteins in α- and dense-granules. These include clotting factors such as ADP and calcium that are significant players in generating platelet activation, as well as clotting proteins fibrinogen and von Willebrand Factor [8].

vWF is a multimeric protein secreted by both Weibel-Palade bodies (WPB) in endothelial cells and α-granules in megakaryocytes [9]. Each monomer of vWF consists of a series of 29 subdomains that function in protein-protein and protein-cell interactions. The 250 kDa monomer will dimerize head-to-head, and the dimers continue to polymerize to create very long vWF chains that may reach sizes of 20,000 kDa [10]. Endothelial cell vWF is released into circulation and remains in plasma, while megakaryocyte vWF is stored in α-granules of platelets as previously mentioned. Both play a role in the formation of arterial thrombi [11]. Under physiological flow, plasma vWF typically circulates in a

globular confirmation due to self-association of the vWF dimers, thereby shielding many of its binding domains. However, in the pathological scenario described below vWF unfolding can initiate the thrombotic process that leads to myocardial infarction and ischemic stroke.

First, a pro-thrombotic surface is established by high shear blood flow disrupting the endothelial cell layer of the artery. Sub-endothelial collagen is then exposed to blood, creating a pro-thrombotic surface. vWF has a mechanosensitive tertiary structure and begins to unravel in the high shear ($> 5000\ s^{-1}$) flow environment as the self-associations of vWF dimers are overcome by the shearing force of the blood flow. This exposes many of the binding domains of the vWF protein, specifically the C3 domain that binds and tethers to the exposed collagen in this case. A layer of vWF proteins begins to accumulate at the wall, creating an even more pro-thrombotic surface for platelets. The A1 domain of vWF, now exposed and at a high concentration on the surface, binds specifically to platelet GPIb. This is able to happen because platelets are pushed toward the vessel walls by red blood cells in flow, and therefore have a higher concentration near the surface [12]. The A1-GPIb bond acts as an extraordinarily fast catch-bond that grabs platelets from the flow. While the GPIb bond is highly reversible, there are several thousand A1-GPIb bonds that keep the platelet tethered [11, 13]. Due to the increased residence time in the high shear zone, platelets become activated [14]. Platelet activation triggers significantly stronger GPIIb/IIIa bonds with vWF, which form to nearly irreversibly tether the platelet. Activated platelets then release α-granules, which secret significantly higher concentrations of vWF to the thrombotic site. Rapid platelet accumulation is then propagated in the area until

occlusive thrombus forms in the vessel, restricting blood flow and leading to complications of myocardial infarction or ischemic stroke [2].

1.3 Current Antithrombotic Therapies

Several drugs exist for the prevention of platelet thrombosis. Each of these therapies targets platelet activation specifically, which would thereby prevent the strong binding of GPIIb/IIIa and the additional release of α-granule vWF from platelets. This section will discuss the targets of common antiplatelet therapies, as well as their performance in the clinic.

1.3.1 Aspirin (Acetylsalicylic Acid)

Aspirin was first utilized as an antithrombotic agent in the 1950's by Dr. Lawrence Craven, and has become a mainstay in preventative therapy ever since [15]. Craven developed his hypothesis after noticing that his patients who chewed aspirin gum exhibited more bleeding complications during surgery. This led to further investigation into the mechanism by which aspirin may be impacting hemostatic function. It was found that aspirin acts by targeting cyclooxygenase (COX-1) dependent platelet activation [16]. The inhibition of COX-1 prevents the necessary synthesis of prostaglandin G2 (PGG2), prostaglandin H2 (PGH2), and thromboxane A2 (TXA2) for the activation of platelets.

Craven developed his own clinical trial for the rates of myocardial infarction in a cohort of 8,000 patients. This study showed that no patients that faithfully stuck to their aspirin dosage experienced a heart attack, which was very striking to the community at the time [17]. However, there is serious speculation that this study (and others that followed) were

not adequately controlled in the wake of recent clinical results. Three large clinical studies reported at the end of 2018 indicate that the effects of aspirin are negligible in primary prevention of MACE. These three studies are the ARRIVE (Aspirin to Reduce Risk of Initial Vascular Events), ASCEND (A Study of Cardiovascular Events iN Diabetes), and ASPREE (Aspirin in Reducing Events in the Elderly) trials. Both the ARRIVE and ASPREE trials indicated no significant difference in the occurrence of MACE between individuals taking aspirin or placebo treatment [18-21]. The same trials also showed a significant increase (hazard ratio 1.38) in the incidence of major hemorrhagic bleeding associated with aspirin use. The ASCEND trial did find a significant difference in the occurrence of MACE between aspirin and placebo groups for diabetic patients, but this was also countered by a significant increase in bleeding events. Therefore, aspirin is likely doing more harm than good in most patients, leading clinicians to start recommending to discontinue aspirin use for primary prevention [18].

1.3.2 P2Y12 Inhibitors

For very high-risk patients (i.e. ACS and patients with stent placement) dual antiplatelet therapy (DAPT) or aspirin and a P2Y12 inhibitor is recommended. P2Y12 inhibitors differ from aspirin in that they block ADP-induced platelet activation. By blocking the P2Y12 receptor of platelets, ADP induced activation of GPIIb/IIIa does not occur.

The most common P2Y12 inhibitor is clopidogrel, also known as Plavix. Clopidogrel is a pro-drug, and as such requires metabolic activation by cytochrome P450 (CYP). However, it has become evident that there is a significantly variable response to clopidogrel within the patient population. It has been identified that polymorphisms in the CYP2C19

allele that codes for the CYP metabolite leads to variants that are unable to metabolize the pro-drug. Therefore, upwards of 30% of the population will not benefit from the antithrombotic effects of clopidogrel [22]. Additionally, the CHARISMA (Clopidogrel for High Atherothrombotic Risk and Ischemic Stabilization, Management, and Avoidance) clinical trial found that DAPT of Plavix and aspirin did significantly reduce the risk of MACE [23].

Three additional P2Y12 inhibitors have been developed as next generation. Prasugrel employs a different metabolic pathway than clopidogrel which should lead to more effective platelet targeting. Ticagrelor and cangrelor are direct P2Y12 inhibitors that bind to the protein without metabolic activity. Each of these drugs has gone through a clinical trial for comparison to clopidogrel efficacy and safety. Prasugrel was found to reduce ischemic events over clopidogrel in the TRITON-TIMI trial but was associated with significantly more bleeding. Ticagrelor reduced the occurrence of MACE over clopidogrel use but was still associated with an 11.2% bleeding rate in the PLATO trial. Finally, cangrelor was not found to be superior to clopidogrel in the CHAMPION clinical trial [22]. Therefore, while improvements in efficacy are being made for P2Y12 inhibitors, bleeding remains a significant issue.

1.3.3 GPIIb/IIIa Inhibitors

The final group of antiplatelets is the GPIIb/IIIa inhibitors. These drugs are intravenously administered and act by direct interaction with the GPIIb/IIIa membrane protein on platelets, thereby inhibiting strong adhesion of platelets to vWF and subsequent aggregation [24]. Two inhibitors of interest in this group are eptifibatide and abciximab.

Eptifibatide was assessed in the PURSUIT (Platelet Glycoprotein IIb/IIIa in Unstable Angina: Receptor Suppression Using Integrillin Threapy) trial and found to reduce the rate of myocardial infarction from 15.7% to 14.2% over the placebo group. However, the risk of bleeding more than doubled (14.1% vs. 6.0%) with the use of eptifibatide [25]. Abciximab, which acts similarly to eptifibatide, presented similar efficacy and bleeding results in the RAPPORT and ADMIRAL clinical trials [26].

1.4 Current Platelet Function Tests

Given the balance needed between efficacy and bleeding risk, a reliable laboratory assay to predict responsiveness to a particular drug and dose is needed. A diagnostic assessment is useful in this context, and several methods have been developed to test platelet function in response to antithrombotic therapy. Thus, these types of diagnostic tests have been generally named as Platelet Function Tests (PFTs). This section will detail current methods for determining platelet function, detailing the strengths and shortcomings of each method in the clinical setting.

1.4.1 Light Transmission Aggregometry (LTA)

LTA was first developed in the 1960s by Born and O'Brien as a methodology for measuring platelet aggregation [27, 28]. This was originally noted by each of these researchers independently after ADP was added to platelet rich plasma (PRP) and a visible change in the opacity of the solution was observed. It has become the gold standard for testing platelet function [29].

LTA is conducted by preparing a PRP sample by centrifuging whole blood and isolating the PRP supernatant off of the red blood cell rich pellet. The PRP sample is then pipetted into a cuvette heated to 37°C and stirred with a small magnetic stir rod. Agonists (i.e. ADP, ristocetin, thrombin, or collagen) are added into the PRP sample in order to activate platelets. The light transmission of the sample is recorded as the platelets begin to aggregate and precipitate out of solution.

The advantages of LTA include the simplicity of the platelet aggregation endpoint, the ability to test multiple agonists for multiple platelet functions (i.e. platelet-platelet and platelet-protein interactions), and the depth of clinical studies that show that LTA can diagnose platelet and bleeding disorders [30].

However, disadvantages of the method include the laboratory workup that is needed to create PRP from whole blood, which takes time and manpower. Additionally, the stirring of the sample may skew results, as there is not a standard stir speed in every lab that conducts the LTA test [29]. Therefore, methodologies that are more automated and robust may provide more clinical utility than LTA.

1.4.2 Chrono-Log Whole Blood Analyzer

The Chrono-Log Whole Blood Analyzer determines platelet function by impedance aggregometry. Impedance aggregometry is the measurement in the changes of electrical impedance between two metal electrodes due to the build-up of a substance layer on them. In this case, that substance is platelets from a whole blood sample. The overall process of testing impedance aggregometry with the Whole Blood Analyzer is very similar to that of the LTA described previously, with the exception of using a whole blood sample rather

than a PRP sample. 500 μL of blood is placed into an equal volume of saline within a cuvette and heated for 5 minutes to a temperature of 37°C. This sample is also stirred with a small magnetic stir bar and an electrode is placed in the sample. Once the electrode is able to establish an impedance baseline, an agonist is added to the blood sample and continuously stirred to adequately mix. As platelets begin to become activated and stick to the electrode surface, the impedance readout rises. The impedance aggregometer then provides three values of Lag Time (the time between agonist addition and for the impedance to rise above 2 Ω, the Amplitude (the maximum change in impedance over the whole reading), and the Area Under the Curve (AUC, the integral of the impedance over time).

Advantages of the Whole Blood Analyzer is that the user is able to test with a whole blood sample rather than PRP as in the LTA, which cuts down on sample processing time. Additionally, this system offers a multichannel setup, which increases the throughput of the device as the user is able to run multiple samples at once. Finally, it is overall cost effective with the base unit approximately $7,000 and the costs to run each test on the order of a few cents.

However, there are disadvantages of the Whole Blood Analyzer. One disadvantage is that the electrodes need cleaned after each assessment, and if this is not properly done then the endpoints may be skewed. This lack of cleaning automation or single-use cartridge/electrode system limits the ability of the aggregometer to make reliable assessments clinically. Additionally, the test does not incorporate physiological flow conditions, which have been shown to be of high importance in the formation of arterial platelet thrombi.

1.4.3 VerifyNow®

The VerifyNow® is perhaps the most commonly used PFT diagnostic in the clinic since it began being marketed in the late 1990's. This device takes the concept of LTA and modified it with two big advantages: use of whole blood and complete automation.

The method involves testing a 1 mL sample of citrated whole blood in a cartridge including a relevant agonist for the assessment (i.e. ADP for P2Y12 inhibitors and arachidonic acid for aspirin). Glass beads that are in the disposable cartridges of the VerifyNow® test are coated with the agonist. Once mixed with whole blood, the light transmission through the glass beads is changed as platelets begin aggregate and coat the surfaces of the glass beads (**Figure 1-1A**). A single light transmission reading is provided after 2-5 minutes of mixing blood with the beads and reported as either ARU ("aspirin response units") or PRU ("P2Y12 Reactivity Units"). Cut-off values for both ARU and PRU have been determined for platelet activity.

Clinically, VerifyNow® has been used extensively, in particular for the PRU test with clopidogrel. Two trials in particular have shown that the VerifyNow PRU test was significant in for MACE occurrence in patients with high vs. low PRU values (235 cut-off). One study of 380 patients undergoing percutaneous coronary intervention (PCI) showed that patients with higher PRU values, indicating high P2Y12 activity, had a significantly higher occurrence of MACE. The other study included 683 patients with acute coronary syndrome and showed similar significant results of MACE occurrence with PRU values [31, 32].

However, The GRAVITAS (Gauging Responsiveness With a VerifyNow Assay-Impact on Thrombosis and Safety) trial of 5,429 patients on dual antiplatelet therapy (DAPT) failed to predict differences in MACE between experimental groups [31]. It also showed that VerifyNow was not able to predict optimal doses of clopidogrel for patients, which is part of the goal of PFTs for directed individualized therapy.

Advantages of VerifyNow® are that it is a fully automated system that utilizes very small sample volumes for its assessment. This allows for a standardized procedure from laboratory to laboratory, so results can be effectively compared. Some studies also indicate it may have some predictive value in MACE occurrence, although this is not demonstrated in every clinical assessment with VerifyNow.

There are some very significant disadvantages with the use of VerifyNow, as well. Most significantly is that the system lacks the pathological hemodynamics of arterial thrombosis, namely a high shear environment. Additionally, the agonists that are utilized in the VerifyNow diagnostic are not relevant agonists in the pathological scenario where sub-endothelial collagen promotes vWF-platelet aggregation. The test is also rather expensive, with each individual cartridge costing the clinical laboratory ~$60 and insurance or the patient is then charged ~$300 for the assessment (personal correspondence).

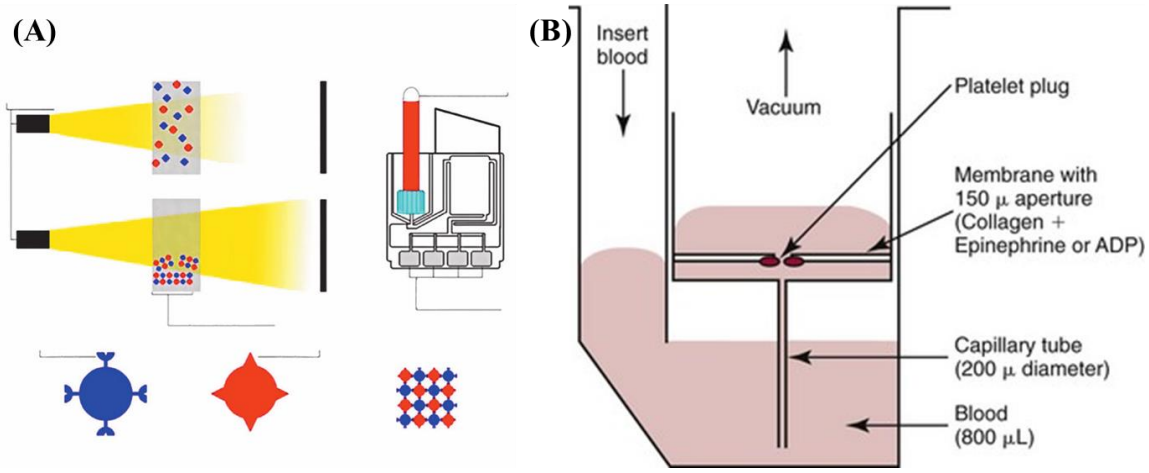

Figure 1-1. (A) VerifyNow cartridge concept of light transmission aggregometry with agonist coated beads (blue) and platelets (red) [33]. (B) PFA-100 concept where blood is aspirated through a membrane orifice coated with agonists to promote platelet plug formation.

1.4.4 PFA-100®

Platelet Function Analyzer-100 (PFA-100®) is the first clinical PFT diagnostic to incorporate high shear flow into its analysis. The system is described as having shear rates between 4,000 and 6,000 s^{-1}, which are in the pathological range. The PFA-100® makes use of a membrane orifice coated with fibrillar type I collagen and epinephrine (C-EPI) or ADP (C-ADP) (**Figure 1-1B**). First, 800 μL of blood is loaded into the cartridge and the aspirated upward through a capillary tube. The blood then enters a second chamber, where it comes into contact with the coated membrane and is forced through the small 100 μm hole that is coated with collagen and epinephrine or ADP. A platelet plug begins to form and occludes the hole in the membrane, leading to the endpoint of closure time (CT) or non-closure (NCT) if the test takes longer than 300 seconds.

The PFA-100 has been extensively used in research of the effects of clopidogrel, aspirin, and GPIIb/IIIa inhibitors. However, PFA-100 has not been able to reliably show

inhibition by antiplatelets like aspirin and clopidogrel using both the C-EPI and C-ADP cartridges, and therefore has not gained much traction in the clinic. Assessments with the PFA-100 found that patients non-responsive to aspirin were 2.1 times more likely to experience MACE; however, 24.8% of patients responsive to aspirin per the PFA-100 still experienced MACE [34-36]. Therefore, the specificity of PFA-100 is poor.

The disadvantages of PFA-100® are the lack of shear prior to the orifice, which creates a sudden flow contraction. The orifice dimensions would be critical for shear rate, but the paper membrane is not geometrically stable under pressure and shear stress. Thus, the geometry of the test section is not anatomically relevant to the case of a stenotic artery. The system apparently does not work with only collagen coating. Thus, the required additions of epinephrine or ADP to the membrane also create a non-physiologic scenario, where only collagen would be present to initiate vWF and platelet adhesion. While the introduction of high shear flow is certainly a step in the right direction, changes to these factors are likely necessary to better recapitulate the pathophysiologic conditions of high shear arterial thrombosis.

1.4.5 Global Thrombosis Test (GTT)

The Global Thrombosis Test was developed by researchers in the UK with the aim of creating a high shear PFT that does not utilize any anticoagulation, thus testing non-treated blood. GTT recreates a physiologic-like flow scenario with relevant shear accelerations across a double ceramic ball-bearing system (**Figure 1-2**) [37, 38]. GTT utilizes two endpoints of occlusion time and thrombolysis time as determined by a drop-based photosensor. Occlusion time is defined as the point at which time between drop readings

is greater than 10 seconds. Thrombolysis time is the time for another drop to occur after occlusion time, following a 300 second thrombus stabilization period. Correlations between thrombolysis time and MACE have been observed, with a sensitivity of 60% and specificity of 80% [38]. No correlations have been found with occlusion time.

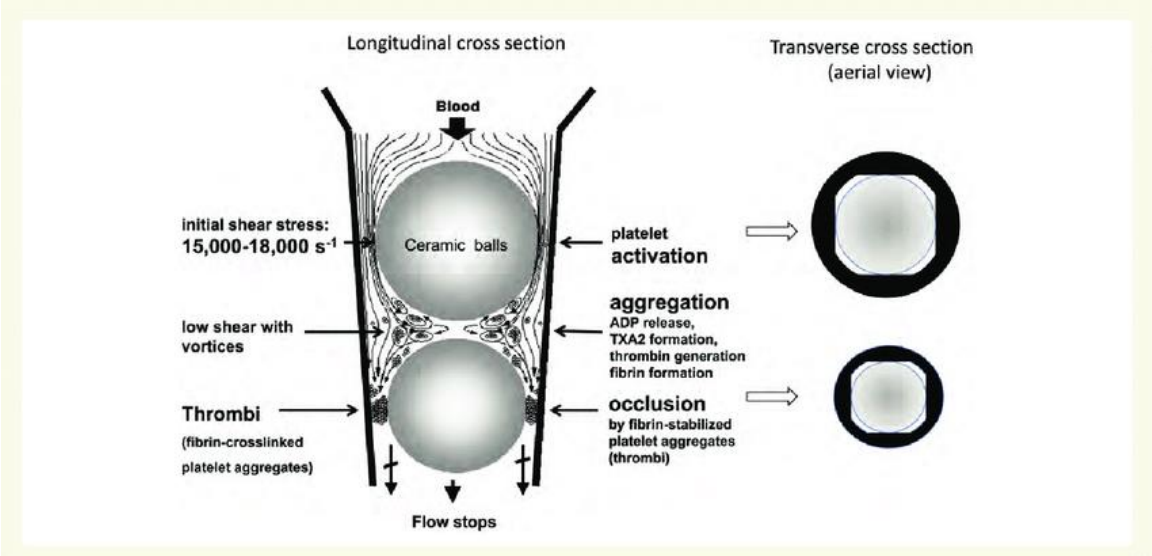

Figure 1-2. Schematic of the Global Thrombosis Test cartridge for high shear thrombosis testing. Blood is injected into a test tube and flows past two ceramic balls in series that create areas of high shear. Thrombi form and occlude these channels between the ceramic ball-bearings and the tube, leading to an occlusion time (OT) metric. Once flow is detected again, the system reports a lysis time (LT) [37].

However, the lack of both a pro-thrombotic surface and any anticoagulation provides some skepticism in the endpoints of this assay. The ceramic flow-contacting surfaces lack any surface coating, such as collagen, to promote thrombus formation. In addition, the test is performed on non-anticoagulated whole blood immediately after blood draw. While there is obvious upside to testing native blood samples, the histology of the clots from the GTT show significant fibrin and few platelets suggesting thrombosis from contact

activation instead of vWF-platelet aggregation that is the sine qua non of arterial white clots [39].

1.4.6 Microfluidic Assays

With the advances and benefits (smaller samples, faster assays) of microfluidic technologies for biological applications over the last 20 years, many experimental microfluidic assays have been developed for the study of platelet thrombus formation [40-43]. I will detail a few significant ones that inspired this work:

Platelet adhesion studies. Several groups have investigated platelet function with a simple straight channel design and a collagen coated surface. A significant group in this research field is the Diamond Lab at the University of Pennsylvania. They have created a reversible bonding microfluidic technology where they collagen coat a 1000 μm thick strip perpendicular to the main flow path, which acts as the pro-thrombogenic "landing zone" for platelets to adhere [44]. Blood is drawn from 8 inlet reservoirs converging into a single outlet, allowing for the simultaneous testing of 8 different blood samples or treatments. As the blood passes over the collagen surface, platelets begin to adhere. However, this single channel system is designed to only assess platelet adhesion at shear rates of ~1,000 s^{-1}, which a normal arterial flow conditions and not as pathophysiologic. As a result, the assay is only useful in assessing platelet adhesion, not bulk platelet thrombus aggregation. Another group has developed an automated well-plate straight channel microfluidic called Bioflux. The procedure requires the fluorescent labeling of platelets and imaging with a fluorescent microscope. While it may provide the same outcomes as the other platelet adhesion studies, it comes at a significant cost of ~$80,000 for the Bioflux flow control

equipment and compatible fluorescent microscope. Not only is this type of system expensive, but it also requires a skilled microscopy technician to conduct the assessment and is not suitable for the clinical diagnostic setting.

Shear-gradient studies. Others have investigated the importance of geometric changes leading to flow accelerations, or shear gradients, on the formation of arterial thrombi in microfluidics. In particular, microfluidic studies from the Nesbitt lab at Royal Melbourne Institute of Technology compared the formation of platelet thrombi in straight channel systems and those with constricted, or stenosed, channels to simulate an atherosclerotic site [45]. The straight channel studies indicated significant platelet adhesion, but unstable bulk thrombus formation. The microfluidic channels that introduced shear gradients through a 2D constriction developed stable platelet thrombi, indicating that flow accelerations may play a role in the formation of arterial platelet aggregates. Therefore, straight channel 2D microfluidic systems may not be a suitable method for investigating platelet aggregation.

T-TAS. The Total Thrombus-formation Analysis System (T-TAS) was developed by a lab at Kagoshima University as a flow-based microfluidic system for generating arterial platelet thrombi. The system makes use of a single inlet reservoir and single outlet for pressure readouts. The test section of the cartridge is split into 25 microchannels coated in collagen, each of a 40 x 40 μm cross section. Blood flows through the microchannels at a shear rate of 2,000 s^{-1} and goes through a shear gradient acceleration as it enters the test section. This system seems promising as a potential high shear arterial thrombosis diagnostic, but does raise a few questions. First, the shear rate is above normal arterial flow conditions, but not high enough (> 5,000 s^{-1}) for stable platelet-vWF capture [14]. Additionally, the dimensions of the device channels are very narrow that emphasizes

collagen wall capture more than rapid platelet accumulation on vWF from mural platelets. This device is intriguing and it will be interesting to see future clinical results from this group.

3D Stenosed Microfluidics. As detailed above, most geometries are two-dimensional (2D) in design, meaning no variation in the z-direction of the channel [42]. This leads to the small height of channels being continuous throughout and not just in the test section zone, leading to high resistances and the need for a pump to drive flow. Our group has previously investigated the ability to make microfluidic stenoses in the z-direction, thus decreasing overall resistance and allowing for gravity to drive flow through the channels. Li et al developed a 4-channel system with a shear gradient leading to a stenotic test zone using a vertical milling machine [46]. While this method was able to create high shear arterial thrombi, the relatively large dimensions of the device (250 x 750 μm cross-section at the stenosis) were more "milli-fluidic" than microfluidic, requiring a significant volume of blood to reach thrombotic occlusion. Therefore, Casa et al investigated CNC micromachining to create microfluidics of channel heights on the order of 70-80 μm. While this approach was successful at achieving lower blood volumes per test (~2-5 mL), the repeatability of channel dimensions was inferior to standard lithography practices. The dimensional variability leads to variable shear rates. This led to high variability > 30% in the endpoint of channel occlusion time (OT), as platelet accumulation rates are dependent on shear rate [47]. An integration of 3D geometries with enhanced dimensional repeatability is still necessary for arterial thrombosis assays.

1.5 Hypotheses and Specific Aims

Currently, clinicians are unable to quantifiable determine if their patients are responding adequately to their prescribed antiplatelet medication. This is due to the lack of a reliable platelet function diagnostic, which should provide insight into individualized responses to therapies. As such, clinicians are prescribing therapies based on risk factors and are blind to the actual effectiveness until an adverse event occurs, either by ineffective therapy (i.e. myocardial infarction or stroke) or overly effective therapy (i.e. bleeding complications). This shows that there is a need for both improved diagnostic tools and antithrombotic therapies in order to decrease the rates of adverse events. To aid in the development of better diagnostics and more reliable antithrombotic therapies, we aim to answer the following questions:

- Can we leverage highly repeatable lithography practices and collagen coating techniques to create a more repeatable microfluidic thrombosis assay?
- Do current anticoagulation methods of platelet function tests have a significant impact on the endpoint of platelet thrombosis?
- Will a less variable assay effectively determine responses to antiplatelet therapies that does not correlate to other PFTs that have proven unreliable?
- Can a low-variability, high shear microfluidic assay be utilized to screen for more effective antithrombotic therapies?

Therefore, the **overall goal** of this work is to develop a low variability stenotic microfluidic thrombosis assay (MTA) that has the able to detect individualized antiplatelet efficacy in the clinical setting, as well as provide a metric by which to test novel antithrombotic therapies in the research setting.

This work has three primary aims:

Specific Aim 1: **Reduction of microfluidic thrombosis assay (MTA) variability through design factors.**

I hypothesize that the main sources of variability observed in previous microfluidic thrombosis assays are due to three fundamental design factors: geometric variability, collagen coating, and anticoagulant selection. To improve geometric precision in current stenotic microfluidic assays, a novel 3D grayscale lithography method will be developed for improved dimensional repeatability. Collagen surface coverage with collagen thin films will be compared to standard fibrillar coatings. Lastly, the most common anticoagulant utilized in PFTs (citrate – a calcium chelator) will be compared to an anticoagulant against thrombin (low-dose heparin).

Specific Aim 2: **Assess the ability of the MTA to quantify antiplatelet responsiveness.**

I further hypothesize that the endpoint of occlusion time in a low-variability assay will provide diagnostic utility for individual antiplatelet responsiveness. To assess the clinical utility of the microfluidic assay developed in Aim 1, a specificity study to antiplatelet therapy will be performed for aspirin and clopidogrel. Samples from healthy individuals will be assayed pre-treatment and post-treatment to determine the assay specificity to antiplatelet responsiveness. A comparative study of acute coronary syndrome (ACS) patients prescribed either aspirin or DAPT will then be performed against two other PFTs: GTT and VerifyNow PRU test.

Specific Aim 3: **Development of a novel nanoparticle antithrombotic therapy.**

Finally, I hypothesize that such a device can be utilized to develop novel antithrombotic nanoparticle therapies. To create a potentially more efficacious antithrombotic therapy, nanoparticles of differing sizes, surface groups, and doses will be assessed in the microfluidic assay. An optimal particle and dose will be determined and assessed in a murine arterial thrombosis model for in vivo safety.

CHAPTER 2. SHEAR INDUCED PLATELET AGGREGATION: 3D-GRAYSCALE MICROFLUIDICS FOR REPEATABLE AND LOCALIZED OCCLUSIVE THROMBOSIS

Results detailed in this chapter have been reported in BioMicrofluidics [48].

Abstract

Atherothrombosis leads to complications of myocardial infarction and stroke as a result of shear-induced platelet aggregation (SIPA). Clinicians and researchers may benefit from diagnostic and benchtop microfluidic assays that assess thrombotic activity of an individual. Currently there are several different proposed point-of-care diagnostics and microfluidic thrombosis assays with different design parameters and end-points. The microfluidic geometry, surface coatings, and anticoagulation may strongly influence the precision of these assays. Variability in selected end-points also persists, leading to ambiguous results. This study aims to assess the effects of three physiologically-relevant extrinsic design factors on the variability of a single end-point to provide a quantified rationale for design parameter and end-point standardization. Using a design of experiments approach, we show that the methods of channel fabrication and collagen surface coating significantly impact variability of occlusion time from porcine whole blood, while anticoagulant selection between heparin and citrate did not significantly impact variability. No factor was determined to significantly impact the mean occlusion time within the assay. Occlusive thrombus was found to consistently form in the first section (333 μm) of the high shear zone and not in the shear gradient regions. The selection of these factors in the design of point-of-care diagnostics and experimental SIPA assays may lead to increased precision and specificity in high shear thrombosis studies.

2.1 Introduction

Myocardial infarction and ischemic stroke are the leading causes of death in the world [49]. Both morbidities occur as the result of an atheroma causing a stenosis in the coronary and carotid arteries with resulting pathophysiological high shear blood flow. If there is a plaque cap rupture causing endothelial damage, then a rapid formation of a platelet-rich clot ensues [2, 3, 50]. Rapid platelet accumulation can grow until occlusive thrombus forms, stopping blood flow in the artery. An assay to quantify a patient's propensity for stenotic thrombosis would significantly aid in the personalized titration of antiplatelet medications to prevent myocardial infarction and stroke occurrence while reducing bleeding complications. However, current clinical and microfluidic systems suffer from high inter- and intra-subject variability causing poor specificity from a test with low precision [51-53].

2.1.1 Failings of platelet function tests

Several platelet assays are available for testing platelets, including VerifyNow®, Chrono-log Whole Blood Aggregometer, and Light Transmission Aggregometry (LTA), PFA-100®, and GTT [34]. Only the PFA-100® and GTT test for platelet response under flow. The other three systems (VerifyNow®, Chrono-log, and LTA) test platelets under stirring conditions rather than shear flow, which is not appropriate for making conclusions regarding arterial thrombosis. Nevertheless, VerifyNow® is the most common platelet assay used clinically [51]. The GRAVITAS (Gauging Responsiveness With a VerifyNow Assay-Impact on Thrombosis and Safety) trial of 5,429 patients on aspirin and Plavix® dual

antiplatelet therapy (DAPT) failed to show statistical differences in death rates due to major adverse cardiovascular events (MACE) between patients with high and low $P2Y_{12}$ reaction units (PRU) as determined by the VerifyNow® assay, thus supporting the claim that VerifyNow® is not suitable to predict patient outcomes [31]. This is likely partially due to the finding that intra-individual variation of the VerifyNow® assay is considerably high, with 25% of individuals having greater than a 20% coefficient of variability (CV) between measurements. This caused 24% of individuals to fluctuate between therapeutic categories between measurements [54, 55].

Of the flow-based assays, PFA-100® is used far more than the relatively new GTT, with more than 600 studies published in peer-reviewed journals. PFA-100® makes use of a membrane orifice coated with fibrillar type I collagen and epinephrine or ADP. This orifice creates an area of high shear flow through a sudden flow contraction that is not hemodynamically relevant to the case of an atherosclerotic, stenotic artery. The additions of epinephrine and ADP to the membrane also create a non-physiologic scenario, where only collagen would be present to initiate von Willebrand Factor (vWF) and platelet adhesion. This is associated with poor predictive value, as 24.8% of patients responsive to aspirin per the PFA-100® still experienced MACE [34-36]. Like VerifyNow®, PFA-100® has high intra-individual end-point variability between 17-37%, which may prevent its clinical utility [56, 57].

In response to the failings of platelet function tests, several experimental microfluidic assays have been developed for the study of shear induced platelet

aggregation (SIPA); however, there remains variability upwards of 35% in the outcomes of SIPA microfluidic assays [40-43, 53]. In 2011, the biorheology subcommittee of the International Society of Thrombosis and Haemostasis made recommendations on four experimental design parameters for the standardization of flow-based thrombosis assays: microfluidic geometry, surface coatings, anticoagulation, and end-point imaging [58]. While these recommendations have been documented for nearly a decade, no specific parameter grouping has been proven to reduce end-point variability within SIPA microfluidics. Therefore, a parametric comparative study is needed to determine the effects of each of these parameters on variability.

2.1.2 Microfluidic Thrombosis Assay Design Parameters

Most geometries are two-dimensional (2D) in design, meaning no variation in the height of the channel. While they have highly repeatable dimensions via lithography techniques, these channels suffer in two major ways. If there is no variation in the width along the channel, then there is a lack of shear gradient important for plasma vWF elongation. Also, for more complex and longer channels there is a high resistance due to the small channel heights that must be overcome through increasing the pressure driving flow, as resistance is inversely proportional to the height cubed (**Equation 2-1**). While this can be accomplished with a pump, undesirable high pressures will develop in the channels as full occlusion forms. Further, utilizing a pump creates a constant flow situation, rather than constant pressure. With constant flow, a single-inlet, multiple-outlet microfluidic device (**Figure 2-2**) would skew flow from a more high resistance channel to a lower resistance channel, thus each

channel is dependent on the thrombotic activity in the other channels. This flow compensation skews results, as blood flow is diverted depending on resistance of the parallel channels. A constant pressure system, however, allows for thrombotic events to occur independently across channels, as flow independently decreases for a given channel as resistance increases due to thrombus formation. This is due to flow being driven by the same pressure difference. Pressure remains constant, resistance rises, and flow decreases in that channel. Flow in other channels will not be affected, as they are governed by their own changes in resistance. Therefore, it is important to be able to establish geometric variations in the height to limit high-resistance areas in the test section of the microfluidic, allowing for constant pressure flow systems. While computer numerical control (CNC) micromachining has been used previously for three-dimensional (3D) microfluidic applications, the repeatability of channel dimensions is inferior to standard lithography practices. The dimensional variability leads to variable shear rates, therefore increasing the channel-to-channel variability. An integration of 3D geometries with enhanced dimensional repeatability is still necessary for high shear thrombosis assays.

$$Resistance = \frac{12\mu L}{wh^3} \quad \textbf{(2-1)}$$

Pro-thrombogenic surface coatings for high shear thrombosis assays have been investigated significantly in the last two decades [59-61]. While fibrillar type I

collagen is the most common in the field due to the specific binding of vWF to collagen fibers [62], the deposition of fibers into flow channels leads to sparse and non-uniform surface coverage [60]. Exploration into soluble collagens has indicated highly uniform surface coverage, but a significant decrease in platelet response due to the lack of structural fibers [63]. One study investigating vWF-III combined with collagen-mimetic peptides GFOGER and CRP and another study of 52 different natural and synthetic coatings investigated platelet accumulation response under flow, and found that several of the coating combinations had enhanced surface coverage, but fibrillar type I collagen led to the strongest thrombotic response under normal arterial shear [64, 65]. Focusing on enhancing the repeatability of fibrillar collagen coatings, Hansen et al induced fiber formation from acid-soluble collagen in order to develop collagen thin films (CTF) [60]. While there was success in achieving high fiber density and coverage, the standard fibrillar coating still had a significantly stronger platelet response in terms of faster adhesion. However, the impact of increased fiber density and coverage on end-point *variability*, such as platelet adhesion and aggregation, was not assessed.

Anticoagulation is utilized to keep blood from clotting between the draw and the test due to contact activation upon introduction to foreign substances, such as the blood collection containers. There have been a range of different anticoagulants used in various assays. Differential effects on platelets based on anticoagulant selection indicate that this choice may impact end-point variability [40, 42, 66]. A commonly utilized anticoagulant in clinical and research applications is sodium citrate [34, 67, 68]. Sodium citrate chelates calcium in whole blood, which is a co-factor for several

steps of the coagulation cascade and platelet activation as integrins are sensitive to calcium ion levels [66, 69]. It has also been reported that vWF requires calcium for platelet adherence, which suggests recalcification is needed prior to testing [70]. However, recalcification to a concentration of 10-40 mM prior to testing often leads to rapid coagulation of the sample during the experiment if not performed on-chip [71]. Methods for on-chip addition of calcium may not mix well with the citrated blood sample due to low Reynold's number flow. Further, it has also been reported that citrate irreversibly reduces the reactivity of platelets and impairs $\alpha_{IIb}\beta_3$ activation even after recalcification [40, 52]. Another anticoagulant option, heparin, acts to increase levels of antithrombin II to inhibit thrombin cleavage of fibrinogen, and is the most commonly used short-acting anticoagulant in clinical settings [72]. Heparin presents the benefit of no secondary recalcification step leading to rapid contact activation of the coagulation cascade, making it easier to work with after the blood draw. Some studies suggest that heparin may inhibit P-selectin function in platelets and their α-granules, which could prevent vWF release during the rapid platelet accumulation phase [40, 73]. Heparin is also reported to potentially have an impact on the thrombin-platelet interaction, but not directly on the vWF-platelet interaction [74].

Finally, imaging of the thrombus development is vital in the determination of an assay end-point through a non-blood contacting method. However, discrepancies in the location of thrombus formation within a stenotic test section are found in the literature. Two different stenosis test sections created thrombus growth in the downstream shear-gradient zone of the channel [45, 75]. However, other reports

indicate that thrombus formation occurs within the stenotic zone [46, 76, 77]. The location of occlusive thrombus in a stenosis with an anatomically relevant throat needs confirmation for the design of a thrombosis imaging end-point.

2.1.3 Objectives and hypothesis

This study aims to assess the main sources of variability of *in vitro* microfluidic SIPA assays. It is hypothesized that current sources of variability are associated with extrinsic factors of channel geometry, pro-thrombotic collagen coverage, and anticoagulant selection. Reducing dimensional and surface coverage variation, as well as use of anticoagulation that does not greatly impair GPIIb/IIIa activation will greatly decrease variability associated with the end-point of thrombotic occlusion time. Further, control of these three factors will lead to a spatially consistent occlusive thrombus within the physiologically relevant 3D microfluidic geometry.

2.2 Methods

2.2.1 Microfluidic Geometry Fabrication

Microfluidic geometries were designed in order to keep platelet-platelet interactions dominant over platelet-surface interactions [41]. Therefore, the minimum stenotic height was set at 70 μm to ensure platelet-platelet aggregation was being studied. The dimensions of the nominal channel sections were determined by CFD estimations (COMSOL Multiphysics, COMSOL Inc.) to establish normal arterial shear rates of 500 s^{-1}, while stenotic arterial shear rates in the test section were designed to be 6,500 s^{-1}. Two methods

of device fabrication were investigated for geometric repeatability and effect on end-point variability: CNC machining and 3D grayscale laser-lithography (GLL).

First, a brass mold was machined with a CNC machine (ProtoTRAK, Southwestern Industries, Inc.). The stenotic geometries were created with a series of mill events. Eight nominal channel segments were fabricated to be 180 µm in height and 475 µm in width with a 1.0 mm milling tool with 2 passes with coolant, as Z feed-rate of 50 mm/min, XYZ feed-rate of 300 mm/min and spindle speed of 150,000 RPM. Stenoses at a height of 80 µm with gradual contraction zones like an atheroma were created from the nominal channels with two cut events from the center of the stenosis to make the upstream and downstream contraction zones. This was completed with the 1.0 mm milling tool using the parameters previously described.

The GLL method was developed to take advantage of highly repeatable lithography and etching processes (**Figure 2-1**), and the development methods are described in detail in Appendix A. In brief, 100 mm silicon wafers were coated with approximately 5.0 µm of photoresist (Microposit SC1827, MicroChem) and variably exposed with ultraviolet light with the use of direct laser writing (Laserwriter LW405, Microtech) to develop defined contraction zones in the photoresist. The wafer was developed to remove exposed photoresist (MF-319, MicroChem). A Bosch etch process (STS ICP) was used to etch the stenotic profile into the exposed silicon wafer to a depth of 180 µm from the wafer surface, followed by an acetone wash of remaining photoresist. A 10 µm photoresist layer (AZ P4620, MicroChemicals) was then spray coated (AltaSpray Coater, SUSS MicroTec), followed by a mask alignment process to align the nominal device geometry on the wafer. Finally, another Bosch etch process was performed to a target nominal depth of 250 µm,

leaving the stenotic height at 70 µm above the wafer surface. A total of four test channels were fabricated for a single inlet (**Figure 2-2**). Quality control measurements at all fabrication steps were acquired through contact profilometry (Dektak, Bruker).

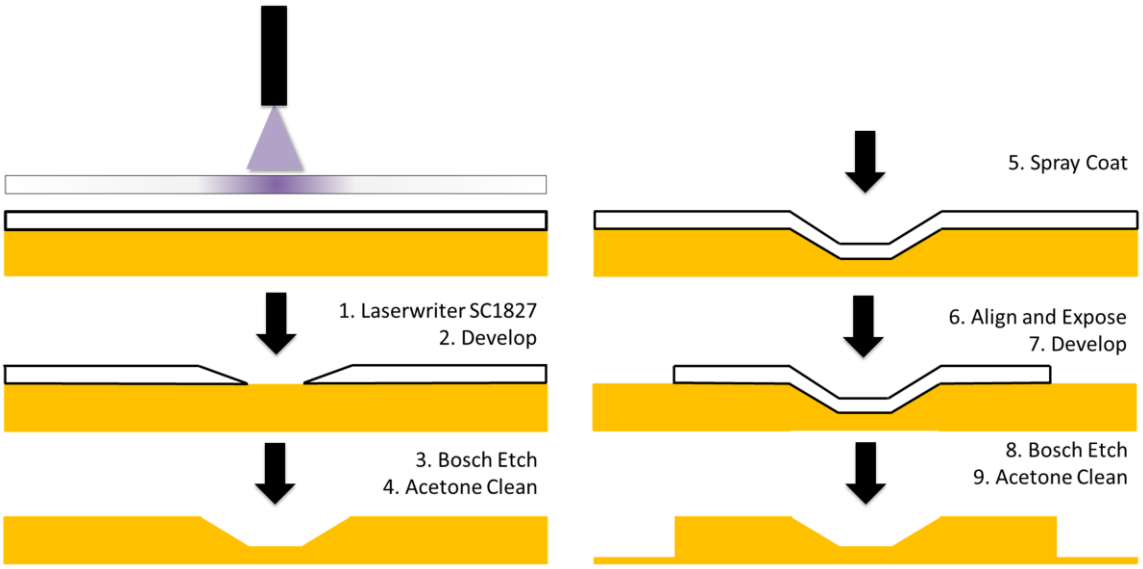

Figure 2-1. Process flow for the development of the novel 3-D 'grayscale' lithography technique. Linear variations in the z-direction were made possible through this method to establish contracting stenotic zones mimicking an atheroma.

Microfluidic chips were created by casting PDMS (Sylgard 184, Krayden) on both machined and lithography molds. PDMS channel height measurements were made with 3D material confocal microscopy (LEXT, Olympus). Average and standard deviation of nominal and stenotic heights, as well as arithmetical mean height (S_a) for surface roughness, were calculated for both methods.

2.2.2 Collagen Surface Coating

Two methods of collagen coating were investigated for coverage repeatability and effect on end-point variability: fibrillar and collagen thin films (CTFs). The fibrillar coating

method was described previously by Casa et al, where microfluidic channels were filled with a 100 µg/mL collagen Type I solution in 0.9% saline (Chronopar, Chronolog, Inc.) and incubated at room temperature for 24 hours [3]. The second method of CTF coating was described by Hansen et al, where microfluidic channels were filled with a 1000 µg/mL soluble collagen solution neutralized with 0.1N NaOH and diluted with PBS [60]. In this experiment, however, the collagen was incubated at room temperature for 24 hours prior to washing and drying.

Characterization of collagen surface coverage was performed by light microscopy (DM6000B, Leica Microsystems) with a 20X objective. Acquired RGB images were converted to grayscale, followed by 55% threshold binary images (MATLAB, MathWorks). The image was divided into equal quadrants and the percent coverage was calculated in each area. The average and standard deviation of the collagen coverage was calculated for both fibrillar and CTF coatings.

2.2.3 Anticoagulation

Whole porcine blood (N = 6) was obtained from a local abattoir (Holifield Farms, Covington, GA) and split into two jars with either unfractionated heparin or sodium citrate so that identical blood samples were utilized in both conditions:

1) 500 mL of porcine whole blood was lightly heparinized at 3.5 USP units/mL, as previously described by Para et al [77]. Blood was stored at room temperature on a rocker prior to testing.
2) 450 mL of porcine whole blood was treated with 50 mL of 3.2% sodium citrate (weight percentage in aqueous solution) and stored at room temperature on a rocker

prior to testing. Blood was recalcified with $CaCl_2$ to a final [Ca^{2+}] of 10 mM immediately prior to each experiment.

All whole blood experiments were performed within 6 hours after blood collection.

2.2.4 Microfluidic Thrombosis Assay

The collagen-coated microfluidic chips were positioned on the stage of a light microscope (DM6000B, Leica Microsystems) with a 4X objective (40x magnification) and connected to an upstream reservoir with Tygon tubing, similar to that previously described (**Figure 2-2**) [3]. A constant pressure head (100 mmH_20) is established for an initial wall shear rate of 6500 s^{-1} in the stenotic zone and 500 s^{-1} in the nominal channels. Downstream tubing led to a discharge reservoir placed on a precision balance (Ohaus Scout SPX222, Ohaus Corp) to measure mass flow rates. Images of thrombus formation were acquired at 1 Hz with a high-resolution CCD camera (Pixelfly, PCO). Image acquisition was facilitated by the μManager open-source microscopy software [78]. Occlusion time (OT) was measured as the time from first blood contact with the stenosis to the time of the initial maximum mass reading.

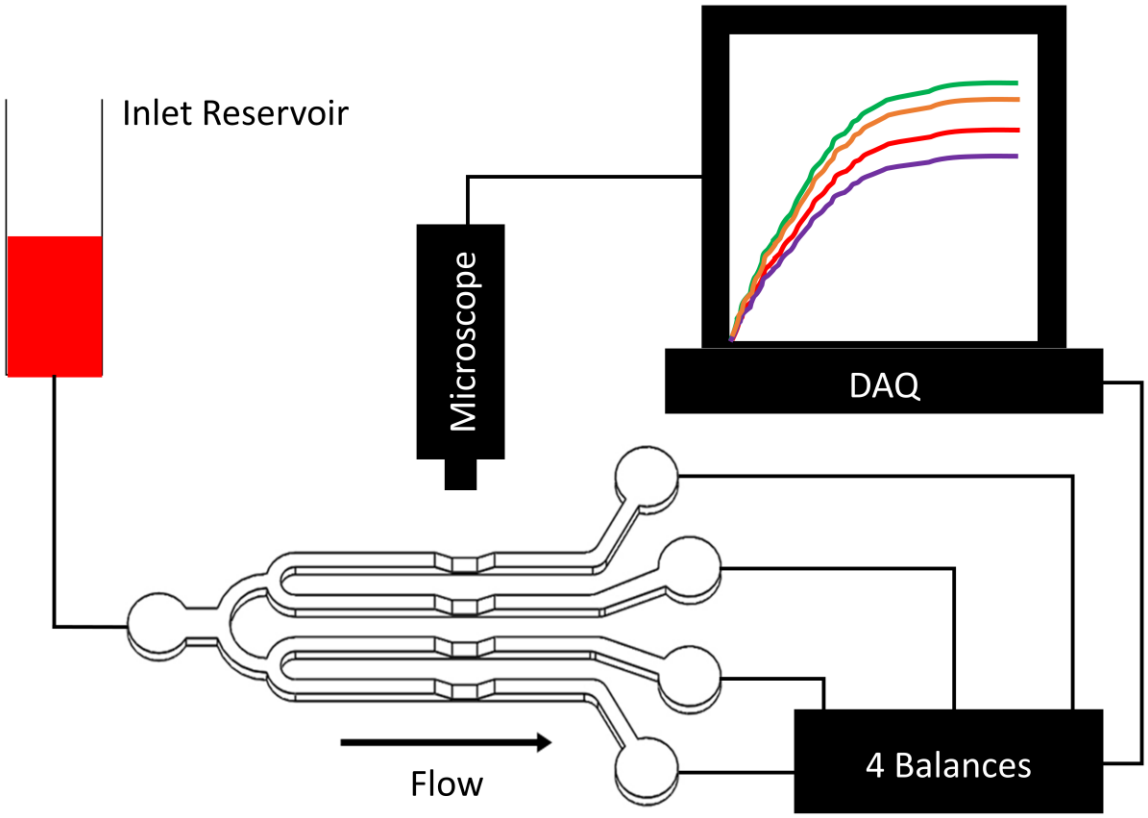

Figure 2-2. Microfluidic SIPA assay setup with gravity driven pressure from an upstream syringe. Blood samples are split evenly between 4 stenotic test section zones and independent mass accumulation readouts from precision electronic balances are sampled at 1 Hz via a National Instruments DAQ. Real time visualization is also performed and recorded at 1 Hz with a PixelFly camera.

Table 2-1. Fractional Factorial Experimental Groups for the three main design factors of geometry fabrication by CNC or GLL, collagen coverage with fibrillar or CTF, and anticoagulation with heparin or citrate.

Group	Geometry	Collagen	Anticoagulant
A	CNC	Fibrillar	Heparin
B	CNC	CTF	Citrate
C	GLL	Fibrillar	Citrate
D	GLL	CTF	Heparin

A total of four experimental groups were assessed in a fractional factorial design of experiments, described in **Table 2-1**. Four blood samples were tested in quadruplicate for each test group, while two additional blood samples had 3 final replicates due to a leak or blockage eliminating one of the four microfluidic channels. The average OT was calculated and standard deviation was determined. Percent variance was determined by dividing the standard deviation by the average occlusion time.

2.2.5 Image Analysis

Images of the stenotic channel gathered by the CCD camera were assessed for location of occlusive thrombus growth. Images were segmented into five regions: 1) inlet gradient, 2) first third of stenosis, 3) middle of stenosis, 4) last third of stenosis, and 5) outlet gradient. At the end of a thrombotic experiment, the intensity of platelet deposition was recorded for each region to determine relative rates of platelet accumulation.

2.2.6 Statistical Analysis

All variability calculations for channel geometry, collagen surface coverage, and occlusion time were performed by dividing the standard deviation by the mean of replicate measurements. Student's t-test was calculated for channel dimension, collagen surface coverage, and clot region measurements. ANOVA was utilized to calculate the f-statistic for each model parameter (geometry, collagen, and anticoagulant) in order to determine each parameter's significance on occlusion time variability [79]. All statistical analyses were performed with JMP Pro (SAS Institute, Inc., Buckinghamshire, England).

2.3 Results and Discussion

2.3.1 Chip Geometric Precision

Assessment of geometric precision of both techniques (CNC and GLL) was performed with the LEXT material confocal microscope and summarized in **Figure 2-3**. For 2D geometric zones (flat along the z-direction) of the channel, the GLL technique proved to have superior precision over the CNC method. However, the GLL yielded surface roughness of 18.9 µm in the sloping geometric zones that ramped into and out of the stenosis, with a periodic peak-to-value distance of 18.8 µm on average. This compares to a surface roughness of 2.3 µm in the CNC ramped zones. As for the stenotic zone, surface roughness of 0.7 µm and 1.3 µm were measured for the GLL and CNC, respectively. The increased roughness in the GLL ramps is likely due to the resolution of the LaserWriter step prior to the Bosch process, as any defect in the photoresist layer will be amplified in the silicon mold due to the etch rates of the two materials (depicted in

Figure 2-1 steps 1-3). Thus, the two techniques have distinctly different strengths, with the GLL giving precise depths, while CNC machining yields smoother ramps. While the surface roughness of the lithography method is not desirable, the heights and effective shear rates in the nominal and stenotic GLL test sections were consistent to 0.2% within an individual channel and across channels. In contrast, the standard deviation of the stenotic heights in the CNC channels was measured to be 2.9 μm, which led to a 3.5% variability in height (**Table 2-2**).

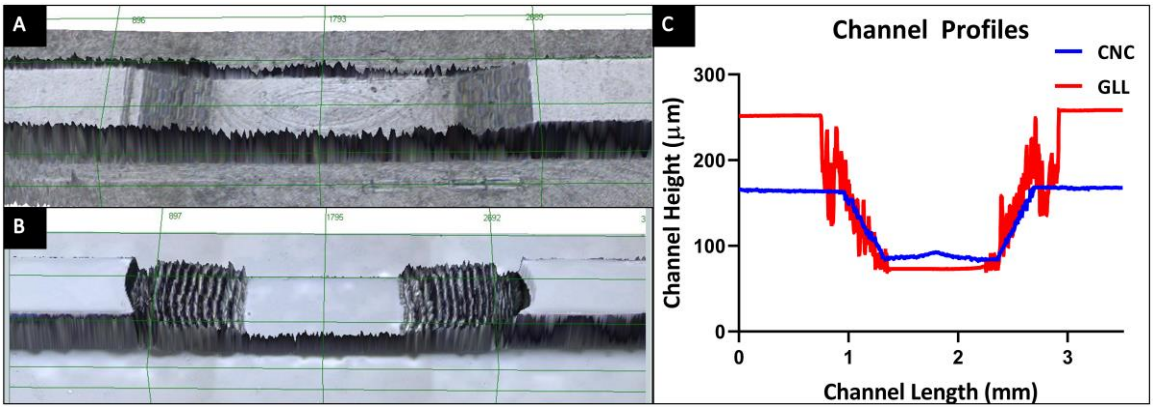

Figure 2-3. LEXT confocal 3-D images of (A) CNC machined and (B) GLL lithography microfluidic channels. (C) Linear profiles indicate the heights of the channels in the nominal and stenotic regions, as well as overall surface roughness characteristics. GLL proved superior in geometric repeatability in the stenotic zone, while CNC was superior in surface roughness in the converging and diverging regions.

Table 2-2. Assessment of fabrication technique dimensional variability for both CNC and GLL methods.

	Stenotic Height (µm)			Nominal Height (µm)		
Method	*Target*	*Actual*	*Variability*	*Target*	*Actual*	*Variability*
CNC (n=8)	80.0	82.4 ± 2.9	3.5%	180.0	182.6 ± 2.6	1.4%
GLL (n=4)	70.0	73.7 ± 0.1	0.1%	250.0	256.0 ± 0.4	0.2%

For our purposes, shear rate in the throat was the dominant factor for the thrombosis endpoint. The wall shear rate in a rectangular channel is dependent on the height squared, so is highly sensitive to errors, as detailed by **Equation 2-2**.

$$\text{Shear Rate} = \frac{6Q}{wh^2} \qquad \textbf{(2-2)}$$

Therefore, with highly repeatable nominal and stenotic heights, the precise lithography channels will have more repeatable flow and shear rates from channel-to-channel. This was confirmed in a water flow rate comparison, where flow rate variability in CNC channels (n = 8) was determined to be 11.7%, while GLL channel (n = 4) variability was determined to be 4.0%.

2.3.2 Collagen Surface Coverage

Collagen surface coverage was determined through light microscopy using a 20X objective and segmentation of the focal area to assess spatial variability in coverage. Qualitatively, fibrillar coatings led to random and sparse deposition of fibers, while the CTF coat provided much more uniform and dense coverage (**Figure 2-4**). This analysis confirms that similar CTF coatings were utilized in this experimental protocol as those utilized by Hansen et al in comparing CTFs with fibrillar collagens in the strength of platelet adhesion response [60]. Quantitatively, the surface coverage of CTFs was determined to be more dense and uniform than fibrillar coatings, as shown and discussed earlier (**Figure 2-4F**). Although the CTF coating was previously studied extensively and found to not exhibit as strong a platelet adhesion response as fibrillar type I collagens, the increased and more uniform surface coverage may lead to repeatable assay end-points [60].

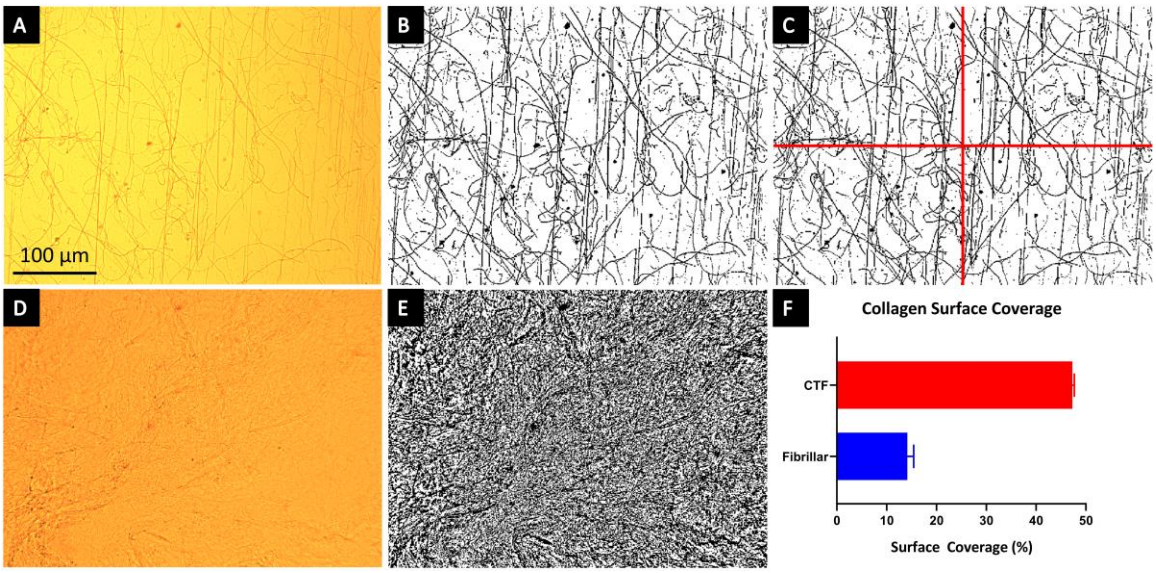

Figure 2-4. Collagen coating assessment performed on fibrillar coatings (A-B) and CTFs (D-E) by light microscopy. Collagen is identifiable in the deep orange colored areas of A and D, which is then converted to a binary distribution map based on the pixel values. (A) indicates much longer, but more sparse collagen type I fibrils, while (D) shows the deposition of microfibrillar CTFs over most of the surface. Images are converted to binary format and divided into quadrants (C). Percent surface coverage of each quadrant was calculated and averaged for both conditions (F). All microphotographs are to the same scale.

2.3.3 Occlusion Time Variance: Fractional Factorial DOE

The multi-parameter design of SIPA microfluidic assays requires an end-point variability analysis to provide guidelines to consider in the future design of such tools. This Design of Experiments can identify the dominant versus secondary factors influencing the endpoint, occlusion time. Therefore, an occlusion time variance analysis was performed for the three design parameters of interest: fabrication technique, collagen coverage, and anticoagulation selection.

Occlusion time was determined for each of the four experimental groups for six porcine samples, from which variance was calculated (**Figure 2-5**). Immediately, group C

(GLL, fibrillar, and citrate) had the least variability in the end-point of occlusion time at 11.5% on average. However, the group analysis was then followed by assessment of each parameter within the experimental design by a standard least squares effect screening.

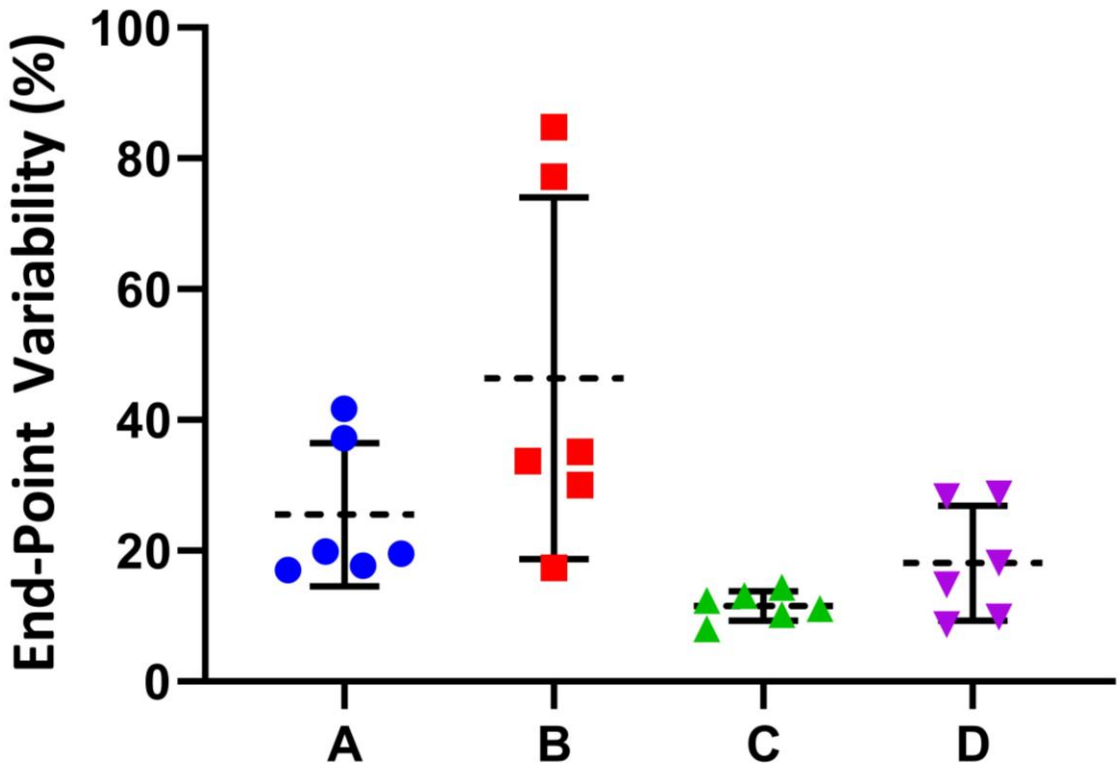

Figure 2-5. Experimental data of average occlusion time (N = 3 or 4) for each sample within each group. The coefficient of variance was calculated by dividing the standard deviation by the average OT and is shown here for each sample. Group C (GLL, fibrillar collagen, citrate anticoagulation) led to the least variability in the occlusion time endpoint as compared to groups A (CNC, fibrillar, and heparin), B (CNC, CTF, citrate), and D (GLL, CTF, heparin). The fractional factorial design ANOVA revealed that GLL geometry ($p < 0.01$) and fibrillar collagen coating ($p < 0.05$) are significant parameters in reducing assay variability. No significant difference was found in assay variability between citrate and heparin anticoagulation. Dashed lines are the mean coefficient of variability and whiskers are the standard deviation of that mean.

First, the parameter that had the largest impact on occlusion time variability was the geometry fabrication technique (**Figure 2-5**; $p < 0.01$). The microfluidic chips

fabricated by GLL led to a significantly more repeatable end-point. As previously stated, shear rates were more consistent between channels, leading to similar rates of platelet thrombus formation. This is consistent with previous work studying and predicting rates of platelet accumulation [14, 80]. This finding also indicates that the surface roughness associated with the contracting zones of the grayscale lithography technique do not greatly impact the end-point of the assay. While the surface roughness could be improved upon, the repeatability of the shear-rates in the nominal and stenotic sections of the channel make GLL a more attractive option than CNC machining methods.

Fibrillar coatings also were found to significantly decrease variability of the thrombosis assay end-point over the use of CTFs, although to a lesser extent than the 3D fabrication method (**Figure 2-5**; $p < 0.05$). This was contrary to our hypothesis that a more uniform collagen fiber surface coverage would lead to less variable end-points. Apparently vWF and CTFs associate weakly, as previously observed in platelet adhesion assessments [60, 63]. These weak interactions may lead to more random adhesion of vWF onto the CTF surface, thus causing the increase in end-point variability. Even though deposition is non-uniform in the flow channel, type I fibrillar collagens lead to a more stable and reliable vWF interaction, which is likely the reason for the decreased variation [62, 63].

Finally, no significant difference was found in the use of unfractionated heparin (3.5 USP) or sodium citrate (3.2%) anticoagulation methods in reducing occlusion time end-point variability for porcine whole blood (**Figure 2-5**). However, from a practical experimental approach, it is beneficial to utilize heparin in the assay as coagulation is not a major factor for the short time scale of SIPA microfluidics (3-5 minutes) and at high shear rates. Recalcification of the citrated whole blood samples can lead to large clots in

the inlet reservoir and tubing, making this technique difficult to manage. Coagulation was observed in several of the recalcification experiments and made timing very important to develop platelet-rich clots before RBC-rich clots obstructed the flow pathway. While this timing could be reduced by methods of on-chip recalcification, this is generally impractical when performing this experiment. Further, in future experiments evaluating antiplatelet or thrombolytic therapies, SIPA experiments will take more time and be more susceptible to coagulation occurring and blocking flow before a complete assessment of platelet thrombosis can be made. While the combination of GLL, fibrillar collagen, and heparin was not part of the DOE analysis, this combination yielded an end-point variability of 11.6% (N = 4), which was consistent with the finding of Group C in the DOE. Therefore, it is simpler to utilize an anticoagulant like unfractionated heparin for SIPA microfluidic assays, where no additional steps for recalcification are required.

Parameter selection did not play a significant role in the time to occlusion. For the geometric differences, this is not surprising as Para reports that in the late stages of thrombus formation, rapid platelet accumulation (RPA) occurs rapidly to overwhelm variations in initial surface height [77]. Therefore, the 10 μm difference in channel heights between CNC and GLL methods did not play a significant role in quantifying occlusion time. What is surprising, however, is that the collagen coating method was not found to significantly impact occlusion time in this assay. With previous reports stating that fibrillar collagen coatings provide a stronger response to platelet adhesion, it might be expected that fibrillar coatings lead to significantly shorter occlusion times. While a small decrease in occlusion time was associated with fibrillar coatings, it was not significant over CTF

coatings. Anticoagulant selection had no significant impact on the time to occlusion within the microfluidic assay.

2.3.4 Spatial Repeatability of Thrombus Formation

Finally, we performed an analysis on the spatial occurrence of SIPA thrombotic formation within the microfluidic assay. After occlusive thrombus was formed, the final images were segmented into five regions of converging, stenotic thirds, and diverging zones (**Figure 2-6**). Intensity values of the white-clot regions were recorded (n = 8).

We observed that the occlusive platelet clot was consistently formed in the first third of the stenotic channel ($p < 0.01$), while significantly less clot formation was observed in the shear-gradient converging and diverging zones ($p < 0.01$). This is consistent with our findings that GLL methods have less variability in occlusion time than CNC methods. GLL provides superior control of the geometry in the stenotic section of the channel, where the occlusive platelet clot forms. The occlusive clot does not form in the gradient sections of the channel, which indicates that the increased surface roughness in those zones by the GLL method does not significantly impact the endpoint. However, this finding is not consistent with a previous report that found platelet accumulation most at the diverging outflow region of the channel [45]. The differences between the previously reported results and ours are likely due to: 1) the prior's lack of collagen and reliance on protein absorption to the PDMS walls to promote platelet accumulation and 2) the very small area at the top of their stenosis. Theoretically, the absorption of vWF would be less likely to occur in the high shear zone due to a decreased residence time in these zones. However, when utilizing collagen as in the current case, vWF fibers in high shear zones tether to the physiologically

relevant surface with more avidity and repeatably form occlusive thrombus in the first third of the channel.

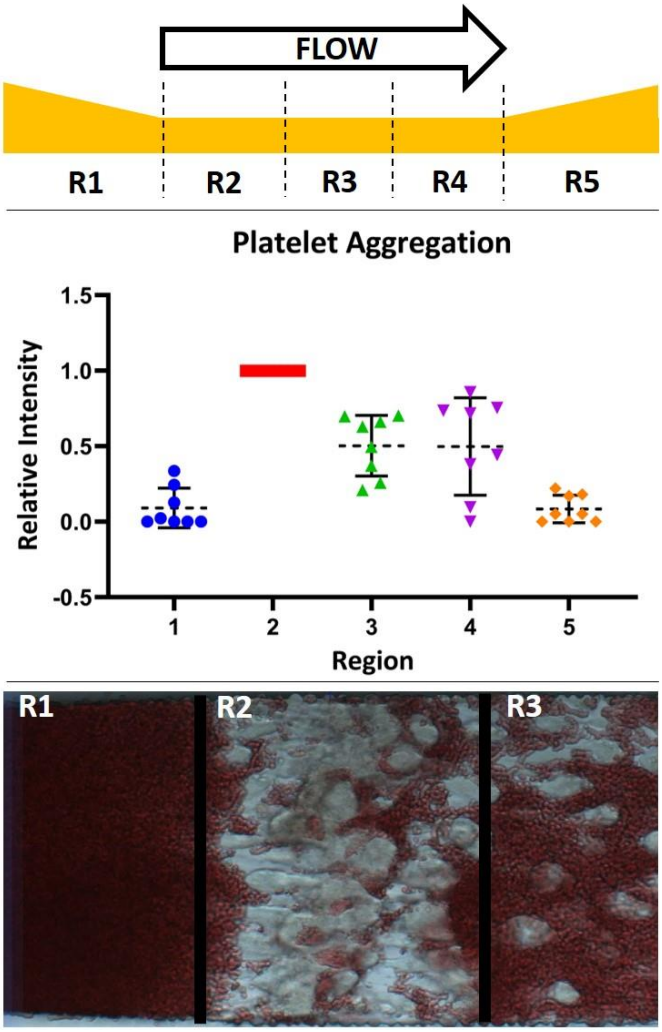

Figure 2-6. Segmentation of the microfluidic channel into 5 regions of interest: 1) converging gradient, 2-4) thirds of the stenotic zone, and 5) diverging gradient. The first third of the converging zone was found to always develop the occlusive thrombus ($p < 0.01$), as shown in the mean intensity analysis of each zone and the bottom representative image of occlusive thrombus. Dashed lines represent the mean intensity and whiskers are the standard deviation of the mean. (Results in collaboration with Dongjune Kim [48])

The relative influence of the factors studied here may prove beneficial in the general design of point-of-care whole blood assays. By designing a shear-activated test section for repeatable platelet thrombosis formation, a microfluidic assay can be globally coated with collagen rather than locally coated through specialized collagen coating techniques that require critical alignment techniques [53, 61]. Development of an optical detection system for clot formation in a limited stenotic zone would allow for an alternative end-point for platelet clot formation when determining thrombotic risk of a patient. Eventually, this type of SIPA microfluidic assay may provide more physiologically relevant results for arterial occlusions than current PFTs in use.

2.3.5 Limitations and future work

Though effective in determining geometric and collagen coating parameters for decreasing occlusion time endpoint variability of the microfluidic thrombosis assay, this work is limited by several fundamental shortcomings. First, this work was performed with porcine whole blood rather than human whole blood. While porcine whole blood is considered to be fairly similar to that of humans, blood plasma protein sequences do differ slightly between the species, which may alter the time it takes for a platelet thrombus to occlude the channel. While this may not have a highly significant impact on an investigation of assay variability, it would dispel any questions regarding its translation to humans if human whole blood had been utilized.

An additional limitation is that the rough, scalloped surfaces developed in the converging and diverging zones of the GLL manufacturing method. While we show that variability of the assay is not highly dependent on the surface roughness of the gradient

zones since the thrombus forms in the constant high shear region, it may limit the level of method adoption due to researchers being averse to the scalloped nature. Therefore, future work into grayscale techniques such as the subtractive manufacturing technique developed in this thesis (see Appendix A) or additive grayscale techniques may benefit the adoption of this type of microfluidic channel.

Lastly, this study only investigated two options for each parameter (geometry, collagen surface, and anticoagulation), while there certainly are more than two approaches to tackle each challenge. This study does not claim to have found the optimal "end-all, be-all" best approach, but rather shows design choices that are proven to limit assay variability. Future methods, such as enhanced fibrillar collagen coatings, were not investigated in this work but may also contribute to decreasing assay variability.

2.4 Conclusion

We quantified the relative importance of several methodological parameters on end-point variability in SIPA microfluidic assays. Two design parameters (geometric fabrication technique and collagen coating method) have significant impact. The development of a 3D grayscale laser lithography technique creates stenotic test sections of precise geometry and enhanced shear rate repeatability, as compared to current CNC machining methods for 3D channel fabrication. Fibrillar collagens were also found to significantly reduce end-point variability as compared to a collagen thin film coating approach, even though the fibrillar coating was non-uniform in surface coverage. Anticoagulation method did not impact variability in the SIPA of porcine whole blood. Finally, it was determined that clot formation

consistently occurred in the first 0.3 mm of the stenotic channel with a constant pressure head, providing a basis by which to design optical detection methods in SIPA point-of-care diagnostic devices.

CHAPTER 3. DIAGNOSTIC POTENTIAL OF THE MICROFLUIDIC THROMBOSIS ASSAY

Abstract

Platelet function tests (PFTs) have the potential to assess antiplatelet efficacy and the risk for major adverse cardiovascular events (MACE) on an individualized basis. However, no current clinical PFT provides significant predictive value for MACE occurrence. We have previously developed a microfluidic thrombosis assay (MTA) that incorporates the major causes of arterial thrombosis: high shear blood flow, collagen pro-thrombotic surface, and significant blood components platelets and vWF. This study characterizes the MTA for its ability to assess antiplatelet function in both healthy and patient populations and compare the patient population to outcomes of two other PFTs: GTT and VerifyNow. Healthy individuals pre- and post-aspirin (N = 20) show that aspirin significantly extends MTA occlusion time (OT) and also shows that blood anticoagulated with sodium citrate has a greater effect on platelet function compared to blood anticoagulated with unfractionated heparin. Significant correlations were found when comparing MTA and GTT OT in patients on aspirin ($\rho = 0.699$; $p < 0.001$; N = 20), but no correlation was found between the two assays in patients on DAPT ($\rho = 0.482$; $p = 0.07$; N = 15). No other correlations were found between the MTA and other PFTs. The findings of this study indicate that the MTA assesses a different platelet thrombosis mechanism than current PFTs and is less sensitive to the effects of antiplatelet therapies, which may prove a more specific assay for predicting MACE.

3.1 Introduction

3.1.1 Antiplatelets for arterial thrombosis

To prevent adverse thrombotic events from occurring, therapies targeting platelet activation and adhesion have been utilized for over 50 years. Two of the most common therapies are aspirin and clopidogrel (also known as Plavix). Aspirin acts by irreversibly inhibiting COX-1, which interferes with thromboxane synthesis. This inhibition prevents activation from platelets by thromboxane production [81]. Plavix is formulated to irreversibly inhibit the P2Y12 platelet ADP receptor, thus permanently inhibiting another platelet activation pathway [82]. However, both drugs may not work as intended for the entire population, as various studies have reported up to 5-60% of individuals are hypo-responsive to therapy, thus exhibiting an "antiplatelet resistance" depending on the study and drug regimen [35, 36, 51, 83-86]. Dual antiplatelet therapy (DAPT) consisting of aspirin and a P2Y12 inhibitor (usually Plavix) is often employed to overcome antiplatelet resistance [51]; however, this may lead to an increase in primary side effects, with 7.4% incidence of fatal and nonfatal bleeding among individuals on DAPT [87]. The observed complications to standard doses of leading antiplatelet agents proves the need to individualize antiplatelet therapy through diagnostic screening with a platelet function test (PFT).

3.1.2 Platelet function test comparison

A PFT may ideally be utilized to quantify a patient's propensity for arterial thrombosis and provide a means for personalized titration of antiplatelet medications to prevent MACE occurrence while reducing bleeding complications. In the previous chapter, we detailed the development and characterization of the microfluidic thrombosis test (MTA) with reduced endpoint variability from previous versions in our laboratory. The MTA incorporates specific design inputs to mimic the pathophysiological condition of

arterial thrombosis: 1) pathological high shear blood flow (>5,000 s^{-1}) [2], 2) flow channel dimensions greater than 50 μm for platelet accumulation to dominate over platelet surface adhesion interactions [41], 3) collagen as a relevant agonist for circulating vWF capture [13, 88, 89], and 4) anticoagulant selection to prevent coagulation from occurring without significant effects on platelet function [40]. By incorporating these parameters, the MTA simulates the physiologic scenario better than the most common PFT, VerifyNow. VerifyNow lacks relevant biophysical stimuli in its test, relying solely on biochemical agonists to detect platelet function. Another PFT, GTT, only incorporates biophysical stimuli in its test without any biochemical agonist (i.e. collagen). The MTA incorporates both high shear and a collagen pro-thrombotic surface in determining platelet function.

We now aim to characterize the utility of the MTA device design in identifying antiplatelet responsiveness in individuals taking antiplatelet medication.

3.1.3 Objectives and hypothesis

We now aim to test the MTA, as compared to VerifyNow and GTT, in the assessment of the effects of antiplatelet therapies aspirin and Plavix in both healthy subjects and cardiovascular patient populations. In order to study these effects, we designed a study to determine the MTA's specificity to detect the effects of aspirin therapy in a healthy population by assessing pre- and post-therapy occlusion time. Through this study we are able to determine normal OT's and a cut-off for therapy responsiveness with the MTA. We are then able to employ this cut-off OT value in a patient population study to compare the MTA with VerifyNow and GTT. It is hypothesized that therapy responsiveness determined

by each PFT will have poor correlation with one another, indicating that each PFT is investigating different clotting phenomena.

3.2 Methods

3.2.1 Materials

Polydimethyl-siloxane (PDMS) was from Krayden, Inc. (Denver, CO, USA). Type I collagen was from Chrono-Log (Havertown, PA, USA). Testing of the MTA was performed on a Leica DM6000B microscope from Leica Microsystems, Inc. (Buffalo Grove, IL, USA), along with Scout SPX222 balances from OHAUS Corporation (Parsippany, NJ, USA) for mass flow rate detection and a high-resolution CCD PixelFly camera from PCO (Kelheim, Germany) for image acquisition. The VerifyNow® (VN) unit from Accriva Diagnostics, Inc. (San Diego, CA, USA) is housed at the clinical lab in Grady Memorial Hospital (Atlanta, GA, USA). The GTT unit from Thromboquest Limited (UK) is housed at the Georgia Institute of Technology (Atlanta, GA, USA).

3.2.2 Blood testing procedures

Microfluidic Thrombosis Assay (MTA). The microfluidic channels were fabricated by gray-scale lithography techniques previously described [48]. Fibrillar type I collagen-coated (100 μg/mL) microfluidic chips are positioned on the stage of a light microscope with a 4X objective and connected to an upstream reservoir with Tygon tubing, similar to previously described [3]. Downstream tubing leads to a discharge reservoir placed on a precision balance to measure mass flow rates. Images of thrombus formation are acquired at 1 Hz with a high-resolution CCD camera. Image acquisition is facilitated by the

μManager open-source microscopy software [78]. Occlusion time (OT) is measured as the time from first blood contact with the stenosis to the time of the initial maximum mass balance reading. Image and flow-rate post-processing was performed with custom code (MATLAB, MathWorks).

VerifyNow® (VN). VN is a PFT that assesses platelet reactivity under low-shear by light transmission. The $P2Y_{12}$ reaction units (PRU) cartridge is utilized in this study. A blood sample collected into a 3.2% sodium citrate 3mL vacutainer is assayed in the cartridge. A PRU value less than 235 indicates drug-induced platelet dysfunction [54, 55].

Global Thrombosis Test (GTT). The GTT is a PFT that assesses platelet thrombus formation and lysis under flow conditions [37, 39, 90]. A single cartridge with two ceramic ball-bearings that create 3 flow-channel gaps is utilized to develop a clot and detect lysis by a drop counter. One 6mL, nonanticoagulated blood sample is injected into the cartridge from a syringe. Occlusion times between 300 and 500 seconds represent normal hemostatic activity, while those faster than 300 seconds indicate platelet hyper-reactivity and those longer than 500 seconds indicate effective therapy. Lysis times earlier than 2000 seconds indicate normal spontaneous thrombolytic activity, while those greater than 2000 seconds indicate low thrombolytic activity.

Complete Blood Count (CBC). A CBC was taken for all healthy individuals participating in the study and recorded from previous lab exams for cardiovascular patients participating in the study.

3.2.3 MTA Specificity Study

Healthy volunteers were older than 18 years of age, had no history of cardiovascular disease, and had taken no antiplatelet medication (aspirin, Plavix, etc.) nor non-steroidal anti-inflammatory drugs (NSAIDS; i.e. ibuprofen) in the 10-days prior to enrollment. Individuals with known anemia (hematocrit < 30%) or transmittable blood diseases were excluded. The MTA was the only PFT utilized in this proof-of-concept study. All subjects were recruited in accordance with the Institutional Review Board of the Georgia Institute of Technology (IRB #H18238).

First, the MTA was assessed in an initial group of eight individuals at two different time points a week apart, prior to beginning aspirin treatment. This assessment was performed with either 3.2% sodium citrate (the most common anticoagulant choice of PFTs) or 3.5 USP unfractionated heparin (an indirect thrombin inhibitor) vacutainers to determine the effects of anticoagulant selection on inter-week variation of the MTA.

The main study cohort then consisted of 20 healthy adults not currently taking antiplatelet, anticoagulant, nor NSAIDS therapy. Prior to starting an aspirin regimen, 39 mL of blood were drawn from each subject using standard phlebotomy practices with a 21G butterfly needle: 18 mL in 3.2% citrate tubes, 18 mL in 3.5 USP heparin tubes, and 3 mL in an EDTA tube for a complete blood count (CBC). Each subject then began a low-dose aspirin regimen (81 mg/day) for 1-week. This regimen was chosen as it is the standard dose prescribed for antiplatelet effects and it has been previously reported that the effects of aspirin therapy on platelets are prevalent after one week of sustained therapy [91]. After taking aspirin on the final day of the week-long regimen, another blood draw of 39 mL was performed. All blood samples were tested within 4 hours after venipuncture. The percentage of aspirin responders was determined based on the cut-off OT time determined

in baseline pre-aspirin measurements. Intra-draw variability of the MTA was also assessed from this group of individuals. Correlations between OT and CBC values were determined.

3.2.4 PFT Comparison Study

The study cohort for a population-based study consisted of 35 adults (18 or more years of age) admitted to Grady Memorial Hospital for an interventional procedure in the Catheterization Lab. Subject recruitment was in accordance with the Institutional Review Board of Emory University and Research Oversight Committee of Grady Memorial Hospital (IRB #00106933). 20 individuals were on aspirin therapy as the only prescribed antiplatelet as part of their care, while another 15 individuals were on DAPT of aspirin and Plavix. The following exclusion criteria were used in patient recruitment: inability to consent, current participation in another study, cardiogenic shock, sepsis, malignancy, bleeding diastasis, thrombolysis therapy, warfarin therapy, GPIIb/IIIa inhibitor therapy, or blood dyscrasia [38]. Demographics (age and gender) were collected from patient records after consent was obtained. MTA and GTT were assessed for all subjects in this cohort, while VerifyNow PRU was assessed only for subjects on DAPT.

After consent was obtained and during the catheterization procedure, 20 mL of blood was collected from either the radial or femoral artery insertion site: 2 mL initial discard, 12 mL for the MTA (6 mL treated with 3.2% sodium citrate and 6 mL treated with 3.5 USP unfractionated heparin), 2 mL for VerifyNow PRU test (treated with 3.2% sodium citrate), and 4 mL for GTT (no anticoagulant). A CBC was already on file for each patient. All blood samples were tested within 4 hours after collection, except the GTT sample which was tested immediately after draw without anticoagulation per the manufacturer's

instructions. The percentage of responders per the MTA were determined based on the cutoff metric calculated in the healthy population study, while responders per VerifyNow and GTT were determined from the manufacturer's set ranges. Correlations of endpoints in all three PFTs with CBC values were also determined.

3.2.5 Statistical analysis

Continuous variables of occlusion time, lysis time, and PRU are presented as mean ± standard deviation. Normality of each dataset was determined by the Shapiro-Wilk test for data sets of small sample size ($N < 50$) [92]. Intra-day and inter-day variation in MTA OT were determined using student's t-test. The cut-off point for the MTA was set as two standard deviations above the healthy individual pre-aspirin OT to determine antiplatelet-effectiveness. Nonparametric analyses for paired (Wilcoxon test) and unpaired (Mann-Whitney test) were used for the healthy and patient subject populations, respectively. For non-normal data sets simple correlation between tests was assessed with Spearman correlation coefficients (ρ), where perfect correlations are represented by ρ of +1 or -1 [93]. Agreement between assays for determining "antiplatelet resistance" was assessed with Cohen's Kappa statistic (κ), where $\kappa < 0.20$ indicates no agreement, 0.21-0.40 as mild, 0.41-0.60 as moderate, 0.61-0.80 as substantial, and 0.81-1 as almost perfect agreement [94]. Correlations between assay endpoints and CBC values were determined by multivariate correlation probability ($p < 0.05$). Statistical analysis was performed in either GraphPad Prism (San Diego, CA, USA) or JMP Pro (Marlow, Buckinghamshire, UK).

3.3 Results

3.3.1 MTA inter-day variability: heparin vs. citrate

First, variability in the MTA OT endpoint was assessed in this protocol to investigate the inter-day variability for heparin and citrate anticoagulation. This was a follow-up to the previous chapter that investigated intra-day variability, only. 3.2% sodium citrate and 3.5 UPS unfractionated sodium heparin were utilized for comparison in a standard venipuncture blood draw with vacutainers. Variability results are represented in **Figure 3-1**. Variability datasets were tested for gaussian distribution by the Shapiro-Wilk test and were determined to be normally distributed. Intra-day variability for blood collected in citrate and heparin vacutainers was 16.6% and 11.8% ($N = 17$; $p = 0.15$), while inter-day variability was 19.7% and 7.2% ($N = 8$; $p < 0.05$), respectively. No significant difference was found between the two anticoagulants for intra-day variability, which is consistent with the results of the previous aim. However, it was determined that inter-day (or week-to-week) variability was significantly less with 3.5 USP heparin vacutainers over 3.2% sodium citrate vacutainers.

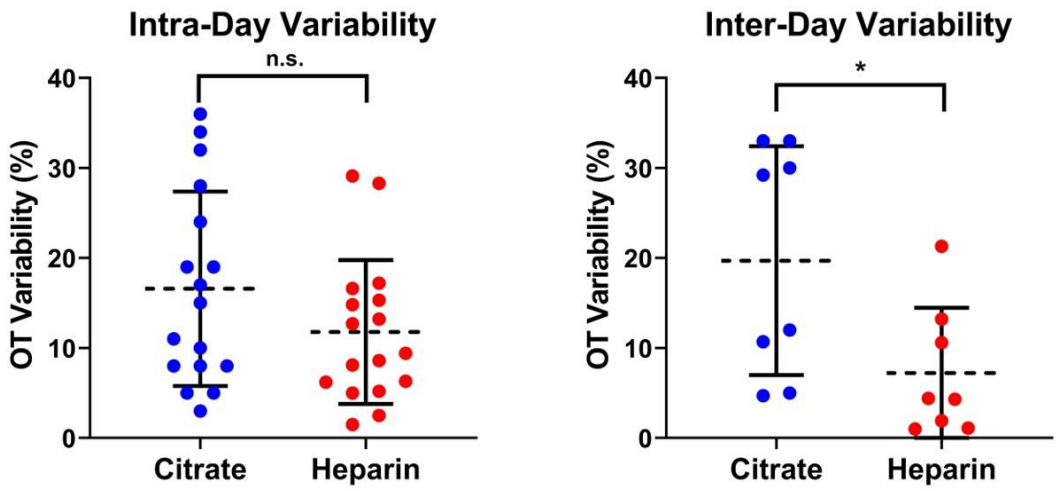

Figure 3-1. Comparison of intra-day (left) and inter-day (right) coefficient of variation of the MTA OT with blood samples collected by venipuncture with either 3.2% sodium citrate or 3.5 USP unfractionated heparin vacutainers. Intra-day measurements were taken from the same blood draw and tested in separate microfluidic cartridges (N = 17; p = 0.15). Inter-day measurements were taken from blood draws of the same donor on separate days to assess variability of different time points (N = 8; p < 0.05). Each data point is an average of 4 OT measurements within the MTA, represented by the dashed line with standard deviation. *p < 0.05

3.3.2 MTA Specificity Study: Low Dose Aspirin

Prior to starting individuals on aspirin therapy, baseline measurements of occlusion time in the MTA were determined for both citrate and heparin treated blood. This provided a population mean and standard deviation in OT for the 20 healthy subjects studied. A cut-off of 300 seconds (dashed line in **Figure 3-2**) was calculated from this population data set as two standard deviations above the mean in both citrate and heparin groups. The cut-off OT represents the point at which an individual is defined as responsive (> 300s) or non-responsive (< 300s) to antiplatelet therapy. This point is applied to any antiplatelet therapy

as it marks a significant inhibition of thrombus formation above the average population value of the MTA.

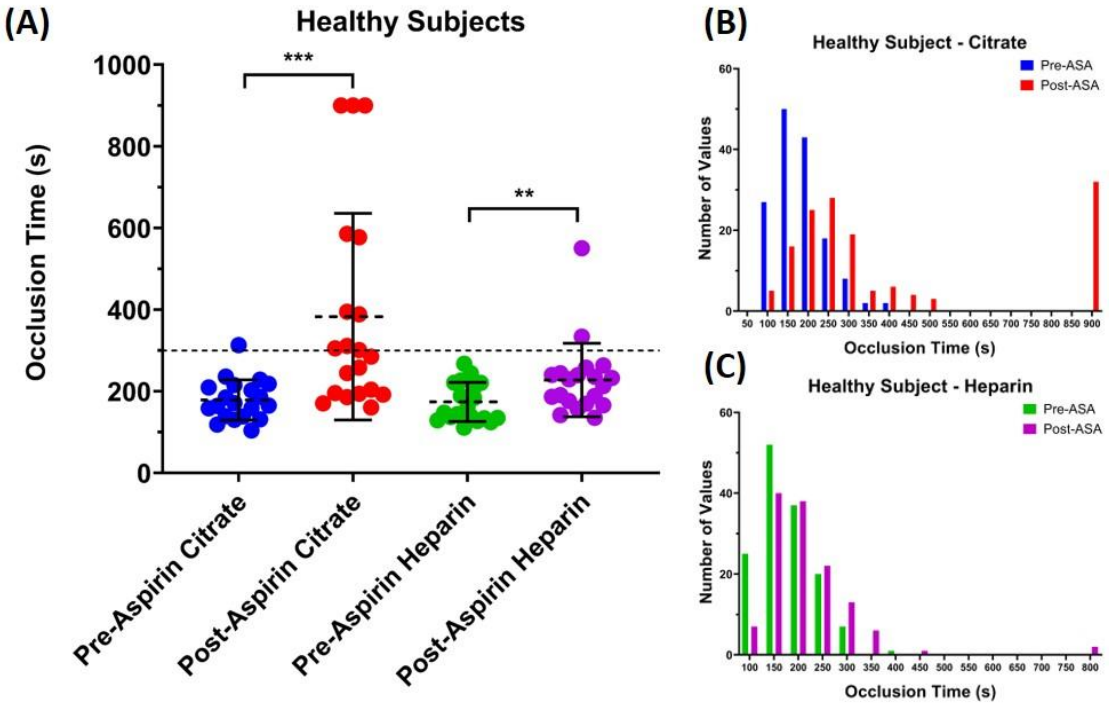

Figure 3-2. Summary of the healthy population week-long drug regimen characterization in the MTA. (A) Occlusion time population data of pre- and post-aspirin (ASA) when collected in citrate or heparin vacutainers. A cut-off of standard occlusion times was determined as two standard deviations above the baseline average and is depicted as the dotted line at 300s. Both post-aspirin groups are found to be statistically different than their respective pre-aspirin condition, indicating that aspirin impacts OT for the population. Log-normal distributions for OT were observed in both (B) citrate and (C) heparin collection methods. (N=20; Each data point is the average of 4 or 8 OT measurements in the MTA; *p < 0.05; **p < 0.01; ***p < 0.001)

After week-long aspirin therapy, individuals were assessed of their thrombotic state with the MTA. Aspirin therapy was determined to have a significant effect on OT measurements in the MTA for both citrate ($p < 0.001$) and heparin ($p < 0.01$), as calculated

by a Wilcoxon test for nonparametric, log-normal datasets. A significant difference in responder rates was also found between the anticoagulation methods, as 10/20 (50%) individuals were aspirin responders when collected in citrate tubes, while only 2/20 (10%) individuals were aspirin responders when collected in heparin tubes ($p < 0.01$). Three individuals' samples did not register an OT by 900s when treated with citrate anticoagulation, at which point the test was terminated. Both individuals who were responders with heparin treated blood were also responders with citrate treated blood. The Cohen's Kappa correlation coefficient between these two anticoagulant methods was 0.200, indicating weak agreement between the two methods. The rate of occurrence of individual occlusion times is also reported for both anticoagulants in **Figure 3-2**, where log-normal distributions are depicted. The effects of aspirin are detailed on an individual subject basis for citrate and heparin in **Figure 3-3**. The heat map of OT's for each condition (pre and post aspirin treatment collected in either heparin or citrate) indicates the level of aspirin-responsiveness, with darker green indicating highly responsive and darker red indicating highly non-responsive (completely white being the 300 s OT therapeutic cut-off). From this heat map and the dot plot, only 2/20 individuals in the heparin group had a faster OT after aspirin. Comparably, only 1/20 individuals in the citrate group had a faster OT after aspirin. This plot is also a good demonstration of the significant differences in PFT outcomes based on anticoagulant selection. From clinical data, it is expected that aspirin will not have a very significant role in preventing shear-induced platelet aggregation. This is better reflected in the heparin anticoagulated data, where only minor individualized differences in OT are observed. Large differences in OT are observed in the citrate group, indicating that citrate may be assisting aspirin in altering platelet function.

Therefore, heparin will be used over citrate as the MTA anticoagulant in the following studies.

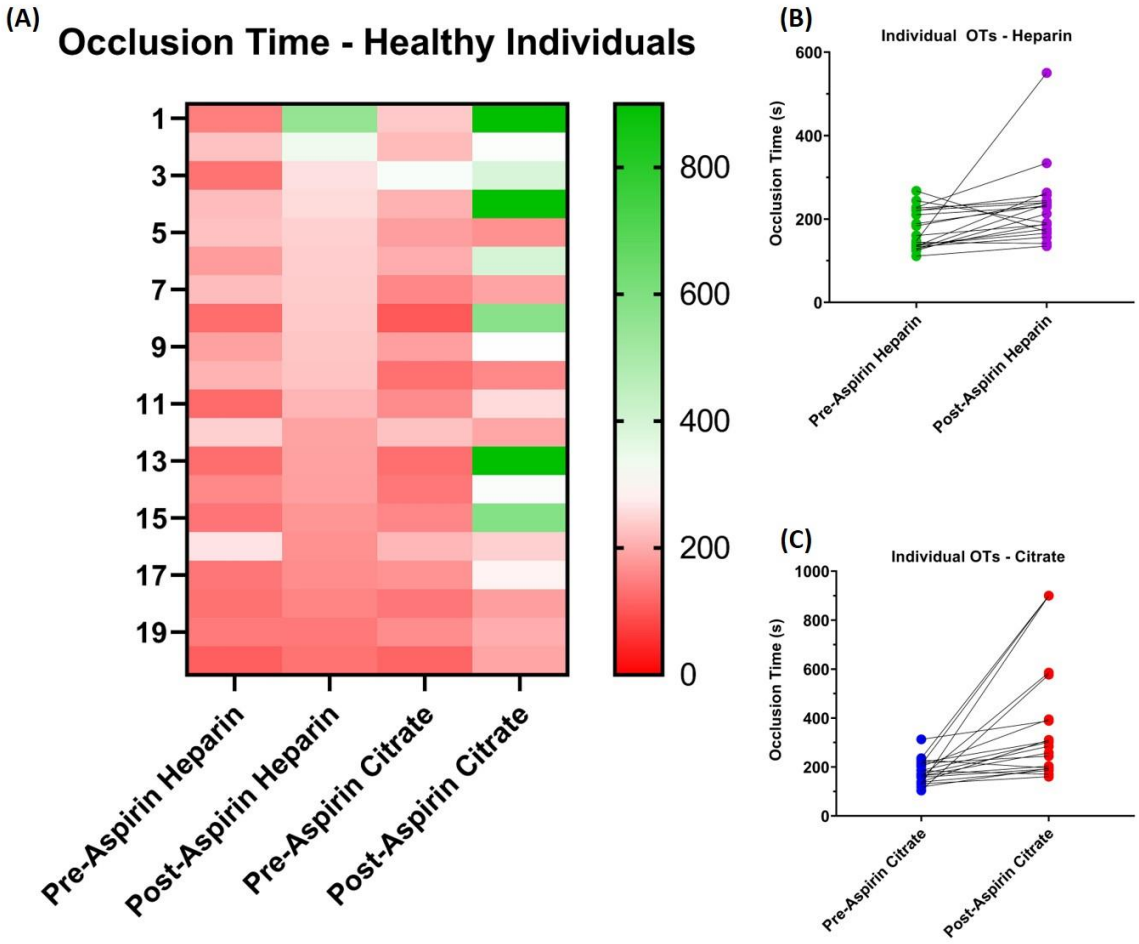

Figure 3-3. Summary of the individualized data week-long drug regimen characterization in the MTA. (A) Sorted by OT values of the Post-Aspirin Heparin (second column). Individual data of occlusion time pre- and post-aspirin (ASA) when collected in citrate or heparin vacutainers. Green indicates responsive to therapy, while red indicates non-responsive on the heat chart. Individual tracking of the OT data from pre-treatment to post-treatment when collected in (B) heparin and (C) citrate also indicates a general increase in OT on an individualized basis. Aspirin is found to have a significant effect on MTA OT for both heparin and citrate anticoagulated blood.

3.3.3 Aspirin responsiveness: MTA vs. GTT

16 cardiology patients undergoing an interventional catheterization procedure on aspirin as their only antiplatelet therapy were assessed with the MTA and GTT platelet function tests. The MTA reported an aspirin response in 3/20 (15%) individuals when collected in heparin tubes, shown in **Figure 3-4**. GTT reports both OT and LT during the same sampling of nonanticoagulated blood, with 12/20 (60%) aspirin responsive per GTT OT and 6/20 (30%) responsive per GTT LT, shown in **Figure 3-4**.

Correlations between the assay endpoints for patients on aspirin as the only antiplatelet agent were calculated using both the Cohen's Kappa test and Spearman Coefficient in **Table 3-1**. A mild correlation was found between the MTA heparin test and GTT OT. This is somewhat evident in the heat maps of **Figure 3-4**. The MTA heat map is sorted from most responsive (top) to least responsive (bottom) to therapy, and the corresponding samples are matched for the GTT OT and GTT LT heat maps. GTT OT has an obvious trend of green toward the top and red toward the bottom, and although not perfectly matching the MTA, it indicates a mild correlation per inter-rater correlation **Table 3-1**. The correlation between individual data points displayed in **Figure 3-5**, however, shows a significant correlation in the absolute values of the MTA and GTT OT endpoints ($\rho = 0.699$, $p < 0.001$). This indicates that a high OT determined by the MTA will likely have a high OT in the GTT, and vice versa. However, the agreement between the tests for the determination of drug responsiveness remains poor (**Table 3-1**). Poor correlations were found between GTT LT and both MTA and GTT OT.

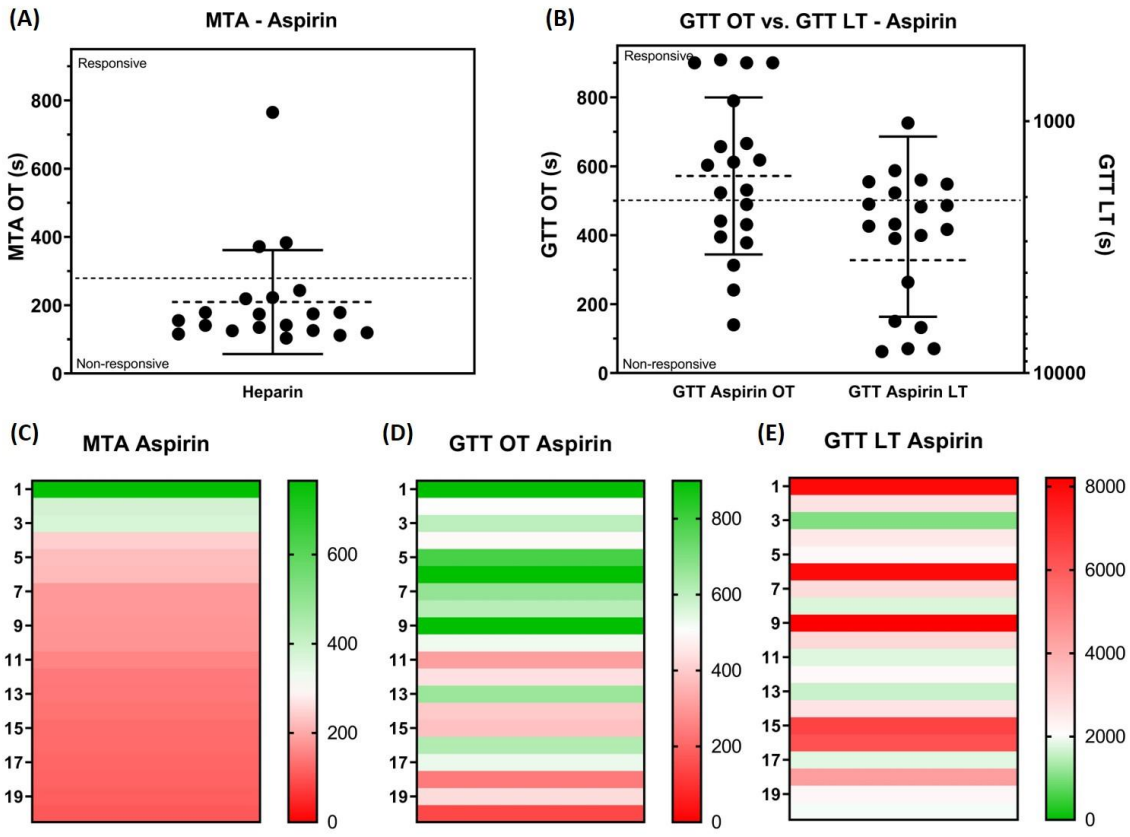

Figure 3-4. Summary of the platelet function test endpoint data for patients taking aspirin as their only antiplatelet therapy. (A) Population data for heparin anticoagulated blood characterized with the MTA. (B) Population data for OT and LT of nonanticoagulated blood characterized with the GTT. (C-E) Summary of the individual responses for the MTA and GTT, with dark green indicating strongly responsive to aspirin therapy and dark red indicating a strong resistance to aspirin therapy. Dotted lines across (A) and (B) indicate the cut-off for drug responsiveness per each metric, with data points above the dotted line indicating responsiveness.

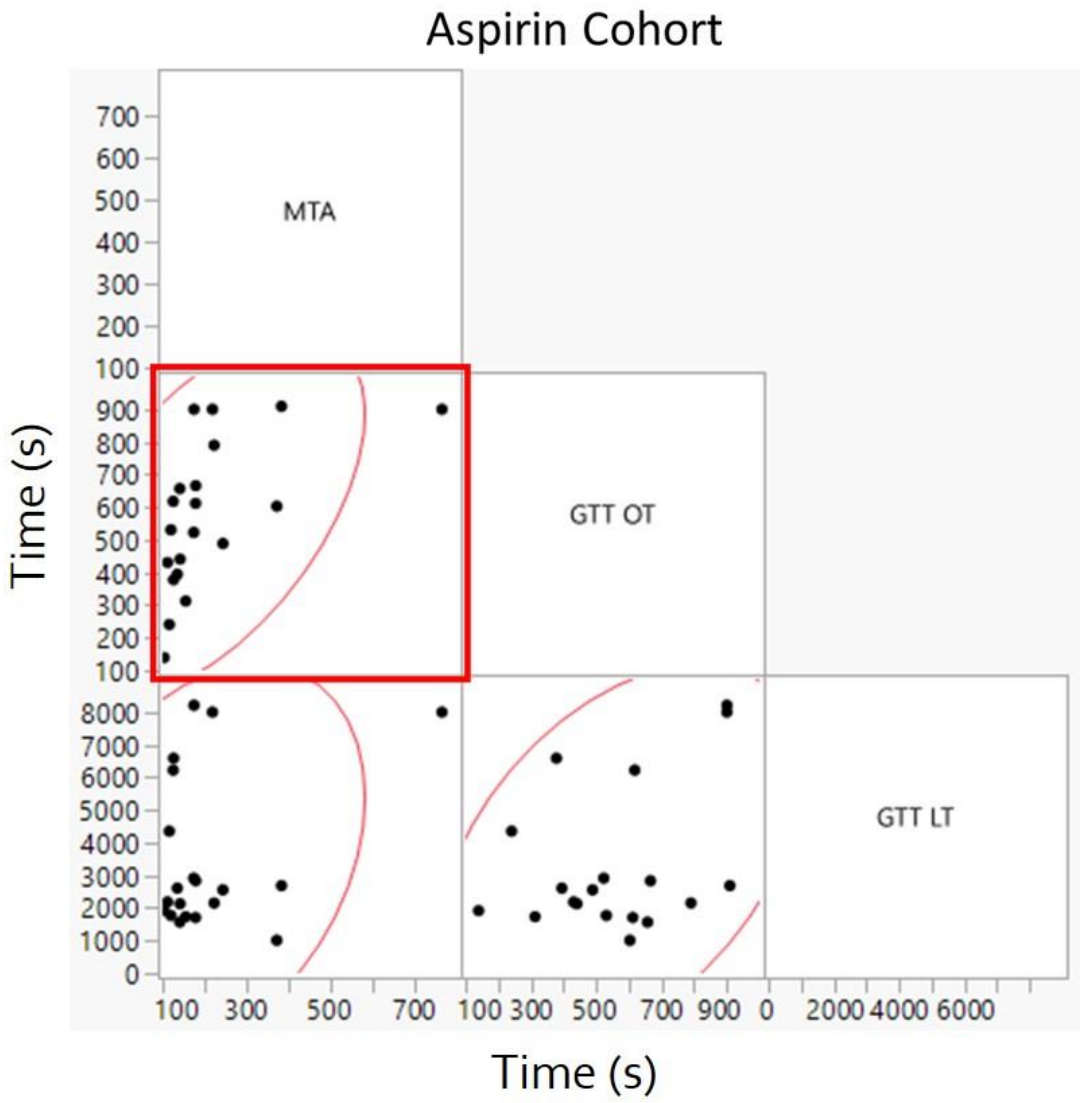

Figure 3-5. Correlation plots of the MTA, GTT OT, and GTT LT results from the patient group taking aspirin only. A significant correlation was observed between the MTA and GTT OT, which is highlighted in the red box. No significant correlations were observed between any other pairing. Red ellipses represent the 95% bivariate normal density confidence interval of the correlation, by enclosing approximately 95% of the data points. The narrowness of the ellipse reflects the degree of correlation of the variables.

Table 3-1. Cohen's Kappa statistic and Spearman Coefficient for agreement of aspirin responsiveness in MTA (N=20) and GTT (N=20) platelet function tests. (*p < 0.001).**

Cohen's Kappa (κ)	GTT OT	GTT LT
MTA Heparin	0.211	0.028
GTT OT	-	0.074
Spearman (ρ)	**GTT OT**	**GTT LT**
MTA Heparin	0.699***	0.103
GTT OT	-	0.297

3.3.4 Comparison of DAPT response in MTA, GTT, and VerifyNow

15 cardiology patients undergoing an interventional catheterization procedure on dual antiplatelet therapy of aspirin and Plavix were assessed with the MTA and GTT, while only 14 of those patients were assessed with the VerifyNow PRU platelet function test. The MTA reported a DAPT response in 3/15 (20%) of individuals, shown in **Figure 3-6A**. GTT reports both OT and LT during the same sampling of nonanticoagulated blood, with 12/15 (80%) DAPT responsive per GTT OT and 5/15 (33%) responsive per GTT LT, shown in **Figure 3-6B**. The VerifyNow PRU test was carried out in 14 of the 15 individuals and found 9/14 (64%) were responders to DAPT, shown in **Figure 3-6C**.

Correlations between the assay endpoints for patients on DAPT were calculated using both the Cohen's Kappa test and Spearman Coefficient in **Table 3-2**. No significant correlation per Spearman Coefficient was found between the MTA and GTT OT, which is different than the aspirin group above. However, a mild correlation was observed in the

inter-rater agreement of the Cohen's Kappa statistic for MTA and GTT OT. This is further evident in the heat maps, where the MTA DAPT is sorted from most responsive to therapy (top) to least responsive to therapy (bottom), and all other PFTs are sorted in the same patient order. The darker green readings for GTT OT are closer to the top, with the less responsive (albeit still light green) are toward the bottom. When comparing the MTA and GTT OT, the major difference between the two is the collagen coat vs. the lack of a pro-thrombotic surface, respectively. The discrepancy in responsiveness rates (MTA = 20%; GTT OT = 80%) may be a result of the coating difference. MTA did not have a significant correlation with either GTT LT nor VerifyNow. Interestingly, VerifyNow significantly correlated with GTT OT in the DAPT group per Spearman Coefficient ($\rho = -0.740$, $p < 0.01$). VerifyNow also had a significant inverse correlation with GTT LT ($\rho = -0.537$, $p < 0.05$).

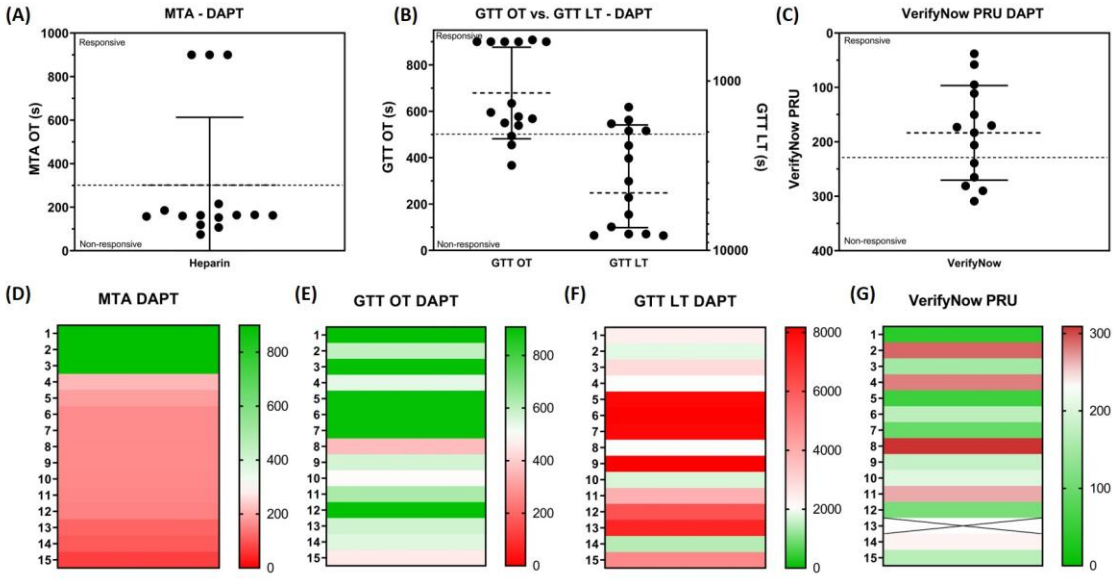

Figure 3-6. Summary of the platelet function test endpoint data for patients taking DAPT of aspirin and Plavix. Population data of characterization with the (A) MTA with heparin anticoagulation (300s cut-off), (B) GTT OT (500s cut-off) and LT (2000s cut-off) without anticoagulation, and (C) VerifyNow PRU test (235 PRU cut-off) with citrate anticoagulation. (D-G) Summary of the individual responses for the MTA, GTT, and VerifyNow, with dark green indicating strongly responsiveness to aspirin therapy and dark red indicating a strong resistance to aspirin therapy.

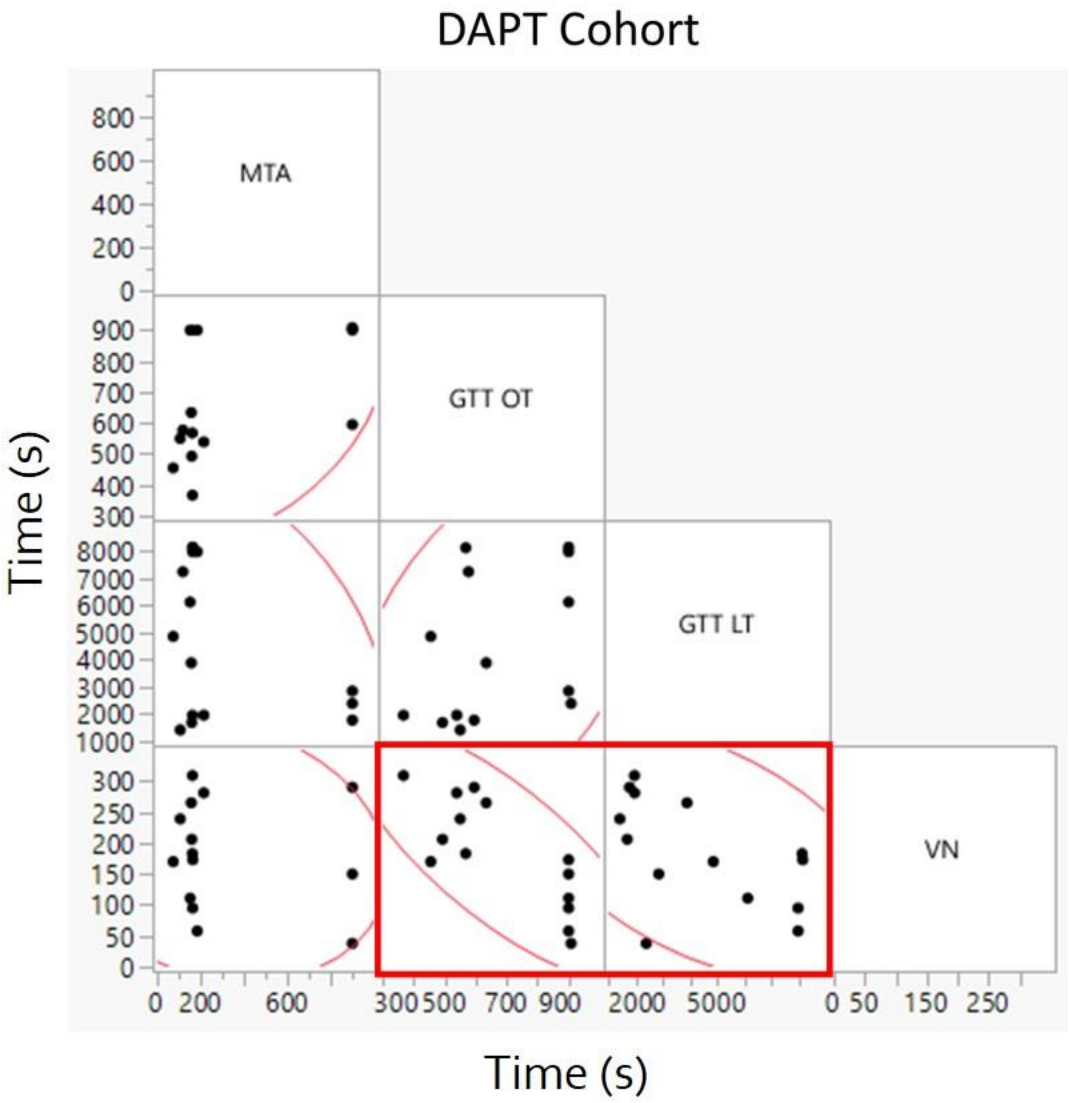

Figure 3-7. Correlation plots of the MTA, GTT OT, GTT LT, and VerifyNow results from the cardiology patient group taking DAPT. A significant correlation was observed between VN and GTT OT, while a significant inverse correlation was observed between VN and GTT LT. No significant correlations were observed between any other pairing, indicating that the values of the MTA do not correlate with either GTT nor VerifyNow for patients taking DAPT.

Table 3-2. Cohen's Kappa statistic and Spearman Coefficient for agreement of DAPT (aspirin and Plavix) responsiveness in MTA (N=15), GTT (N=15), and VerifyNow (N=14) platelet function tests. (*p < 0.05; **p < 0.01).

Cohen's Kappa (κ)	GTT OT	GTT LT	VerifyNow PRU
MTA Heparin	**0.118**	**0.000**	**0.018**
GTT OT	**-**	**-0.222**	**-0.024**
GTT LT	**-**	**-**	**-0.585**
Spearman (ρ)	**GTT OT**	**GTT LT**	**VerifyNow PRU**
MTA Heparin	**0.482**	**-0.036**	**-0.126**
GTT OT	**-**	**0.451**	**-0.740****
GTT LT	**-**	**-**	**-0.537***

3.3.5 MTA and CBC correlations

For all groups tested, no statistically significant correlations were found between PFT endpoints and CBC values. A summary of the average CBC data can be found in **Table 3-3.**

Table 3-3. CBC averages for pre- and post-aspirin healthy population (N=20) and both patient populations taking either aspirin (N=20) or DAPT (N=15). No statistically significant correlations were found between CBC values and PFT endpoints.

	Healthy Pre-Aspirin (N=20)	Healthy Post-Aspirin (N=20)	Patients Aspirin (N=20)	Patients DAPT (N=15)
WBC	5.15 ± 1.64	5.16 ± 1.55	7.02 ± 1.85	6.75 ± 2.33
RBC	4.92 ± 0.50	4.92 ± 0.52	4.34 ± 0.53	4.52 ± 0.79
HGB	15.1 ± 1.4	15.0 ± 1.2	12.6 ± 1.0	12.8 ± 2.3
HCT	42.9 ± 3.9	42.7 ± 3.8	37.7 ± 2.8	38.9 ± 6.6
MCV	87.5 ± 4.3	87.1 ± 4.0	87.9 ± 7.8	86.5 ± 5.8
MCH	30.6 ± 1.3	30.6 ± 1.4	29.2 ± 2.7	28.4 ± 2.1
MCHC	35.2 ± 1.6	35.1 ± 1.8	33.3 ± 0.5	32.9 ± 1.1
RDW	12.0 ± 1.2	11.9 ± 1.2	14.7 ± 1.2	15.1 ± 1.9
PLT	234.5 ± 43.0	232.5 ± 41.5	248.6 ± 67.7	238.4 ± 61.7
MPV	7.83 ± 1.50	7.83 ± 1.60	8.58 ± 0.67	8.42 ± 1.04

3.4 Discussion

This study evaluates the Microfluidic Thrombosis Assay (MTA) for measuring the effects of aspirin and DAPT on high shear thrombosis leading to occlusion. The MTA incorporates high shear rates similar to an arterial stenosis, and exposure of fibrillar collagen similar to a plaque cap rupture using whole blood from human subjects. The MTA demonstrates consistent patterns of occlusive thrombosis in normal subjects and patients with coronary heart disease. Aspirin was able to lengthen the occlusion time in a small subset of normal subjects (10%), but did not completely inhibit total occlusion in any subjects. This aspirin effect was similar in patients with cardiovascular disease (15%) and did not lead to complete inhibition in any subjects. Plavix plus aspirin (DAPT) lengthened the occlusion time in a larger subset of patients (20%) and effects with complete prevention of occlusion. These ratios of subjects benefiting from aspirin or DAPT is consistent with large scale clinical results.

The use of the MTA for formation of occluding thrombi is affected by the choice of an anti-coagulant to allow delayed testing. Heparin is a commonly used anti-coagulant that has its primary effect on the coagulation pathway [40]. Its effects on vWF-platelet adhesion should be minimal. Use of heparin led to the fastest occlusion times and the smallest intra- and inter-day variability by subject (~11-14%). Citrate is widely used for platelet studies, but is known to affect platelet adhesion, aggregation, and activation [40, 51]. Here, citrate led to greater variability and differences in shear induced occlusion from heparin. The results also indicated that citrate potentiates the effects of aspirin and Plavix on subject responsiveness with a possible worsening of specificity of effectiveness. Thus, we do not recommend use of citrate for assays of high shear thrombosis.

The MTA results can be compared against the VerifyNow. The MTA showed DAPT responsiveness in 3/15 (20%) while VerifyNow showed effectiveness in 9/14 (64%). Two of the patients overlapped in effectiveness. Comparison against VerifyNow cutoffs for aspirin effectiveness measures show poor statistical correlation indicating that the two devices assay for different effects.

The MTA results can be compared against the newer Global Thrombus Test (GTT) assays of occlusion time and lysis time. The GTT exhibited prolonged occlusion times from DAPT in 13/15 (86%) while Lysis Time was shorter for 12/15 (80%). This is quite a different result from the GT-MTA with correspondingly poor correlation. Thus, the MTA is clearly measuring different thrombotic mechanisms than the GTT. The occlusion times by MTA with collagen are significantly shorter than GTT with ceramic and plastic surfaces, even though the shear rate ranges are comparable. This highlights the necessity of including both high shear *and* collagen to mimic arterial thrombotic occlusions.

3.4.1 MTA aspirin specificity

Within the healthy population that was tracked before and after week-long aspirin therapy, the MTA shows that post-aspirin occlusion times are statistically longer than pre-aspirin. This demonstrates that aspirin therapy does have an impact on high shear thrombus formation. However, this effect is strongly affected by the sample preparation. The findings indicate the influence of the choice of anticoagulants. The aspirin response in the healthy patient population was found to be significantly different in the MTA when whole blood was treated with sodium citrate (50% response rate) vs. heparin (10% response rate). Additionally, 3/20 (15%) of normal controls tested did not develop an occlusive clot during

the study with a 15-minute endpoint when the blood was treated with sodium citrate, while all controls developed an occlusive clot when blood was treated with unfractionated heparin. This suggests that sodium citrate has a strong effect on platelet function, which is aligned with the interpretation that has been presented in previous literature that platelet membrane protein $\alpha_{IIb}\beta_3$ is irreversibly altered upon citrate administration [40, 95]. While the healthy population pre-aspirin data indicates no significant difference between citrate and heparin, there may be a compounding factor in citrate/aspirin interactions in preventing platelet adhesion, activation, or accumulation that would explain the significant difference in the outcomes of the two anticoagulants post-aspirin. This finding is of significance because the two major platelet function tests utilized, VerifyNow and PFA-100, both use sodium citrate as an anticoagulant. We have previously mentioned that the current PFTs are not designed with the relevant factors for arterial thrombosis, such as high shear and collagen surfaces, but now we suggest they also may not be using an appropriate anticoagulant in their assessment [48].

When looking at recent clinical results of the ASPREE and ARRIVE studies tracking the clinical outcomes of aspirin use on prevention of major adverse cardiovascular events (MACE), it is shown that aspirin does not significantly change outcomes over placebo in primary prevention [18-21]. The results presented herein of the MTA with heparinized blood may provide support to why aspirin is not useful in the prevention of MACE. Although OT was found to be delayed significantly on a population basis, every individual still developed an occlusive clot under high shear conditions. This would indicate that if an atherosclerotic injury is present in vivo, a clot will likely still develop even if aspirin is used. When looking at studies of VerifyNow for assessing aspirin

effectiveness with the Aspirin Response Units (ARU) test, aspirin was found to have a 100% response in individuals [96]. This indicates that the MTA design may be better suited for assessing antiplatelet function than VerifyNow.

3.4.2 MTA OTs in healthy and patient populations

Comparing the MTA OT data for both the healthy individuals and patients only on aspirin antiplatelet therapy, there was no significant difference in the population averages. The average OT for the healthy individuals was 227.4s (N=20), while the average OT for the patients taking aspirin was 209.3s (N = 20). These two averages are not significantly different from one another ($p = 0.649$), indicating that clotting times are similar across healthy and "at risk" populations. Therefore, the patient group is not more "at risk" for a cardiovascular event due to their blood biochemistry, but rather another underlying factor such as grade of atherosclerotic injury would make them more "at risk".

3.4.3 MTA and GTT OT correlation

Comparisons of the MTA to GTT OT showed a significant correlation in the patient population taking aspirin only. The major similarity between the two assays (other than the endpoint of OT) is the fact that they both incorporate high shear rates > 10,000 s^{-1}. Therefore, they are both using biophysical high shear flow to induce platelet aggregation, which is one of the major causes of arterial thrombosis. However, two other major factors differ between the tests: methods of anticoagulation (heparin vs. nonanticoagulated) and thrombotic agonists (collagen vs. ceramic). These differences may account for why the correlation between assay endpoints was no longer significant in the DAPT group, where the MTA was more sensitive to DAPT in its OT endpoint. We argue that the MTA

accurately simulates the formation of a platelet-rich arterial clot, as the system is designed with all three causes of arterial thrombosis in mind: high shear, pro-thrombotic collagen surface, and vWF/platelets. In addition, the use of heparin anticoagulation prevents the formation of fibrin-rich blood clots from the coagulation cascade. The GTT OT, however, does not utilize anticoagulation and may be forming fibrin-rich clots in the recirculation zones of the flow channel as a result, but this cannot be verified due to lack of clot visualization in the tool. However, it is possible that if the GTT were modified to incorporate collagen coating and heparin, the MTA and GTT OT may become nearly identical tests and correlate strongly for all therapy groups.

3.4.4 VerifyNow Correlations with GTT

As expected due to the lack of major arterial thrombosis causes of high shear flow and non-physiological agonists, VerifyNow had very poor correlation with both the MTA OT endpoint. However, as mentioned previously in the results, VerifyNow did exhibit significant correlation with GTT OT for DAPT patients. This is a peculiar finding, as they are very different methods for testing platelet function. GTT OT utilizes high shear flow, while VerifyNow mixes blood samples at very low shear. In addition, much of the argument for GTT OT is that it does not utilize an anticoagulant, thereby testing fresh native whole blood. VerifyNow, on the other hand, uses citrate anticoagulation, which has been suggested in this thesis and by other research groups to impact platelet function irreversibly [51, 52]. One potential explanation is that both tests may be better suited for tested fibrin clotting events, as the GTT group has shown large amounts of fibrin formation on the surfaces of these clots and VerifyNow tests in the low shear regime more suitable for fibrin-rich clots [90]. Additionally, VerifyNow was found to inversely correlate with

the GTT LT metric. Lower VerifyNow values (indicating antiplatelet responsiveness) correlated with higher GTT LT values (indicating lack of thrombolytic activity), showing further disagreement between PFT methods.

3.4.5 Testing antiplatelet in vivo vs. in vitro

In a previous study from our laboratory, aspirin was administered in vitro into blood samples and assessed in the "milli-fluidic" MTA model previously described [7]. The results of that study showed that addition of aspirin across multiple doses ranging from 0 to 2.0 mM in whole blood did not significantly change the OT in 5 samples at a shear rate of 10,000 s^{-1}. While the OT of the milli-fluidic was higher at the dose of 2.0 mM than at baseline, it was not statistically different. This is similar to the assessment presented here of testing aspirin after ingestion, as the OT of the MTA was not drastically different than the baseline pre-aspirin value and was only statistically different for the population due to the higher sample size (N = 20). The same likely cannot be said for Plavix or other antiplatelets that must undergo a very complex metabolic pathway to become an active drug. In those cases, an in vivo assessment will likely be needed over in vitro administration of the drug. However, this comparison of aspirin results indicates that in vitro assessments with the MTA may do a suitable job in reflecting how the therapy may perform in vivo.

3.4.6 Limitations and future directions

The primary limitation of this study is the small sample sizes in both healthy and patient groups. These sample sizes may have limited the power of correlation calculations between assays and CBC levels, although CBC levels alone should not dictate antiplatelet regimens on an individualized basis. Additionally, having a small sample opens the study

to sampling bias and not be representative of a larger population. Another limitation of this study is the potential for poor drug compliance, particularly in the patient population that was studied. While more checks were in place to determine drug compliance in the healthy group taking aspirin, the only check for the patient groups taking aspirin or DAPT was verbal confirmation prior to drawing blood. This, however, is a limitation of most drug related studies as drug compliance is a major issue not only in research but also in the clinical setting. Finally, effects of Plavix alone were not able to be assessed in this study as all patients taking Plavix were also taking aspirin (DAPT). Therefore, all outcomes from PFTs in the DAPT group cannot be assumed to be the effects of Plavix alone, but rather potentially synergistic effects of aspirin and Plavix therapy.

There are a few future directions for this work. The next step for this research would be to plan and initiate a larger clinical study with follow-up to determine the MTA's ability to predict MACE in a patient population. Another "lower hanging fruit" study that may be useful to complete is to make modifications to the GTT to incorporate collagen coatings and heparin may essentially mimic the MTA. It would be interesting to make those modifications and compare the two tests again to see if a stronger correlation exists.

3.5 Conclusion

In summary, the MTA is a rapid assay (<10 min) that requires a small amount of whole blood (< 5ml) to create clots in microfluidic channels. The assay can be utilized to assess patient propensity to thrombotic occlusion while being treated with aspirin or DAPT. The MTA is a functional assay that is significantly different from VerifyNow and GTT that show poor correlation to the MTA or clinical antiplatelet effectiveness. The results further

demonstrate that citrate may be a poor choice for preserving specimens for later testing of high shear thrombosis. Heparin can maintain liquid whole blood with minimal effects on SIPA. Future larger-scale clinical studies may demonstrate the MTA's ability to predict MACE in a patient population.

CHAPTER 4. ANTITHROMBOTIC THERAPY BY CHARGED NANOPARTICLES

Results detailed in this chapter regarding CNP in porcine whole blood have been reported in BioMicrofluidics [76].

Abstract

Platelet accumulation under high shear rates at the site of atherosclerotic plaque rupture leads to myocardial infarction and stroke. Current antiplatelet therapies remain ineffective for a large percentage of the population, while presenting significant risks for bleeding. We explore a novel way to inhibit arterial thrombus formation. Theoretically, a negative charge may influence the tertiary structure of vWF to favor the globular configuration by biophysical means without the use of platelet inactivating drugs. We tested this hypothesis experimentally for negatively charged nanoparticles (CNP) to inhibit arterial thrombus formation in a microfluidic thrombosis assay (MTA). Several different CNPs demonstrated the ability to inhibit or retard thrombotic occlusion in a laboratory microfluidics model that has been validated by clinical arterial thrombosis testing. Our hypothesis that particle charge and size matter for antithrombotic CNP is proven. Further, the effect is present with particles of widely varying base compositions, indicating that biochemical effects are not dominant. A preliminary study of safety in mice shows that bleeding times are not markedly prolonged. The CNPs tested here show promise as a new class of antithrombotic therapies that act by biophysical means rather than biochemical pathways.

4.1 Introduction

4.1.1 Current antithrombotic methods

The main target of current antithrombotic therapies for high shear thrombosis is platelet activation. Therapies utilized for this end have been termed more specifically antiplatelet drugs. The most commonly utilized antiplatelet is aspirin, which is prescribed nearly universally by cardiologists [18, 97]. Aspirin may act as an antiplatelet agent by irreversibly inhibiting cyclooxygenase-1 (COX-1) function, thereby interrupting thromboxane (TXA_2) action that normally induces platelet aggregates [81]. However, confidence in aspirin as an antiplatelet agent has greatly diminished with the recent clinical results in the ASPREE (randomized and blinded; n = 19,114) and ARRIVE (randomized and double blinded; n = 12,546) trials [18-21]. The primary endpoint of each trial was the occurrence of cardiovascular death, myocardial infarction, unstable angina, stroke, or transient ischemic attack. The outcomes of myocardial infarction, stroke, and ischemic attack all result from thrombotic events. Both trials indicated no significant difference in the occurrence of major adverse cardiovascular events (MACE) between individuals taking aspirin or placebo treatment. The ASPREE trial showed that death related to cardiovascular disease was comparable between aspirin (1.0%) and placebo (1.2%) groups [19, 20]. The ARRIVE trial showed that the occurrence of MACE was similar between both aspirin (4.3%) and placebo (4.5%) groups, as well.

The same trials also showed a significant increase in the incidence of major bleeding associated with aspirin use. The ASPREE trial explored bleeding safety endpoints of major hemorrhagic bleeding, with an incidence of 8.6 events per 1000 person years in the aspirin group and 6.2 events per 1000 person years in the placebo group ($p < 0.001$) [20]. Meanwhile, the ARRIVE trial investigated rates of intestinal bleeding, with 0.97% of

patients on aspirin experiencing gastrointestinal bleeding complications compared to 0.46% of individuals in the placebo group ($p < 0.001$) [21]. Therefore, aspirin is likely doing more harm than good in most patients, leading clinicians to start recommending to discontinue aspirin use [18].

Other clinically used therapies, such as clopidogrel, abciximab, eptifibatide, and PAR-1 antagonists (vorapaxar and atopaxar), aim to inhibit platelet activation and interaction with proteins such as vWF and thrombin (**Figure 4-1**) [24, 25, 86, 98, 99]. However, multiple studies found that these drugs do not reduce the rates of mortality in patients [98, 99]. Specifically, clopidogrel was investigated similarly to aspirin in the "clopidogrel versus aspirin in patients at risk of ischemic events" (CAPRIE) and "Clopidogrel and metoprolol in myocardial infarction trial" (COMMIT) trials [100, 101]. The CAPRIE study is a blinded, randomized trial of 19,185 patients taking either aspirin or DAPT. The rate of MACE in patients taking aspirin alone was 5.83%, which was significantly reduced to 5.32% in individuals taking DAPT ($p = 0.043$) [100]. The COMMIT trial investigated clopidogrel against placebo in a blinded, randomized study of 45,852 patients. Clopidogrel was found to significantly reduce MACE occurrence from 10.1% in the placebo group to 9.2% in the clopidogrel group ($p < 0.01$) [101]. While both studies found statistical significance between groups, the reduction in MACE rates was a fraction of either the aspirin or placebo group. Both studies show that over 90% of individuals that would experience MACE in the non-clopidogrel group will still experience MACE when adding clopidogrel therapy. Therefore, from a clinical perspective current therapies are not significantly pushing the needle, and more effective therapies are still needed.

Prior to undertaking these large clinical studies (ASPREE, ARRIVE, CAPRIE, and COMMIT) that take several years to complete (5-9 years) and large amounts of funding, preclinical investigations are required. Per the FDA approval report, the preclinical investigations for safety and efficacy of clopidogrel made use of several animal models: mice, rats, guinea pigs, baboons, and dogs. However, the scientific community has placed an emphasis on finding methodologies that can reduce, refine, or replace the animals used in preclinical research [102]. Therefore, *in vitro* assessments for drugs and therapies are being developed to replace animals for a large percentage of preliminary assessments [102]. By leveraging these *in vitro* technologies as high throughput screening systems, significant reductions in drug development costs can be achieved and faster characterizations may be accomplished [103].

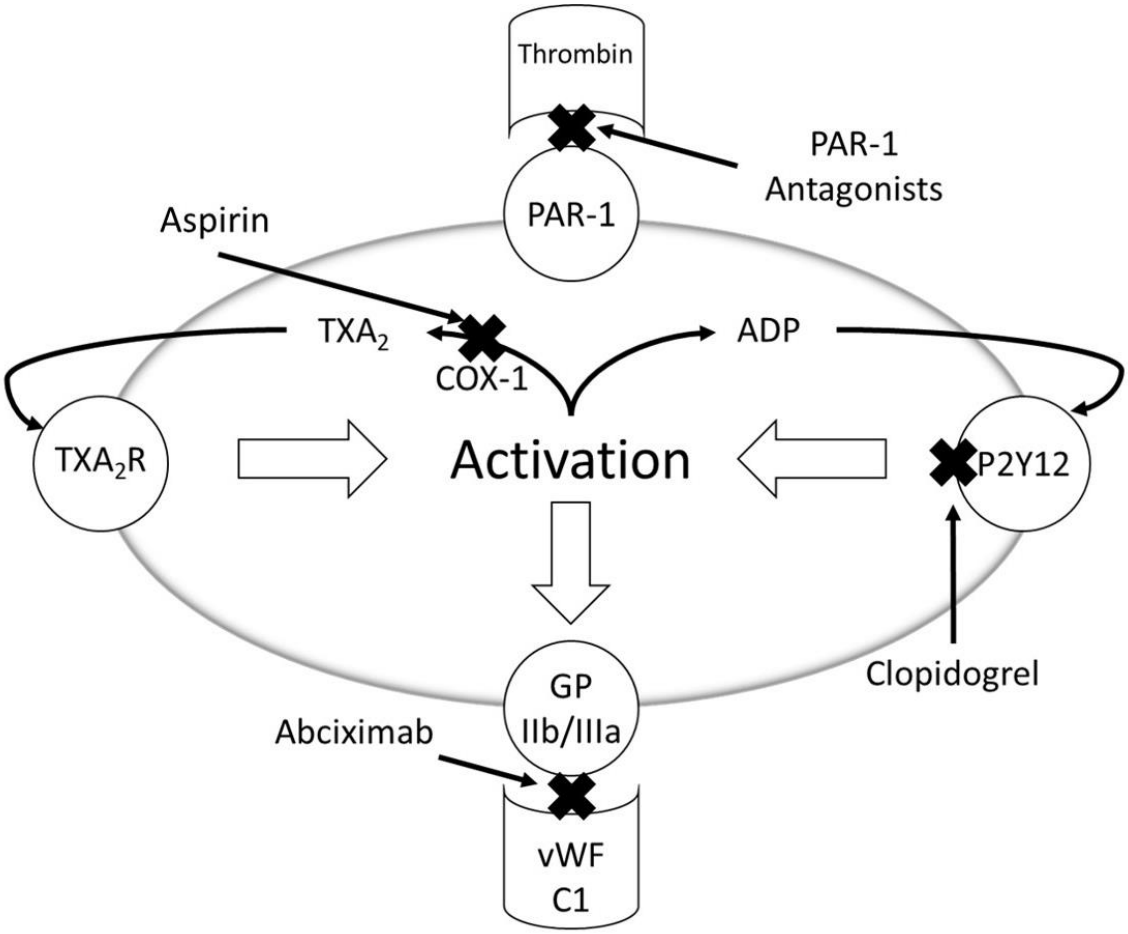

Figure 4-1. Depiction of antiplatelet mechanisms of action for irreversible inactivation (Aspirin and Clopidogrel) or protein receptor inhibition that aim to prevent platelet adhesion events to proteins (Abciximab and PAR-1 antagonists).

4.1.2 Issues with targeting platelet activation

Currently utilized therapeutic methods for targeting platelet activation have serious drawbacks. In some instances, the drug is not able to be metabolized properly due to the individual lacking the necessary enzyme, such as the CYP2C19 gene for metabolism of clopidogrel [104, 105]. Further, bleeding complications arise due to the irreversible inactivation of platelets, leading to platelets circulating in a dummy-like state unable to activate in normal hemostatic processes [20, 87]. These side effects/safety issues will

continue to arise if antiplatelet therapies are continually designed to act through irreversible biochemical inhibition. Therefore, a fundamentally new approach may prove superior in the prevention of arterial thrombosis.

4.1.3 Nanoparticles for biophysical interactions

There are several requirements for arterial platelet thrombosis, including vWF unfolding under high shear, vWF adhesion to a collagen surface, activation-independent platelet adhesion to vWF, and platelet activation leading to rapid platelet accumulation. While a majority of current therapies target the latter, interfering with any of these stages in the process would prevent or inhibit the formation of an arterial thrombus. The initial stage of high shear platelet thrombus formation is vWF unfolding under flow and is therefore an interesting candidate target that warrants investigation. Preventing vWF unfolding under flow, thereby maintaining its globular state, would limit the amount of vWF binding to collagen. This in turn could inhibit the subsequent stages of arterial platelet thrombosis, without altering internal mechanisms of platelet activation that are necessary for healthy hemostatic processes.

Such interactions may include electrostatic protein interactions with biomaterials, thereby changing protein conformations temporarily while that interaction persists [106-108]. Nanoparticles present a feasible option to promote these protein-biomaterial interactions, as it is well known that a plasma protein corona forms around the surface of the nanoparticle after entering the blood stream [109]. If multiple nanoparticle materials effectively inhibit thrombotic formation, it would be indicative of a mechanism that is not dependent on individual material biochemical interactions with blood components. Rather,

interactions would be more likely due to general physical characteristics of the nanoparticle, such as size and charge.

4.1.4 Nanoparticles for biomedical applications

Three nanoparticle materials that have been commonly utilized in biomedical applications are polystyrene, PLGA, and gold. Polystyrene (PS) is a biocompatible material that is not biodegradable. This material has been utilized in nanoparticle applications of biosensors, photonics, and self-assembled nanostructures [110, 111]. It is considered an easy material to work with and sterilize for biomedical applications; therefore, it is often used as a model material for nanoparticle investigations.

Poly(lactide-co-glycolide) (PLGA) is an attractive material for nanotherapeutic applications as it combines favorable properties of biocompatibility and biodegradability [112-116]. Further, PLGA particles carry a distinct advantage as they have already been approved by the FDA as vehicles for drug delivery [117]. PLGA has been utilized extensively in drug delivery applications because of its biodegradation allowing for sustained release of the drug of interest [118, 119]. The degradation takes the form of PLGA hydrolytically breaking down to lactic and glycolic acid that are, in turn, metabolized via the Krebs' cycle and eliminated as carbon dioxide and water [117, 120]. Therefore, PLGA has been utilized extensively in biomedical applications such as vaccination and treatment of cancer, inflammatory diseases, or cerebral diseases [118]. However, PLGA nanoparticles for biophysical interactions have not been explored and thus present a new therapeutic option by which PLGA based particles may be utilized.

Finally, gold has also been utilized in bioacoustics, DNA sensors, and bioconjugation for drug delivery applications [121]. It is an attractive material for biological applications of nanoparticles due to its stability and biocompatibility. Gold nanoparticles are also very easy to synthesize and conjugate with other biomolecules, making them adaptable to many biological applications [122]. Like PS and PLGA nanoparticles, gold nanoparticles have few to no applications in biophysical applications and therapeutics, therefore there are unexplored applications for this base material.

Nanoparticles in systemic circulation.

One of the difficulties with utilizing nanoparticles in vivo is that they are rapidly cleared from the blood stream via opsonization by the mononuclear phagocyte system (MPS). This drastically decreases the efficacy of particles if the target is anything other than the mononuclear phagocyte system (MPS). Additionally, for biostable materials such as PS and gold, this creates issues of liver and spleen toxicity over time as these organs cannot break down the material. Therefore, targeted renal clearance is required for such particles. Surface modifications to a polystyrene and gold nanoparticles with thiol mediated binding of a polymer such as PEG have been utilized previously to decrease biodistribution to the liver and spleen to alleviate this issue [123].

The reason for the rapid clearance of PLGA particles from the systemic circulation is due to the hydrophobic nature of the PLGA [118]. This has been alleviated in part due to advancements in surface coatings of the PLGA base material. Two general methods have shown a significant increase in circulation time. One is through the use of a PLGA-PEG block co-polymer [120, 124, 125]. Through an oil/water (o/w) emulsion synthesis with

PLGA-PEG block co-polymer, particles with a PLGA base and PEG surface may be fabricated. While these particles have shown significant increases in circulation time, they are termed “stealth particles” due to PEG coatings having decreased interactions with biomolecules and proteins [125]. Another method for increasing circulation time is through nanoprecipitation synthesis of PLGA with a PVA surfactant [126]. Excess PVA in the aqueous phase of the synthesis process interacts with the PLGA particle surface and remains there as a stabilizer. The resulting particle has increased hydrophilicity due to the PVA coating, therefore increasing the circulation time of the particle. Higher PVA concentrations and molecular weights enhance this effect. Therefore, simple modifications to the synthesis process may increase particle circulation time.

Tuning the size of nanoparticles.

Selection of a suitable nanofabrication method is critical to achieve desired sizes during synthesis. Polystyrene nanoparticles are most often fabricated by emulsion polymerization, with sizes being altered by changing the polymeric concentration in solution and temperature [127]. The three most common methods for polymeric nanoparticle synthesis are double emulsion, nanoprecipitation, and spray drying. Double emulsion and spray drying techniques typically lead to the production of larger PLGA nanoparticles greater than 200 nm [126, 128]. Nanoprecipitation allows for greater size control at lower diameters by altering the polymer concentration and synthesis temperature [126]. By increasing the batching temperature of the aqueous phase close to boiling and decreasing the PLGA concentration in the organic phase, particles smaller than 100 nm may be fabricated, while larger particles are fabricated through the reverse properties.

Nanoprecipitation, therefore, presents an easy to use methodology for fabricating PLGA particle sizes in the 50 to 200 nm range.

Fabrication of gold nanoparticles is typically done through reduction of gold ions with sodium citrate in aqueous solution. By tuning the ratio of gold to citrate ions, the size of the particle can be controlled. More citrate ions leads to more rapid and stronger stabilization of the gold in solution, creating smaller gold nanoparticles, and vice versa [129]. Additionally, the size of the particles can be altered by batching temperature, with increases in temperature leading to smaller particle formulations [129]. Sizes can be tuned in the 1 to 100 nm range [130, 131].

The effects of nanoparticle charge.

The surface charge, or zeta potential, also carries a significant role in the design of nanoparticles for biomedical applications. Several studies have shown that positively charged nanoparticles are opsonized more rapidly than negatively charged particles, likely due to the net negative charge of amino acid residues on the surfaces of circulating cells [119, 132]. Positively charged PS nanoparticles were found to enhance platelet aggregation over neutrally and negatively charged particles [106]. Further, positively charged PLGA particles induced an increased cytotoxic effect, while negatively and neutrally charged PLGA particles had no such effect [132]. The surface charge can be altered through the use of different surfactants or surface modifications to the nanoparticle base material [133]. Surfactants such as PVA create negatively charged surfaces. More neutrally charged particles may be achieved through PEG surface modification, which can then be subsequently altered by capping the PEG with different end groups.

4.1.5 Objectives and hypothesis

In order to study the effects of charged nanoparticles on thrombotic inhibition, we employed two thrombosis models: the microfluidic thrombosis assay (MTA) for *in vitro* screening and a murine carotid stenosis *in vivo* model. The MTA was utilized to screen for the effects of nanoparticle size, surface charge, and blood concentration with easy to use polystyrene particles. From the MTA, we will be able to identify the most effective nanoparticle parameters in order to translate into a biocompatible nanoparticle synthesis scheme that will also be assessed with the MTA. The most effective particle will also be further characterized in the *in vivo* murine tail bleeding model. I hypothesize that a nanoparticle on the same order of size of a vWF monomeric unit (50-60 nm) and matching negative charge (~ -50 mV) will provide a strong and repeatable antithrombotic response.

4.2 Preliminary CFD Results

Collaboration with Dr. Cyrus Aidun's research group for computational fluid dynamics analysis aided in the design and development of the experimental hypotheses and methods [76, 134]. The supporting computational methods and results are reported in this section.

4.2.1 Computational Methods

We developed and validated the application of the lattice-Boltzmann (LB) method for direct numerical simulation (DNS) of dense suspension of particles in viscous flow [135-138], deformable capsules [139, 140], and cellular blood flow [141]. A multiscale computation approach has been developed where the CNP and vWF are modeled with a

Langevin dynamics (LD) approach fully integrated and coupled with the LB method (LB-LD) [134, 142]. The vWF is modeled as a chain of N beads (each representing a dimer) as done in many previous studies [143-147]. The total force on the particle or bead in LD consists of hydrodynamic, Brownian and non-hydrodynamic forces which include any external body forces, such as the Lennard-Jones (LJ) potential (employed for attraction force between monomers) and electrostatic forces. The electrostatic force is modeled by a Coulomb potential as an effective pair potential that describes the interaction between two point-charges. The connectivity force between neighboring vWF monomers is modeled through a finitely extensible nonlinear elastic (FENE) spring potential, U_s [146, 148]. The same LD approach is applied to charged nanoscale particles with $U_s = 0$. The LD method for modeling the vWF and CNP has been extensively validated including modeling the vWF transition from globular to elongated phase at the critical shear rate [13, 134, 142, 145, 146].

Electrostatic interactions with vWF are induced because of large patches of positive charge at the A1 interface. Although the electrostatic charge is not constant, it can be estimated to be about on average 6 to 10 kT/e (150 to 250 mV) [149]. In our simulations, we take an average of +8 kT/e for the A1 domain implemented as a point charge in each dimer. Modeling the charge of the A1 domain as a point particle in each dimer is an assumption that requires further experimental verification. The average charge of CNP for the simulations is -50 mV [150].

4.2.2 Computational Results

The conformational dynamics and motion of vWF proteins were simulated using the LB-LD method outlined above. The natural vWF exhibits periodic stretching, tumbling and folding events under linear shear flow (**Figure 4-2A**). Without the CNP, the vWF re-elongates frequently, going through periodic cycles of stretching and relaxation. The patterns of elongation in **Figure 4-2A** are representative of the elongation and folding model described previously in Schneider et al [13]. These patterns form independently of initial conditions.

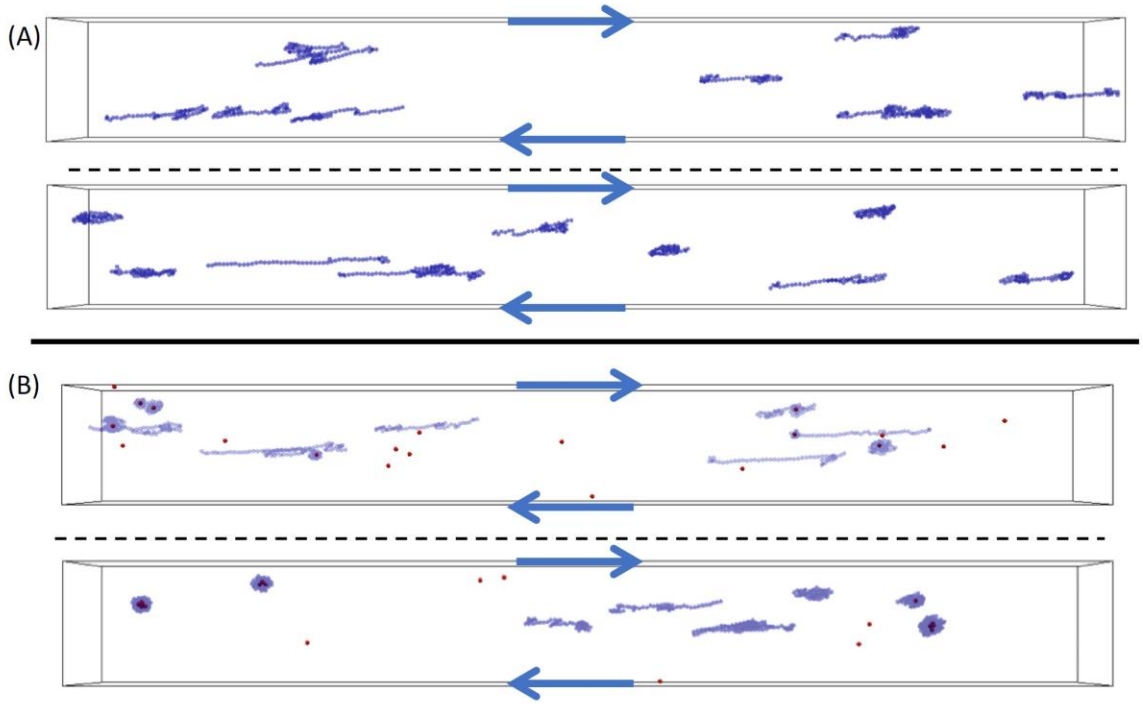

Figure 4-2. (A) vWF (blue) without CNP in shear flow (6500 s^{-1}) with arrows indicating flow direction. vWF undergoes dynamic elongation and folding, but does not remain in a stable globular shape under high shear as indicated by the two screenshots above. (B) vWF (blue) immersed in experimental concentrations of CNP (red) in shear flow (6500 s^{-1}) with arrows indicating flow direction. vWF polymers

fold back into globular form (dense balls) after interaction with CNP, and remain in the globular conformation under the same shear rate [76].

Electrostatic attraction by charged particles was introduced to counteract the elongation of vWF from drag forces of high shear stress. The vWF-CNP interaction simulations demonstrate that CNP have a demonstrable effect on conformation of vWF under shear flow conditions. In the simulation, there are 20 CNP and 10 vWF proteins each consisting of 50 dimers. A ratio of two CNPs available per vWF filament was chosen to match the relative CNP:vWF concentration used in experiments. The addition of negatively charged CNP radically altered the behavior of the vWF in high shear flows.

Figure 4-2B illustrates the interaction of CNP (red) and vWF (blue) in a constant shear flow of 6500 s^{-1}. The elongated vWF wraps the charged CNP into the interior of the coiled form, stabilizing this conformation. When the simulation reaches dynamic equilibrium, each coiled vWF (6 out of 10 in the bottom snapshot, 2 strands have self-associated) contains one or more CNP. The vWF-CNP compound maintains the globular conformation and does not elongate again at this shear rate. The vWF-CNP effective length, i.e. the projected length in flow direction, drops by more than 2/3 to less than 30% of its maximum length, suggesting a significant drop in capture power of vWF or a lengthening of occlusion time when CNP are mixed in blood. The failure of vWF-CNP to elongate would be expected to severely reduce the ability of vWF to capture platelets under high shear rate conditions.

The computational simulation was then used to assess the importance of charge sign. The model predicts that CNP with a neutral or positive charge would not hinder the

elongation of vWF nor would it induce a preferred globular form of vWF. Only the negatively charged nanoparticle is predicted to have an effect on vWF elongation and, subsequently, less thrombosis.

4.3 Experimental Methods

4.3.1 Materials

Polydimethylsiloxane (PDMS) was from Krayden, Inc. (Denver, CO, USA). Type I collagen was from Chrono-Log (Havertown, PA, USA). Resomer 50:50 (PLGA) was purchased from Sigma Aldrich (St. Louis, MO, USA). Polyvinyl alcohol was purchased from Sigma Aldrich (St. Louis, MO, USA). PEG-thiols with either carboxyl or methyl end groups were purchased from Sigma Aldrich (St. Louis, MO, USA). HAuCl4 was purchased from Sigma Aldrich (St. Louis, MO, USA). Calcein AM was purchased from BD Biosciences (San Jose, CA, USA). Unfractionated sodium heparin was purchased Fisher Scientific (Hampton, NH, USA).

Testing of the microfluidic thrombosis assay (MTA) was performed on a Leica DM6000B microscope from Leica Microsystems, Inc. (Buffalo Grove, IL, USA), along with Scout SPX222 balances from OHAUS Corporation (Parsippany, NJ, USA) for mass flow rate detection and a high-resolution CCD PixelFly camera from PCO (Kelheim, Germany) for image acquisition.

4.3.2 Nanoparticle synthesis and characterization

Polystyrene, poly lactic-co-glycolic acid, and gold nanoparticles were utilized in this study. 50-60 nm and 200 nm polystyrene particles with no modification (PS-CNP) or carboxyl surface modification (PSC-CNP) were purchased at a concentration of 10 mg/mL from either Bangs Laboratories (Fishers, IN, USA) or Phosphorex, Inc. (Hopkinton, MA, USA). Both PLGA and gold nanoparticles were synthesized in house by the methods below (**Figure 4-3**).

PLGA Nanoparticles. Biodegradable PLGA-CNP were fabricated in house by nanoprecipitation, similar to previously published methods [132]. 100 mg of RG503H Resomer® (Sigma Aldrich) was dissolved in acetone. The dissolution was performed over 5 minutes at 150 g stirring. Ultrapure water was added with continued stirring at 150 g for 3 hours to create a final PLGA-CNP concentration of 10 mg/mL. PLGA-PVA particles were also fabricated by addition of a 5% PVA (~20,000 MW) solution rather than ultrapure water. Particles on the order of 50 nm were synthesized at 90°C, while particles on the order of 150 nm were synthesized at room temperature (~25°C). Particles were washed by microcentrifuge at 4,500 x g for 20 minutes.

Gold Nanoparticles. Gold nanoparticles modified with Poly (ethylene glycol) carboxyl thiol (PEG-C) and PEG-methyl ether thiol (PEG-M) were utilized in this study. PEG-Carboxyl thiol (7500 M_n) and PEG-methyl ether thiol (6000 M_n) were purchased from a supplier (Sigma Aldrich). 1 mM bulk solutions of each substance were created using deionized water. The PEG solutions were then stored in a freezer at -20˚C prior to use. Spherical citrate capped gold nanoparticles were synthesized as described by Manson *et al* and Wang *et al* [151, 152]. Deionized water (198 mL) and 25 mM gold(III) chloride trihydrate ($HAuCl_4 \bullet 3H_20$, 8 mL) was boiled and refluxed in a 250 mL flat-bottom beaker

on a temperature-controlled hot plate with continuous stirring. Sodium citrate solution (18 mL of 20 mM solution) was added to the boiling chloroauric acid solution, removed from heat and left to stir for 20 minutes to ensure completion of the reaction. Varying concentrations of PEG-C and PEG-M were added to the citrate capped nanoparticles in order to create 100 mL solutions of PEG-capped AuNPs. After thawing and agitating each of the 1 mM PEG solutions, the following PEGylated nanoparticle solutions were created: PEG-AuNP-C (141 µL of PEG-C solution) and PEG-AuNP-M (141 µL of PEG-M solution). Each solution was left to rapidly stir overnight at room temperature to complete the exchange of citrate molecules and PEG. The PEGylated AuNP solutions were then washed by microcentrifuge at 4,500 x g for 20 minutes. The supernatant was removed, leaving the AuNP pellet at the bottom of each centrifuge tube. The pellet was washed by adding 100 µL of phosphate-buffered saline (PBS) to each tube, agitated and re-spun in the centrifuge using the same settings. This process was repeated to remove excess PEG and other reactants [151]. This process, which takes several hours across two days, yielded approximately 3 mL of gold nanoparticles at a concentration of 2.0 x 10^{13} CNP/mL. Additionally, the use of PEG in the gold nanoparticle formulation substantially increases the batching cost from ~$0.19/mL for citrate stabilized gold CNP to ~$2.77/mL for PEG stabilized gold CNP, representing a 1458% increase in price.

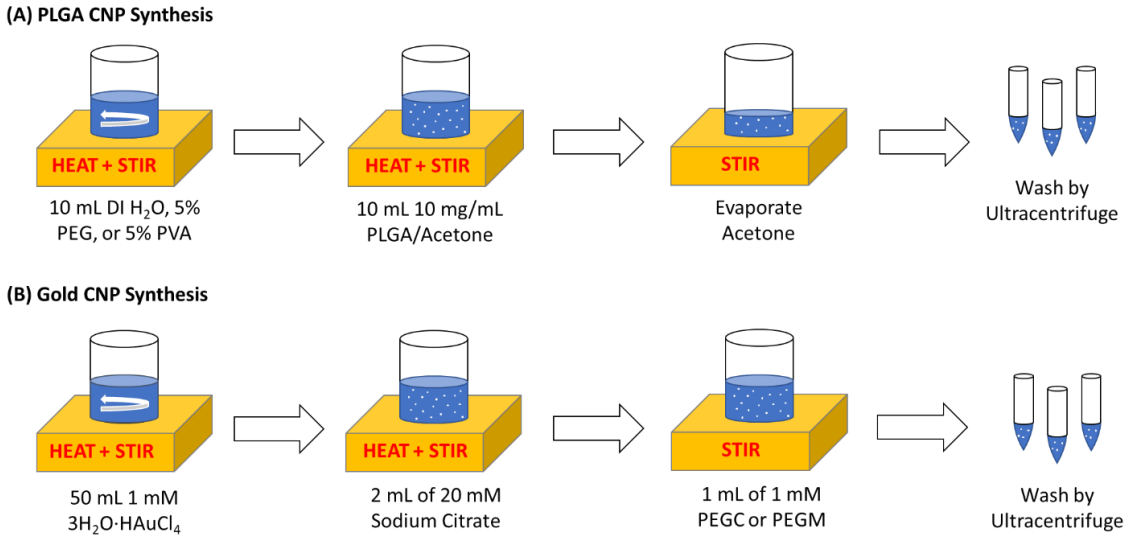

Figure 4-3. Synthesis protocol for (A) PLGA and (B) gold CNP. Polystyrene particles utilized in the study were purchased from either Bangs Laboratories or Phosphorex, Inc. [76]

All particles (PS, PLGA, and gold) were stored at 4° C until needed for characterization or blood treatment. Prior to use, the CNP were vortexed for 10 seconds to evenly disperse and minimize agglomeration. Characterization of average diameter and zeta potential was performed by addition of 100 µL of the 10 mg/mL CNP mixture to 900 µL of deionized water for a final test concentration of 1 mg/mL. Diameter was measured by dynamic light scattering, while zeta potential was measured by photon correlation spectroscopy (ZetaSizer Nano-ZA, Malvern Instruments).

4.3.3 Blood collection

Porcine. Porcine whole blood was obtained from a local abattoir (Holifield Farms, Covington, GA) and lightly heparinized at 3.5 USP units/mL, as previously described by Para et al [77]. Blood was stored at room temperature on a rocker prior to testing. All testing was completed within 8 hours after collection.

Human. Healthy volunteers were older than 18 years of age and had no prior history of cardiovascular disease and no antiplatelet medication in the 10-days prior to enrollment. Individuals with known anemia (hematocrit < 30%) or transmittable blood diseases were excluded. The MTA was the only PFT utilized in this proof-of-concept study. All subjects were recruited in accordance with the Institutional Review Board of the Georgia Institute of Technology (IRB #17315).

4.3.4 Blood treatment with CNP

Blood samples were treated with varying concentrations of CNP immediately before the flow assay. Estimations of the appropriate dose were based on average plasma vWF molecule concentrations. An approximate vWF concentration was calculated at 1.4 x 10^{11} molecules/mL of blood, assuming a mass concentration of 5 μg/mL and average length of 4μm for plasma vWF. Values were converted to a stoichiometric CNP:vWF ratio, given the relative CNP dose to the approximated amount of vWF molecules in a whole blood sample. Concentrations of CNP investigated in this study ranged from 0.5 to 10 CNP:vWF. Stoichiometric concentrations of PLGA-CNP and AuNP-CNP were selected based on results of the PS-CNP investigation.

4.3.5 In vitro microfluidic thrombosis assay (MTA)

The microfluidic channels were fabricated by gray-scale lithography techniques previously described [48]. Fibrillar type I collagen-coated (100 μg/mL) microfluidic chips are positioned on the stage of a light microscope with a 4X objective and connected to an upstream reservoir with Tygon tubing, similar to previously described [3]. Downstream tubing leads to a discharge reservoir placed on a precision balance to measure mass flow

rates. Images of thrombus formation are acquired at 1 Hz with a high-resolution CCD camera. Image acquisition is facilitated by the μManager open-source microscopy software [78]. Occlusion time (OT) is measured as the time from first blood contact with the stenosis to the time of the initial maximum mass balance reading. Image and flow-rate post-processing was performed with custom code (MATLAB, MathWorks).

4.3.6 Platelet surface coverage analysis

An assessment of platelet surface coverage in the microfluidic was also performed to determine the effects of CNPs on overall platelet adhesion. The MTA was utilized again for this assessment, was fixated on the stage of a fluorescent microscope (AxioObserver, Zeiss). Human whole blood samples were treated with optimal nanoparticle doses, as determined in the OT assessment described previously. Immediately prior to testing the blood samples in the MTA, Calcein AM was added to the blood sample at a concentration of 1.0 μM (BD Biosciences). Samples were processed in the MTA per the methods described above. Fluorescent images were collected and processed with MATLAB counting the number of pixels with fluorescence, indicating platelet surface coverage.

4.3.7 In vivo murine tail bleeding model

Although the microfluidic device mimics the *in vivo* atherosclerotic environment, it does not allow for an assessment of bleeding risk; therefore, it is necessary to perform *in vivo* hemostatic safety experiments. A tail-bleeding model was utilized to determine the effect of each agent on normal hemostasis. Animals were anesthetized with a ketamine/xylazine cocktail injection (87.5 mg/kg ketamine, 12.5 mg/kg xylazine, 0.1 mL cocktail / 20g mouse weight). Ten (10) wild-type (C57B1/6) mice were separated into two

groups (n = 5 per group): CNP (n=5) or PBS placebo (n=5) was injected into the tail vein of the mouse. The number of animals was selected based on sample sizes utilized in similar tail-bleeding assessments of a previous study [153]. This was followed by cleanly cutting 1 cm off from the tip of the tail and submerging the injured tail into a vial of saline. The bleeding from the tail was timed until blood ceased to flow into the saline vial, indicating hemostasis at the site of injury.

4.3.8 In vivo murine carotid thrombosis model

In order to study *in vivo* efficacy, a relevant animal model of thrombosis must be selected. The murine ferric chloride thrombosis model is a popular choice in this field [154, 155]. However, recent reports have indicated that the chemical-induced injury leads to abnormal clot formation [156]. Therefore, an arterial physically-induced injury model was utilized in this study through the modified-Folts model, which creates a high shear environment [153].

Ten (10) wild-type (C57B1/6) mice were separated into two groups (n = 5 per group): CNP treated and negative control non-injury. The number of animals was selected based on statistically significant results found in a previous study using similar sample sizes in the modified-Folts model [153]. Animals were anesthetized with the same protocol as above. Mice were placed on their back with a midline incision performed on the neck to isolate the right common carotid artery. A flow probe connected to a blood flowmeter was gently placed around the isolated artery. Silk suture was lightly tied distal to the flow probe and continually tightened until flow has decreased by 50%. Prior to inducing injury, CNP or PBS placebo injection was performed via intravenous bolus through the tail vein.

Arterial injury was induced by crushing the artery with artery forceps directly over the suture [153]. Flow rates were monitored over the course of the 60-minute experiment to monitor the development of occlusive thrombi and vessel perfusion. After 60 minutes, the animals were euthanized by cervical dislocation.

4.3.9 Statistical methods

All data is presented as the average and standard deviation, unless otherwise specified. A student's t-test was used to determine statistical differences between experimental groups and control values at the same concentrations for both in vitro and in vivo data [77].

4.4 Results

4.4.1 Effects of PS CNP Charge on Porcine In Vitro Thrombosis

In an initial screen of the effects of CNP on porcine whole blood thrombosis, three different surface modifications of 60 nm polystyrene were assessed: carboxyl, amine, and non-treated. These modifications represented negative, positive, and neutral charges of CNP, respectively (**Table 4-1**). Doses of nanoparticles were varied between 1.2-12 x 10^{11} nanoparticles/mL of blood, which corresponds to estimated ratios of 1:1 to 10:1 CNP to vWF molecules in whole blood samples. Porcine blood samples (n = 4) were subjected to a high shear rate environment of 10,000 s^{-1} with a fibrillar collagen surface in the MTA. Images acquired during the duration of the experiment made it possible to qualitatively determine the level of platelet accumulation and observe thrombus formation (**Figure 4-4**). The amount and rate of thrombus formation was comparable for both control and PS-CNP

conditions. However, significant differences in the amount of light transmitted between the control and PSC-CNP (60 nm) groups were found at time points of 90, 120, and 180 seconds (**Figure 4-5**). The control group (saline addition) occluded quickly (t_{occ} = 133 seconds). In contrast, the PSC-CNP treated group remained in the initial platelet adhesion phase (lag phase), with accumulation occurring at a much slower rate than normal. Although the images of PSA-CNP might indicate that they were also effective in inhibiting thrombus formation, video evidence from all samples treated with PSA-CNP showed large platelet emboli passing through the channel, occasionally getting stuck in the stenotic region or upstream. Therefore, PSA-CNP were eliminated from further assessment as they induced platelet aggregation.

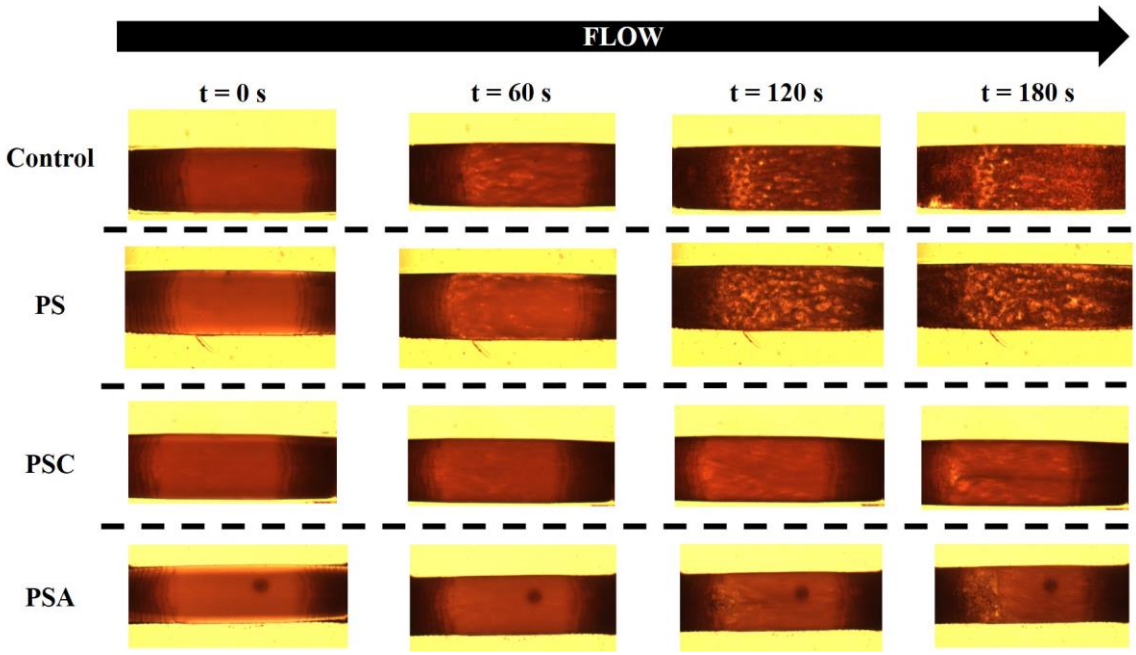

Figure 4-4. Experimental results comparing the control (untreated) whole blood condition and the addition of 60 nm polystyrene (PS), polystyrene-carboxyl (PSC), and polystyrene-amine (PSA) nanoparticles at a concentration of 1.8 x 10^{11} nanoparticles/mL. Flow is from left to right in each image. The comparison indicates similar thrombotic events in control and PS, while thrombus formation is delayed in PSC. Although hard to see in the still frames, samples treated with PSA had several

microthrombi form and pass through the channel, sometimes lodging in the upstream portion, which caused channel occlusion rather than thrombus formation on the collagen coated surface.

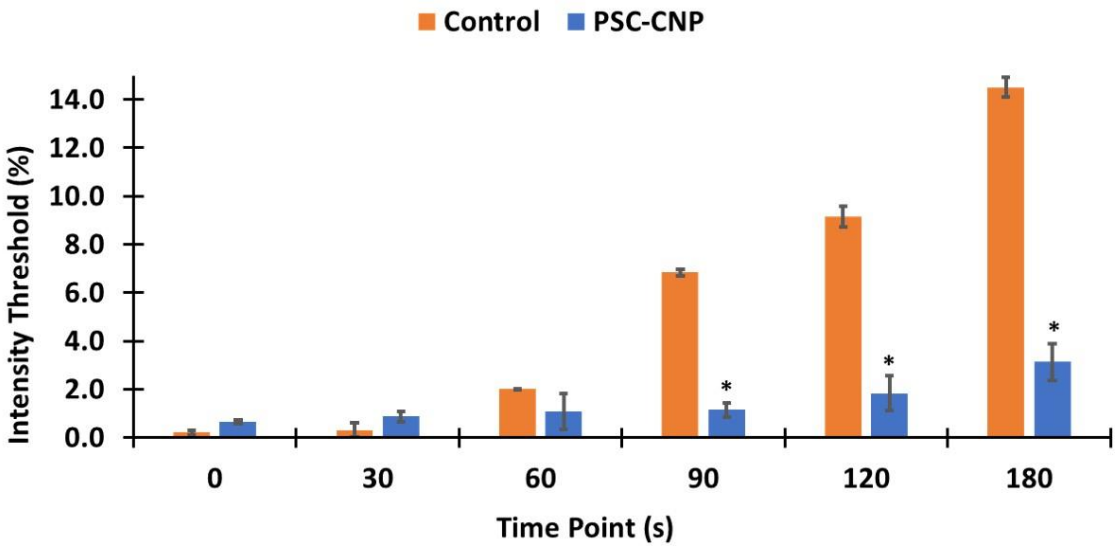

Figure 4-5. The PSC-CNP significantly retarded thrombus formation as quantified by light transmittance (1.8 x 10^{11} nanoparticles/mL). The overall light transmittance in the channels was found to be significantly different between the control and PSC-CNP at times of 90, 120, and 180 seconds (*p-value < 0.01, n = 4; error bars represent standard deviation).

PSC CNP delayed occlusion time up to 4X

Across the dosing scheme of 1.2-12 x 10^{11} nanoparticles/mL, the 60 nm PSC-CNP were found to have a narrow efficacy range in their ability to inhibit thrombus. The peak concentration was found to be around 2.0 x 10^{11} particles per mL of blood and with an approximately 4-fold increase in occlusion time compared to the control group (**Figure**

4-6A-B). However, the effect of the PSC-CNP began to diminish as the concentration was increased beyond this range.

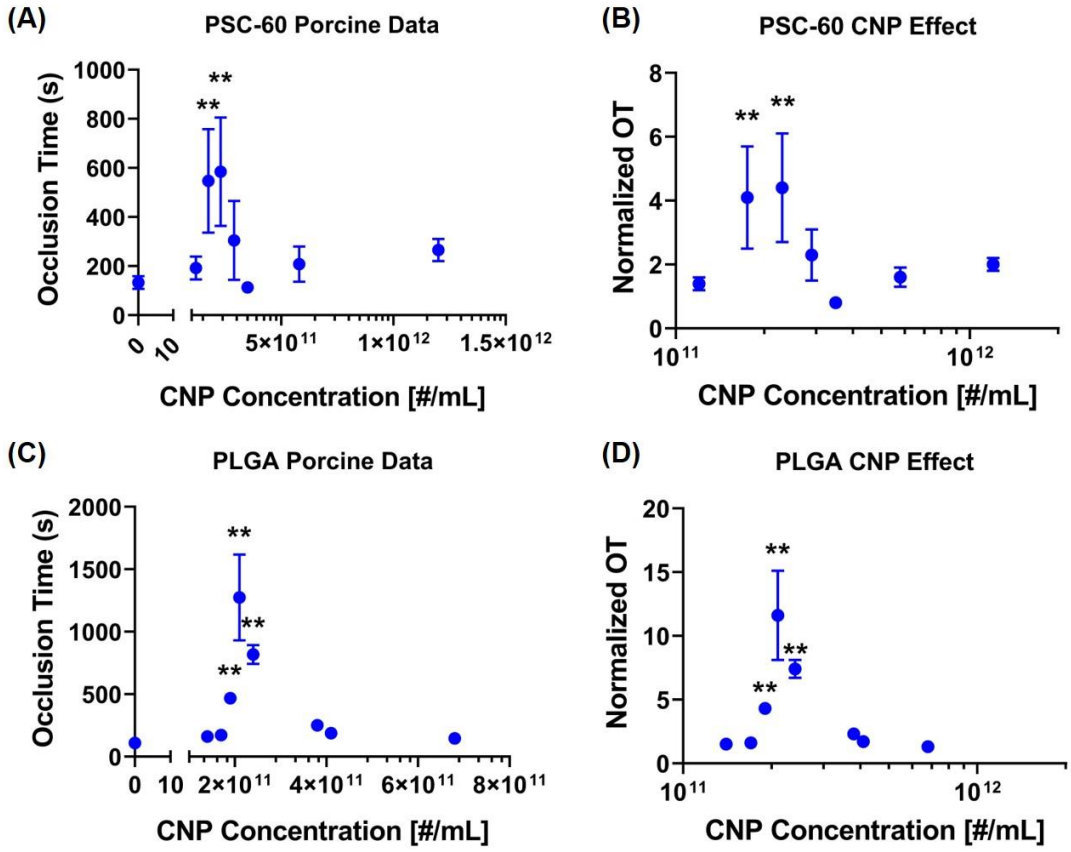

Figure 4-6. Occlusion time dose response of both PSC 60nm CNP and PLGA CNP in the arterial thrombosis microfluidic assay. (A) 60 nm PSC-CNP had a narrow dose response, with a maximum effective concentration between that led to an approximate 4X increase in OT (B). (C) PLGA-CNP had a peak at a similar concentration to that of the PSC-CNP, but led to an approximate 12X extension in OT (D). Statistical significance was determined from treated group compared to the untreated group (p-value < 0.01; n = 4 to 32 per data point).**

4.4.2 *Effects of PLGA CNP on Porcine In Vitro Thrombosis*

Next, we investigated whether this effect was also observed with another negatively charged particle. PLGA-CNP were synthesized at room temperature using nanoprecipitation methods and were found to have a size of 155nm and zeta potential of -32.1 mV (**Table 4-1**). The concentrations of PLGA-CNP tested in the arterial thrombosis assay was then varied around the peak observed with the 60 nm PSC-CNP, with eight calculated ratios between 1.0-10 x 10^{11} particles per mL of blood.

The results of the MTA with porcine whole blood indicated a similar peak in this range of CNP concentrations, with a maximum effective concentration found at approximately 2.0 x 10^{11} PLGA-CNP per mL of blood (**Figure 4-6**). At this concentration, the occlusion time was delayed by an even greater **12-fold** from the control case. This effect also diminishes to nearly baseline occlusion times at concentrations outside the optimal ratio, similar to the 60 nm PSC-CNP.

Nanoparticle Characterization from in vitro porcine experiments

PS-, PSC-, PSA-, and PLGA-CNP characterization of hydrodynamic diameter (D_{CNP}) and zeta potential (ZP_{CNP}) were determined with the use of a ZetaSizer instrument (ZetaSizer Nano-ZA, Malvern Instruments; **Table 4-1**). The purchased polystyrene particles were within the manufacturer's range of size distributions.

Table 4-1. Quantified characteristics of CNP utilized in the porcine whole blood testing.

	D_{CNP} (nm)	ZP_{CNP} (mV)
PS-CNP	65.0	-6.1
PSC-CNP	80.0	-48.0
PSA-CNP	62.0	+26.0
PLGA-CNP	155.0	-32.1

4.4.3 Polystyrene CNP parametric analysis in human whole blood

The high shear MTA was utilized to confirm that the results found previously with porcine whole blood translated to human whole blood [76]. Given the hypothetical mechanism of CNP and vWF interaction previously proposed [76], a screening experiment was designed ranging from an approximate 1:2 to 2:1 CNP to vWF ratio. An approximate vWF molecular concentration in blood is 1.4×10^{11} molecules per milliliter of blood, given a soluble vWF mass concentration of 5 µg/mL and average length of 4 µm/molecule [157-159]. Polystyrene nanoparticles of either 50 or 200 nm diameter and carboxyl-functionalized (PSC50 or PSC200) or non-functionalized (PS50 or PS200) surface were investigated in blood collected from five donors with four experimental replicates for each donor. All particles were characterized for charge and size prior to testing (**Table 4-2**). PSC50 significantly inhibited thrombosis at three of four concentrations tested, with the exception of 1.4×10^{11} particles/mL (**Figure 4-7**). PS50 significantly inhibited thrombus formation only at 1.4×10^{11} particles/mL (**Figure 4-7**). Neither PSC200 nor PS200 significantly inhibited thrombus formation at any concentration tested. After normalizing

to baseline occlusion times for each sample, PSC50 was found to have a peak effect at a concentration of 1.8 x 10^{11} particles/mL, which was statistically significant to all other particle types (**Figure 4-7**). Inhibition was significantly greater for PSC50 at this concentration than all other particle types, which is behaviorally consistent with previous results of similarly sized particles in a porcine whole blood model [76]. PSC200 particles were found to have a similarly significant impact in only 2 of 5 individuals investigated, indicating a decreased response as particle size is increased.

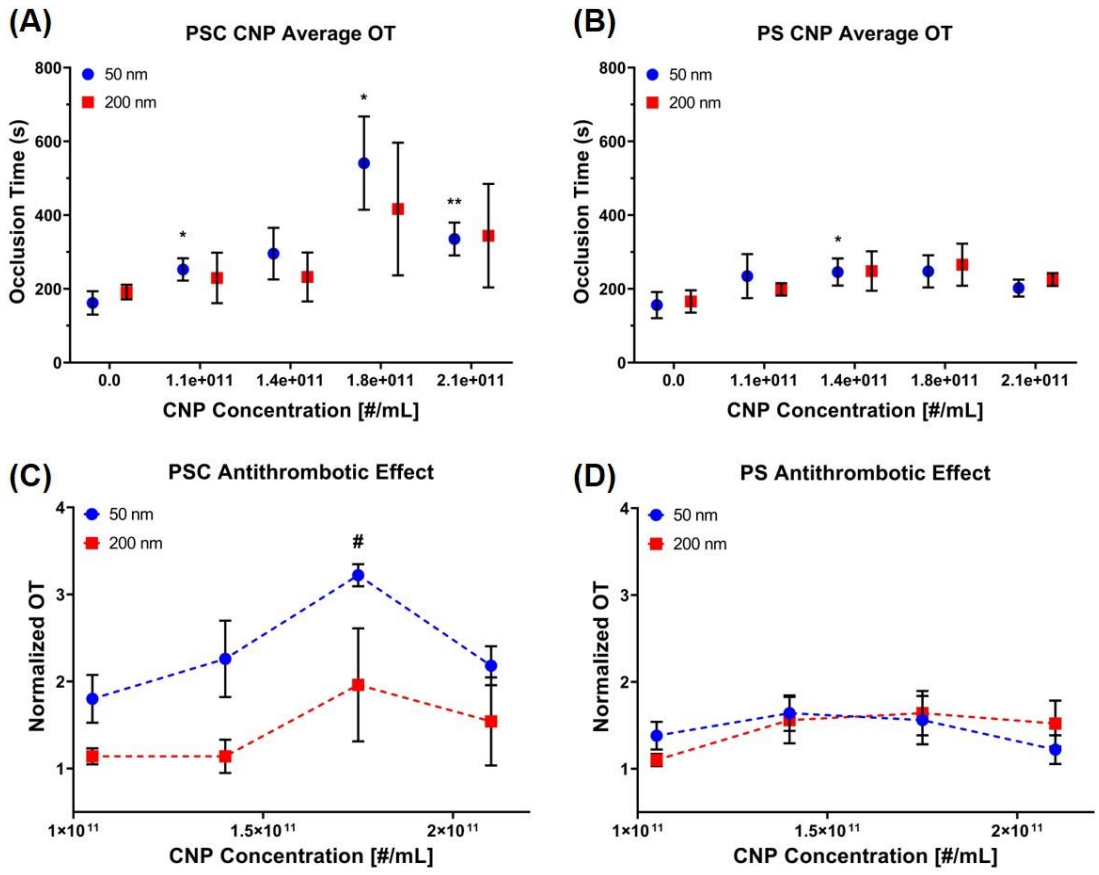

Figure 4-7. Polystyrene CNP results in the MTA with human whole blood. Average occlusion times across the human blood samples for polystyrene-carboxyl (A) and native polystyrene (B) CNP (n = 5 samples, 4 experimental replicates per samples). Significant differences were calculated for each particle type with respect to the baseline value for each particle (*p < 0.01). Occlusion times were normalized to the baseline value for each particle type for each particle type (C-D). The peak value of PSC50 particles at 1.8 x 10^{11} particles/mL of blood was found to be statistically significant compared to all other particle types at the same concentration ($^{\#}$p < 0.05).

4.4.4 PSC50 CNP inhibit human platelet surface coverage in vitro

An investigation into the amount of platelet adhesion over time was also performed utilizing fluorescent microscopy. The top performing polystyrene particle (PSC50) was selected for characterization at its optimal dose of 1.8 x 10^{11} particles/mL. Adhesion of

platelets was delayed, and surface coverage was less dense in the PSC50 CNP group over the saline-treated control group (**Figure 4-8**).

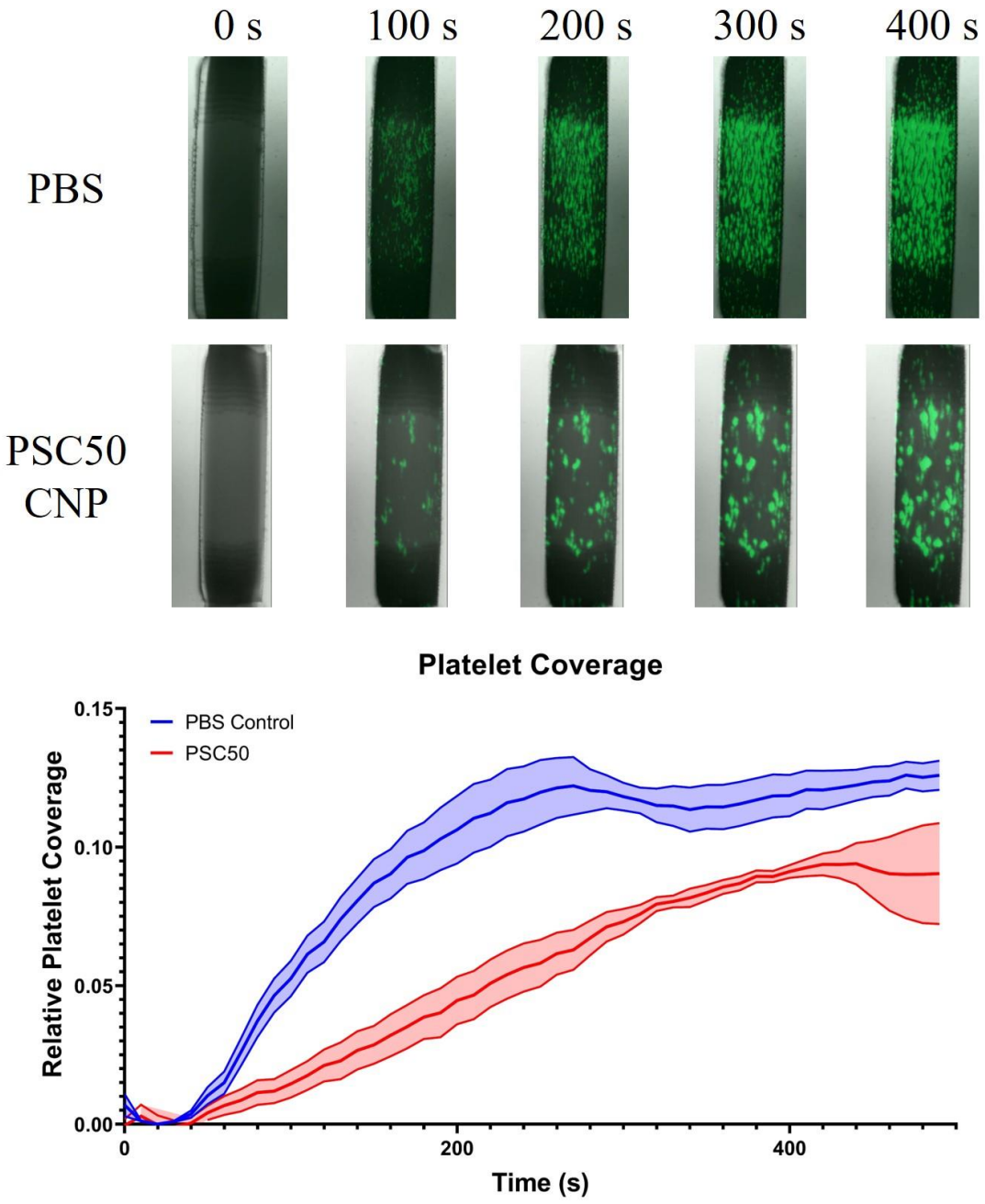

Figure 4-8. Calcein platelet stain comparing the adhesion and accumulation of platelets in the stenotic MTA over time for PBS (control) and PSC-50nm conditions (flow is from top to bottom). The shaded regions represent the standard deviation of

the surface coverage for the average across the assessed channels at each time point (N = 4).

4.4.5 PLGA CNP inhibits thrombosis in human whole blood

In addition to assessing polystyrene CNP in vitro in human whole blood, we aimed to assess the effects of other nanoparticle base materials. Unmodified PLGA particles were then investigated for their antithrombotic properties in human whole blood in vitro. Particles close to 80 nm in diameter were synthesized by nanoprecipitation at 95°C. In addition, 150 nm particles were synthesized at room temperature as previous results indicated a powerful antithrombotic response of 150 nm PLGA particles in porcine whole blood [76]. Smaller PLGA CNP did not have a strong antithrombotic effect (**Figure 4-9**). However, the larger PLGA CNP (150 nm) had a large antithrombotic effect, with a peak effect leading to OTs that are 4 times longer (**Figure 4-9**). However, the unmodified PLGA particles have practical limitations for in vivo use, as their hydrophobic nature causes them to be rapidly cleared from the blood stream. Therefore, surface modifications to increase the hydrophilicity of the PLGA CNP were investigated.

PLGA with a PVA surfactant modification was synthesized at both small (~80 nm) and large (~150 nm) diameters. Similar effects based on size were observed for both surface modifications as with the unmodified PLGA CNP (**Figure 4-9**). PLGA-PVA 150 nm had a sustained response across multiple doses to extend OT by approximately three times the baseline value. Therefore, the antithrombotic effect of unmodified PLGA is preserved after surface modifications to create a more hydrophilic CNP for in vivo assessment (**Figure 4-9**).

The larger PLGA-PVA was then assessed for platelet adhesion and surface coverage over time compared to PBS control by fluorescent microscopy (**Figure 4-10**). Full occlusive thrombus was formed by 250s for the PBS control, while significantly less adhesion was observed over time in the PLGA-PVA treated condition (**Figure 4-11**), similarly to the previous comparison of PSC50 CNP and PBS (**Figure 4-8**). The intensity analysis indicates that the platelet adhesion plateaus in about twice as much time and with significantly less platelet coverage in the channel.

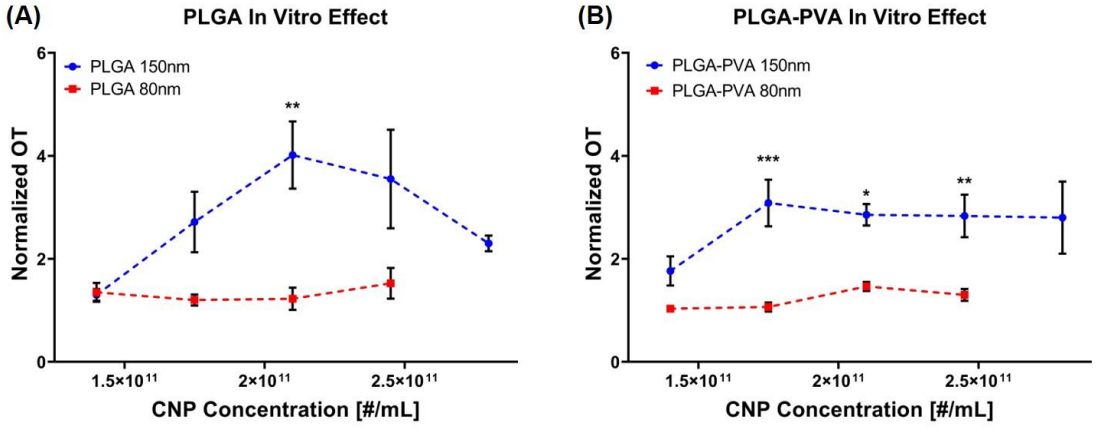

Figure 4-9. Other biocompatible CNP formulations of (A) PLGA (n = 4-6) and (B) PLGA-PVA (n=4-7) CNP show an effect on occlusion time in the MTA. Each PLGA-based particle type was investigated at a particle size of approximately 150 nm and 80 nm. For each type of PLGA-based particle, the larger sized particle led to a stronger inhibitory effect on thrombus formation, which was not consistent with the findings of the polystyrene particles. (*p < 0.05; **p < 0.01; ***p < 0.001).

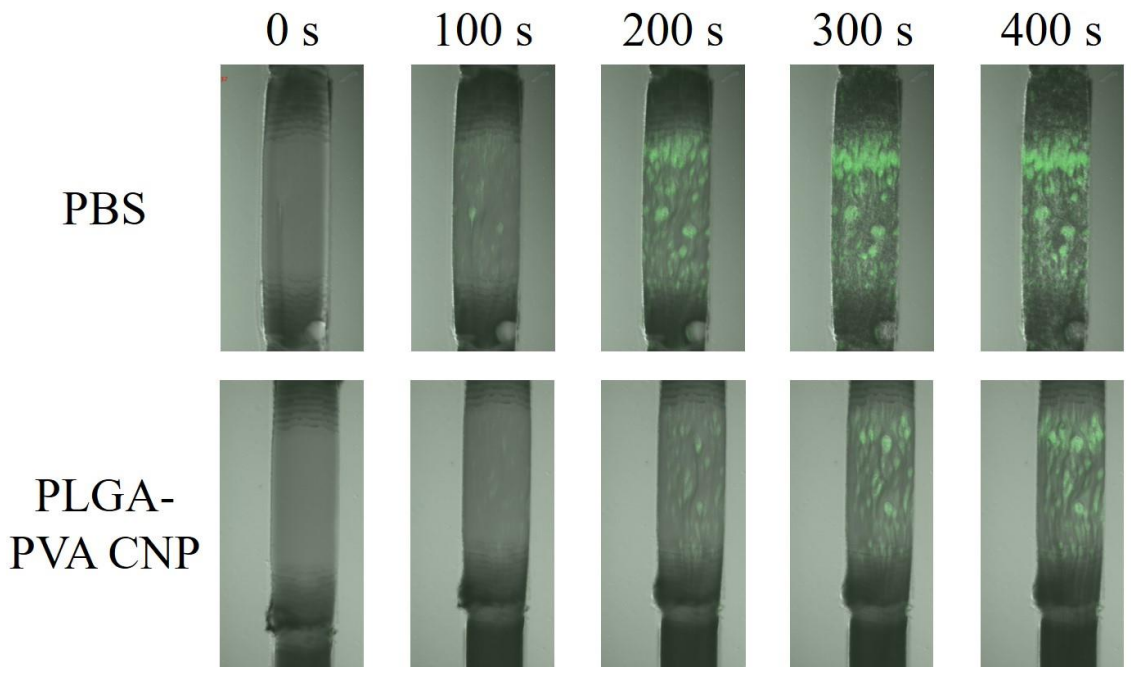

Figure 4-10. Calcein platelet stain comparing the adhesion and accumulation of platelets in the stenotic MTA over time for PBS (control) and PLGA-PVA CNP conditions (flow is from top to bottom).

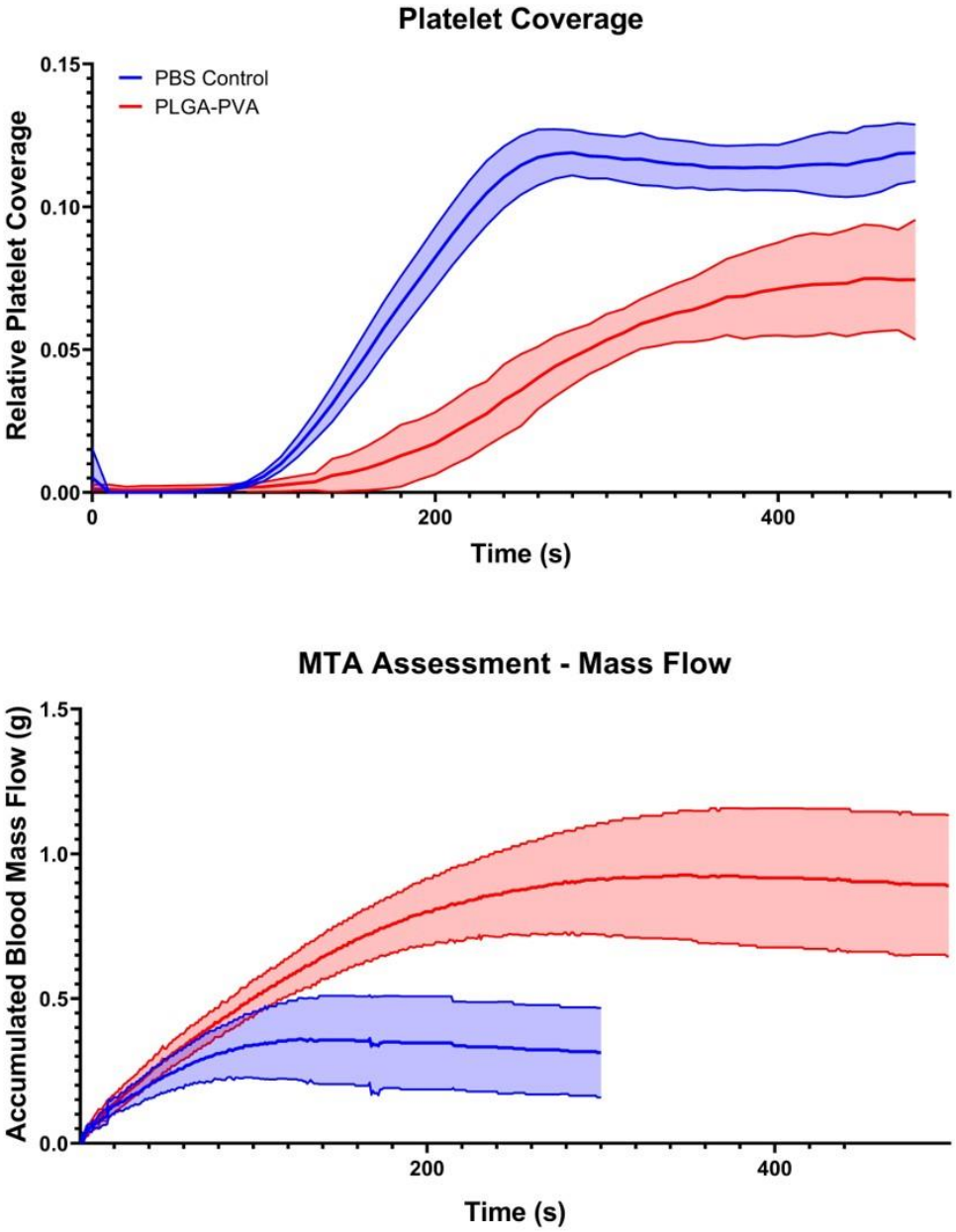

Figure 4-11. Rates of platelet adhesion (top) and blood mass accumulation from the outlet (bottom) during the MTA assessment for both PBS-treated control and PLGA-PVA CNP treated groups (N = 4). PLGA-PVA CNP treated whole blood led to significantly slower and less platelet coverage than the PBS-treated control group, which corresponds to the OT's determined from the mass flow data. Therefore, CNP decrease the rates of platelet adhesion, subsequently elongating OT in the MTA. The shaded regions represent the standard deviation of the surface coverage for the average at each time point across the assessed channels.

4.4.6 AuNP loses mild antithrombotic effect with PEG coatings

After the screening assay for the effects of size and charge indicated that a 50 nm, negatively charged particle led to a significant effect on thrombus formation, gold (AuNP) was utilized as a base material to fabricate a biostable, biocompatible particle. AuNP stabilized by citrate ions was fabricated by reduction of gold ions. This led to particles of size 45 nm and -38.0 mV. The AuNP were assessed in the MTA at the same concentrations as the polystyrene CNP (**Figure 4-12A**). A significant effect of citrated AuNP over baseline conditions was found at 1.8×10^{11} CNP/mL, but was not to the same level of inhibition as the PSC50 CNP.

The synthesis was also modified to fabricate gold particles that were more hydrophilic in nature and would thus have increased circulation times in an *in vivo* setting. Polyethylene-glycol (PEG) was utilized as a surface modification to enhance blood circulation time. Two PEGs capped with either a carboxyl (PEGC) or methyl (PEGM) group were utilized to create zeta potentials similar to the PSC50 and PS50 CNP, respectively (

Table 4-3). AuNP-PEGM had a very mild inhibitory effect, similar to the PS50 particles, in the MTA in human whole blood. However, AuNP-PEGC did not yield similar inhibition to the PSC50 particles, with a very similar dosing profile to the AuNP-PEGM (**Figure 4-12**).

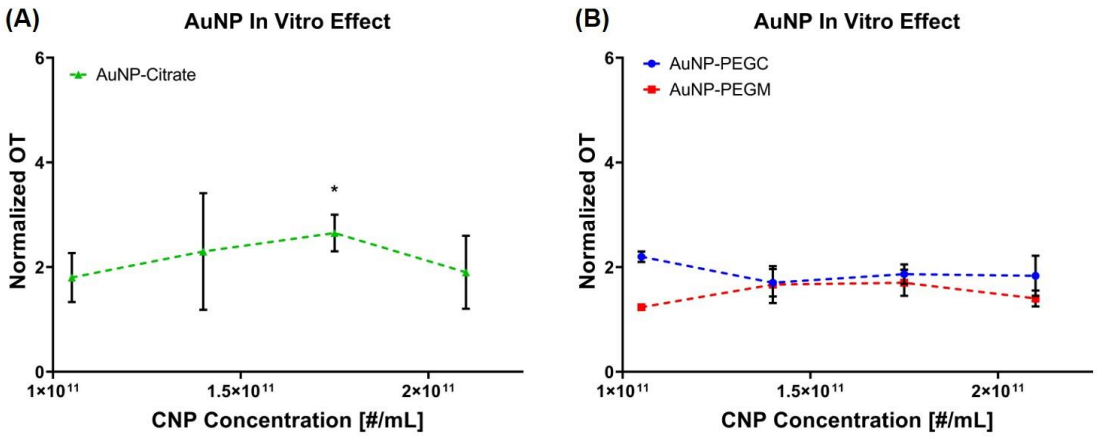

Figure 4-12. (A) Citrate stabilized gold nanoparticles (AuNP) at ~50nm investigated at the same doses as the polystyrene CNP (n = 4). A significant inhibitory effect was found at the same dose as PSC50 CNP, although the effect was smaller. (B) More neutrally charged AuNP-PEGM (n = 3) mimics the behavior of PS50; however, the more negatively charged AuNP-PEGC (n = 3) does not mimic the magnitude of effect observed with the PSC50 CNP (*p < 0.05).

4.4.7 CNPs do not affect in vivo hemostasis

PSC50 CNP were investigated in a murine tail bleeding model to determine the effects of each agent on normal hemostasis (**Figure 4-13**). In order to counter rapid clearance of the PSC50 CNP in vivo within the first few minutes of administration a dose of 1.8 x 10^{13} PSC50 CNP/mL was administered as previous studies suggest approximately 1% of similar polystyrene-carboxyl particles remain in the blood 1-3 hours after venous injection [131, 160, 161]. No significant difference in bleeding time was found between CNP and PBS controls, indicating that the CNP does not alter normal hemostatic processes.

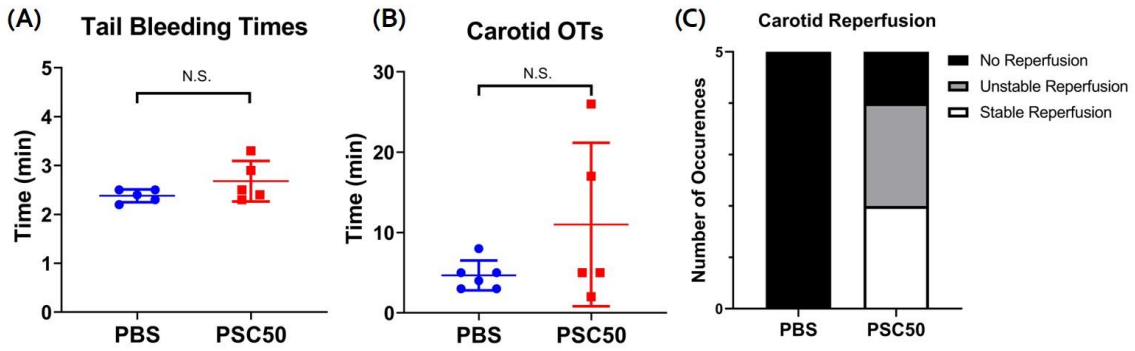

Figure 4-13. (A) Assessment of PSC50 CNP and PBS placebo in a murine tail bleeding model found no difference in tail bleeding times, indicating that CNP do not impact hemostatic function. (B) Carotid OTs were determined for both PBS and PSC50 CNP treated mice, which found no statistical difference between the two groups. However, two of the PSC50 CNP treated mice led to OTs that were approximately 3-4X longer than control OTs. (C) Reperfusion of the carotid artery after clot formation did not occur in any of the PBS treated mice. However, unstable perfusion leading to other clot formations occurred in 2/5 of PSC50 CNP treated mice and stable reperfusions with no subsequent clot formation occurred in another 2/5 of CNP treated mice. This indicates that CNP have an impact on in vivo clot formation and stability.

4.4.8 CNP's Impact on In Vivo Thrombus Formation

PSC50 CNP were investigated in a modified-Folts murine carotid arterial injury model and compared to a phosphate buffered saline (PBS) placebo (**Figure 4-13**). In order to counter rapid clearance of the PSC50 CNP in vivo within the first few minutes of administration, a dose 100-times greater the optimal dose in vitro was administered as previous studies suggest approximately 1% of similar polystyrene-carboxyl particles remain in blood 1-3 hours after venous injection [131, 160, 161]. The PBS placebo dose led to stable clot formation in an average of 4.7 minutes (N = 5) and no reperfusion of the clot was observed during the 60-minute observation period. When dosed with CNP, occlusive clots formed in an average of 11.0 minutes (N = 5), which was not statistically

different than the control condition. However, 2/5 of the mice developed OTs that were approximately 3-4 times longer than the control OTs, indicating that CNP were impacting thrombotic activity in those animals. Additionally, 4/5 of the clots in the CNP-treated mice led to either stable or unstable reperfusion shortly after. This indicates that the strength of the clot was also affected by the CNP. However, a negative side-effect of increased respiratory activity was noticed in the mice treated with PSC50 CNP vs. PBS.

4.4.9 Characterization of CNPs

Characterization of the hydrodynamic diameter (D_H) and zeta potential (ZP) for all nanoparticles utilized in this study were performed with Malvern ZetaSizer and Malvern NanoSight instruments. The values for each parameter are summarized in **Table 4-2**, **Table 4-3**, and **Table 4-4**.

Table 4-2. Characterization of purchased polystyrene CNP hydrodynamic diameter (DH) and zeta potential (ZP) of the stock solutions.

	PSC50	**PS50**	**PSC200**	**PS200**
D_H (nm)	53.7	44.9	185.8	189.2
ZP (mV)	-33.8	-12.4	-26.6	-9.4

Table 4-3. Characterization of synthesized biostable AuNP CNP hydrodynamic diameter (DH) and zeta potential (ZP) of the stock solutions.

	Au-PEGC	Au-PEGM	Au-Citrate
D_H (nm)	61.3	40.6	45.7
ZP (mV)	-40.0	-6.7	-37.7

Table 4-4. Characterization of synthesized biodegradable PLGA CNP hydrodynamic diameter (DH) and zeta potential (ZP) of the stock solutions.

	PLGA80	PLGA150	PLGA-PVA80	PLGA-PVA150
D_H (nm)	90.1	146.7	85.6	130.4
ZP (mV)	-33.3	-34.8	-34.3	-32.1

4.5 Discussion

Prevention of arterial thrombosis has generally been through irreversible biochemical targets of platelet activation. In the present study, we present a new approach to retard arterial thrombosis by altering the physical tertiary structure of vWF rather than destroying platelet activity. Since vWF elongation is necessary for rapid platelet aggregation, negatively charged particles may attract positively charged A1 domains into

a compact, globular structure that resists elongation by high shear. We find that several such negatively charged nanoparticles can retard thrombotic occlusion time in a high shear/collagen microfluidics assay. The nanoparticles made of multiple materials with no conjugated pharmacological agents demonstrate antithrombotic properties that are more effective than aspirin or Plavix. The prolongation in occlusion time is more consistently effective over a wide range of samples of whole blood from many porcine and human subjects. Additionally, CNP showed to have an effect on carotid thrombus stability in vivo. Thus, CNP may be an inexpensive alternative to the effective, but very expensive ReoPro [162]. Further, the nanoparticles did not prolong tail bleeding time for mice at high doses indicating a margin of safety different from current antiplatelet pharmaceuticals.

4.5.1 vWF as a target for CNP

The two major blood components in arterial thrombosis, vWF and platelets, may be likely targets for this CNP interaction. vWF appears to be a likely target for this interaction, as the approximate stoichiometric ratio between vWF and the effective CNP concentration is on the order of 1:1. In silico models from our research group have shown that such an electrostatic interaction between CNP and vWF molecules at this ratio can possibly alter the folding of the protein to prevent elongation under high shear arterial flow [76, 134, 142]. Flow based single-molecule studies of vWF elongational dynamics similar to those performed by Fu et al may prove to be useful in elucidating this hypothesis [159]. This single-molecule methodology has already been utilized to show that electrostatic interactions in high saline concentrations can alter vWF folding under high shear, thus a similar mechanistic experiment with CNP may allow for the smart-design of CNP parameters to prevent vWF elongation by electrostatics under flow [163].

The CNP demonstrate an unusual therapeutic dose curve with a peak around 2.0 x 10^{11} CNP per mL of blood and return to near baseline rather than having the sigmoid dose-response curve of pharmaceuticals. This peak effect may be due to competing physical interactions between plasma proteins. The protein corona significantly changes over time, with the corona forming within 30 seconds and specific protein concentrations going from low to high and vice versa while incubated in blood [164]. Along with time effects, size and material of the nanoparticle play a critical role in plasma protein corona formation [109, 165, 166]. Changing the concentration of nanoparticles effectively changes the amount of biomaterial surface area, which may in turn impact the protein interactions in blood flow. Another potential reason for the decreased effect at higher concentrations may be due to electrostatic repulsion between negatively charged nanoparticles as they become more concentrated, which may alter interactions with blood components. Multiple negatively charged particles on the same vWF molecule may induce repulsive elongation rather than attractive compaction. This would create a mountain peak dose-response curve instead of the sigmoid curve of saturation.

4.5.2 CNP efficacy compared to aspirin and DAPT

The in vitro results of the CNP antithrombotic effect are also promising in the wake of the results observed in the previous aim of this thesis characterizing the antithrombotic effects of aspirin and Plavix. For this discussion, only results of the MTA with heparin anticoagulation will be used for comparison to the CNP, as that was the same anticoagulant utilized in this aim. The MTA found an effect of aspirin in in only 2/20 (10%) of healthy individuals on week-long therapy, and this effect was mild across the population with the average OT increasing by only 1.3 times the pre-aspirin baseline. Looking at the cardiology

patients, only 3/20 on aspirin therapy and 3/15 on DAPT had extended OTs. PSC50 increased the average OT by 3.2 times the baseline value at its optimal dose and extended OT by at least 3 times for each of the 5 blood samples tested. PLGA-PVA similarly extended OT by approximately 3 times in each of the 7 blood samples tested. And while no significant difference was found between PBS and CNP in time to occlusion in vivo, it appears that CNP may alter clot stability and strength as reperfusion occurred in 4/5 animals treated without a significant increase in bleeding time. Therefore, further pre-clinical development of the nanoparticle therapy and delivery should be investigated and directly compared to current antiplatelets.

4.5.3 CNP effects: human vs. porcine whole blood

Another interesting finding was the decrease in CNP antithrombotic efficacy in human whole blood compared to porcine whole blood. In particular, PLGA-CNP had a greater than 10-fold impact on occlusion time in porcine whole blood, while similar doses only had a 4-fold impact in human whole blood. Assuming that the mechanism of CNP anti-thrombotic effect is electrostatic interaction with vWF, a potential reason for this difference between the two species is that the vWF proteins are slightly different [167]. Porcine vWF lacks four continuous residues in the GPIb binding site region of the vWF-A1 domain, and also has additional positively charged residues in its sequence. Therefore, vWF-A1 binding with GPIb may be inherently weaker in porcine whole blood, as well as enhanced electrostatic interactions with negatively charged nanoparticles due to an increase in positive domains of the protein. The combination of these two properties of the porcine vWF may explain why there is such a difference in CNP efficacy as compared to

human whole blood. We will explore optimization of a wider range of CNP efficacy to human blood in the future.

4.5.4 Limitations and future work

This work is limited by several shortcomings. First, there are many possible nanoparticle formulations based on size, charge, and base material (among other factors) that were not assessed in this aim. The assessment with the polystyrene and PLGA nanoparticles show that the size alone inhibits thrombus formation differently across different base materials. Therefore, each base material should be assessed across a series of sizes to determine the optimal size for each material. Delivery and persistence of nanoparticles was not addressed as different materials are cleared from circulation by different mechanisms. A localized delivery method could be utilized to better control dosing and limit systemic metabolism of CNP. A possible approach might be to utilize shear-responsive microparticles detailed by Korin et al [168]. Another limitation is that although significant delays in thrombotic formation were observed with CNP use, experiments still ended in the ultimate formation of an occlusive thrombus. It is unknown whether clinical effectiveness requires complete prevention or only reduction in thrombus growth rates to prevent MACE. Additional uses for CNP could include acute injection during MACE to slow down thrombus formation during transport to an emergency facility.

4.6 Conclusion

This study effectively demonstrates a new therapeutic for reducing acute arterial thrombosis based on preventing the shear elongation of circulating vWF. CNP administered into whole blood significantly prolonged occlusion times by up to 12-fold in

an arterial-like microfluidic system with high shear rates and collagen that routinely goes to thrombotic occlusion. The effect is seen in multiple particles of differing size and charge, with a non-sigmoid dose-response curve, illustrating the non-pharmacologic mechanism of anti-thrombosis. Further, in vivo murine studies show no significant increase in bleeding due to CNP. This study opens the door for further investigation into CNP modifications and pre-clinical assessments to increase antithrombotic potential of CNP. Thus, CNP may be an inexpensive alternative to the effective, but very expensive ReoPro, without the inherent bleeding side-effects. As such, CNP may lead to a new type of antithrombotic therapy that acts through biophysical means as opposed to less effective pharmacological pathways of inhibiting platelet activation.

CHAPTER 5. CONCLUSION

5.1 Original Contributions

The following peer-reviewed journal articles have been published previously from this work:

1. **Griffin MT**, Kim DA, Ku DN. "Shear-Induced Platelet Aggregation: 3D-Grayscale Microfluidics for Repeatable and Localized Occlusive Thrombosis." Biomicrofluidics, 2019. 13(5): 054106.
2. **Griffin MT**, Zhu Y, Liu Z, Aidun CK, Ku DN. "Inhibition of High Shear Arterial Thrombosis by Charged Nanoparticles." Biomicrofluidics, 2018. 12(4): 042210.
3. Zhu Y, Liu Z, **Griffin MT**, Ku DN, Aidun CK. "Conformational Dynamics of Charged Polymers Interacting with Charged Particles." APS, 2018.
4. Hastings SM, **Griffin MT**, Ku DN. "Hemodynamic studies of platelet thrombosis using microfluidics." Platelets, 2017. 28(5): 427-33.

The following patent application is pending:

1. **Griffin MT**, Aidun CK, Ku DN. "Compositions and Methods for Inhibition Shear Induced Platelet Accumulation." US 2019/0343871 A1. Published 14 November 2019.

The following publications are in preparation:

1. **Griffin MT**, et al. "Platelet Function Test Comparison of the Microfluidic Thrombosis Assay (MTA), GTT, and VerifyNow PRU Test."
2. **Griffin MT,** et al. "Non-Pharmacologic Charged Nanoparticles Inhibit Shear-Induced Platelet Aggregation."

We have presented following peer-reviewed abstracts at major conferences:

1. Zhu Y, Liu Z, **Griffin MT**, Ku DN, Aidun CK. "Behavior of Von Willebrand Factor (VWF) and Platelet Interaction Under Shear Flow." 71st Annual Meeting of the APS Division of Fluid Dynamics. 11/2018.
2. **Griffin MT**, Zhu Y, Liu Z, Aidun CK, Ku DN. "Inhibition of Arterial Thrombosis with Charged Nanoparticles." BMES 2018. Atlanta, GA – 10/2018.

3. **Griffin MT** and Ku DN. “Arterial Thrombosis Microfluidics: Control of the Third Dimension by Grayscale Lithography.” Micro and Nano Flows 2018. Atlanta, GA – 9/2018.
4. Zhu Y, **Griffin MT**, Liu Z, Ku DN, Aidun CK. “Controlling the Conformational Changes of vWF in Shear Flow with Charged Nanoparticles.” Micro and Nano Flows 2018. Atlanta, GA – 9/2018.
5. Ku DN, **Griffin MT**, Zhu Y, Aidun CK. “Challenges of thrombosis modelling.” ISTH Congress. Dublin, Ireland – 7/2018.
6. Ku DN, **Griffin MT**, Zhu Y, Aidun CK. “Hemodynamics Controls Thrombosis to Cause Heart Attacks and Strokes.” World Congress of Biomechanics 2018. Dublin, Ireland – 7/2018.
7. **Griffin MT** and Ku DN. “Grayscale Lithography to Create 3-D Channels: Applications to High Shear Thrombosis Assays.” SB3C. Tucson, AZ – 7 /2017.
8. Ku DN, **Griffin MT**, Zhu Y, Liu Z, Aidun CK. “Nanoparticle Inhibition of Shear Induced Platelet Aggregation.” ISTH Congress. Berlin, Germany – 7/2017.

5.1.1 Aim 1: Reduction of microfluidic thrombosis assay variability through design factors.

This aim 1 led to the development of a grayscale lithography technique for creating ramped sections to change the z-dimension of microfluidic geometries. Although we apply this technique specifically to high shear thrombosis microfluidic technology, it certainly is not specific to this application and may benefit others aiming to accomplish a similar lithography technique. Therefore, we published this work in the journal *Biomicrofluidics* so that the technique might reach a broader group of researchers [48].

Through our parametric screening design, we were able to show that the 3D grayscale laser lithography technique creates stenotic test sections of precise geometry and enhanced shear rate repeatability, as compared to current CNC micromachining techniques. Additionally, we showed that fibrillar collagens

provide superior repeatability in the MTA over collagen thin films, even though thin film approach provides a significantly more uniform surface. Although comparisons have been made between fibrillar and collagen thin films before for the strength of platelet responses to the type of collagen coating, this is a new finding showing that sparse fibers still produce a more repeatable platelet test. Additionally, we show in this study that the anticoagulation method (citrate vs. heparin) does not significantly impact the endpoint variability across experimental replicates. Finally, it was determined that clot formation consistently occurred in the first 0.3 mm of the stenotic channel with a constant pressure head, providing a basis by which to design optical detection methods in SIPA point-of-care diagnostic devices.

5.1.2 Aim 2: Assess the ability of the MTA to quantify antiplatelet responsiveness.

This aim 2 was focused on the continued development of in vitro diagnostics for thrombosis and antiplatelets. First, we were able to demonstrate that the MTA is capable of detecting antiplatelet effects in a group of healthy individuals taking low-dose aspirin therapy. This is significant because it determined a therapeutic cut-off value for the OT metric from baseline values that was able to be utilized in the study of cardiology patients. Further, we were able to show that the MTA does not correlate strongly to VerifyNow, which only uses biochemical agonists, and GTT, which only incorporates high shear and not biochemical agonists. It was also found that the MTA was less sensitive to antiplatelet medications than each of the other two devices, indicating that the combination of biochemical agonists (i.e. collagen) and high shear may lead to the development of a more stable clot more similar to the one that develops in the in vivo setting. This lower sensitivity

may lead to higher specificity of the MTA in determining if a patient truly is responsive to a given antiplatelet therapy.

5.1.3 Aim 3: Development of a novel nanoparticle antithrombotic therapy.

This study effectively demonstrates the antithrombotic potential of CNP when administered in vitro and assessed in the MTA. We defined parameters for negatively charged, 50 nm polystyrene nanoparticles in order to achieve a reliable, strong antithrombotic response in vitro. The CNP decrease the rate of platelet adhesion and also decrease the total amount of platelet surface coverage within the stenotic zone of the MTA, indicating that clots form slower and are potentially weaker than clots under normal conditions. We also demonstrated that nanoparticle parameters of size and charge do not necessarily translate equally to other nanoparticle materials, as both gold and PLGA based nanoparticles of the same size and charge do not demonstrate the same effect. Therefore, conclusions about an antithrombotic response with one material cannot be made for another material even if all other factors are equal.

While efficacy results in vivo are modest and paired with concerns of respiratory complications after high-dose administration in mice, this study opens the door for further investigation into CNP modifications for increasing circulation residence time, and thus decreasing the effective dosing. Further, the in vivo experiments show no significant increase in bleeding due to CNP. As such, CNP may open the door to a new type of antithrombotic therapy that acts through biophysical means as opposed to traditional biochemical pathways of traditional agents.

5.2 Future directions

5.2.1 Diagnostics for antiplatelet therapies

Future directions of the MTA diagnostic are first to create a fully automated system that can detect occlusion time without the use of a microscope or mass balances. The quickest option to do so is to investigate modifications with the automated GTT unit. The GTT already incorporates high shear through a microfluidic-like channel in its cartridge. The material of the ceramic balls may have to be changed to something that is more thrombogenic. Also, anticoagulation with heparin is recommended for blood samples tested for high shear occlusion so that samples do not need to be tested immediately after the blood draw, making it easier on the technician or phlebotomist running the diagnostic. A comparative study of these modifications with the current state of the MTA will be useful to see if they provide the same OT endpoint. If not, then a custom automated system for the MTA with either a drop-counter or laser-diode optic at the stenosis could be developed.

Following the creation of an automated device, the MTA should be validated in a large, multi-center study designed to test individuals who are at risk for MACE and taking an antiplatelet therapy of interest (i.e. DAPT). Those patients could then be followed-up over the course of a multi-year study to see if they experienced a major event. The sensitivity and specificity of the MTA could then be determined for predicting MACE. Similar studies have been performed for all of the other major PFTs and would certainly be valuable to validate the MTA for MACE prediction.

5.2.2 CNP Antithrombotic Therapy

Significantly more work can be performed to further the research of the CNP antithrombotic therapy. First, CNP should be tested in an *in vivo* murine stroke model to

determine its effect on thrombus formation. This can be accomplished at a much lower loading dose with PLGA-PVA CNP over PSC50 CNP, as the PLGA-PVA are designed to remain in the blood circulation for a much longer time period due to their hydrophilic nature. While this was not performed in this thesis, it should be performed to see if this antithrombotic effect found *in vitro* can be replicated *in vivo*.

If the PLGA-PVA CNP were proven to be effective, further work would need to be accomplished in order to specifically define the blood circulation half-life of these particles and determining their "effective" half-life after venous injection. Particles will need to have an effective half-life over 24 hours so that particle dosing would be at most a daily occurrence. This can be initially characterized in the mouse carotid stroke model, where longer time points greater than tracking flow for 60 minutes post injury can be performed.

An investigation into the mechanism of action by CNP can also be undertaken to better understand what CNP are doing, which may help in the smart design of CNP for antithrombotic effects. Based off of our hypothetical mechanism of CNP-vWF interactions preventing vWF-platelet interactions at high shear, one could perform single-molecular studies on vWF proteins under flow. By adhering a single vWF domain to a surface within a microfluidic chamber, vWF extension can be characterized under a range of flow rates. By adding CNP into the flow chamber with the vWF molecule, the effects of CNP on vWF extension could be monitored and quantified. Fluorescently tagging the CNP would also be useful, so that if changes in folding dynamics are not observed, direct CNP-vWF interactions that do not impact folding but rather impact vWF sterically can also be observed. If the mechanism is not through CNP-vWF interactions, then additional studies

investigating CNP-platelet interactions may need to be developed as the next logical target of CNP action.

APPENDIX A. GREYSCALE LITHOGRAPHY WITH DIRECT LASER WRITING

High shear thrombosis assays are utilized in both clinical and research settings to analyze and assess platelet function and thrombus formation characteristics. However, these assays are susceptible to large amounts of variability due to factors such as individual blood biochemistry, anti-coagulation methods, experimental setup, and device channel geometry. It is worthwhile to reduce all sources of variability in order to acquire the most accurate metric that is desired in the assay. While all four areas require attention, this report details a method by which to reduce variability due to the geometry of the device.

Previous microfluidic applications in the field of high shear thrombosis have largely utilized standard 2-dimensional (2D) lithography approaches in device fabrication. However, 2D lithography, by definition, is limited to geometric variations in the x- and y-directions of the wafer substrate. The height (z-direction) is therefore conserved at typically 100 μm or less in both the nominal and constricted or stenotic test sections of the flow channel. This leads to a drastic increase in total resistance along the flow path, making it difficult to achieve physiological shear rates (500-1000 s^{-1} in the nominal and > 5000 s^{-1} in the test sections) under constant pressure due to gravity driven flow. Therefore, these assays must make use of pumps to drive flow, which can lead to large undesirable increases in pressure within the flow channels as an occlusive thrombus forms.

3-dimensional (3D) lithography approaches have the potential to alleviate the issues presented within standard methods of high shear platelet assays. The introduction of 'greyscale lithography' provided a drastic change in microfabrication technology;

however, it remains an expensive option that is limited mainly to industry. A few simulated greyscale approaches have been devised, such as with the use of a liquid photomask with axial variations in dye concentration along the channel, thus altering the amount of UV exposure to the substrate. However, the control of dye concentration along the channel is not highly regulated and can thus lead to variations arising from channel to channel. CNC machining is an alternative for 3D geometries, but is not as desirable as lithography in terms of surface roughness and geometric repeatability. An automated lithography practice is therefore preferred in the development of 3D geometries in microfluidics. This report introduces a method for the creation of a microfluidic chip for physiologically relevant high shear thrombosis assays through the use of an automated 'greyscale' 3D lithography approach.

A.1 Lithography Methods

100 mm silicon wafers were coated with positive photoresist (Microposit SC1827) to a desired thickness of approximately 4.75 to 5.0 microns. The wafer was spun at 500 rpm for 10 seconds, followed by a 5 second ramp to 1500 rpm for 40 seconds, but was later increased to 1750 rpm in order to decrease the thickness (noted when this change occurred). The coated wafer was then baked at 115°C for two minutes in order to crosslink the photoresist. After exposure with the laserwriter, the wafer was developed in MF-319 with agitation for a time specified in each condition. All measurements were acquired through the use of a contact profilometer (Dektak). All etch steps were performed with a BOSCH etch process in the Pettit cleanroom STS ICP; however, the number of cycles depends on the individual process being run and should be determined separately for each project.

Characterization of Intensity, Gain, and Bias

In order to develop a defined slope gradient on a silicon wafer, a greyscale lithography approach was taken with the use of direct laser writing (Microtech Laserwriter LW405). Initially, it was important to investigate the effects of laser intensity, gain, and bias on the resulting photoresist height. Eleven different gain and bias pairings were selected, and eleven different ridges of varying laser intensities were exposed for each of those pairings. The wafer was developed for 50 seconds after exposure.

Two comparisons can be made with this data in **Figure A-1**. The first is by holding the gain constant at 30.1 and varying the bias from 2.1 to 12.0 over the array of exposure intensities. Secondly, we can hold the bias constant at 8.0 and study the effects of varying the gain from 20.0 to 40.0 over the array of exposures. From these results, we can see that a constant gain slightly converges as the laser intensity increases, while the constant bias scenario diverges from a single thickness value as laser intensity increases. Bias controls the thickness in the low intensity regime, while gain controls thickness in high intensity. After an initial exposure, it appears that the thickness and intensity are nearly linearly related, with the exception of the data shown at 59% intensity, which was consistent across all settings.

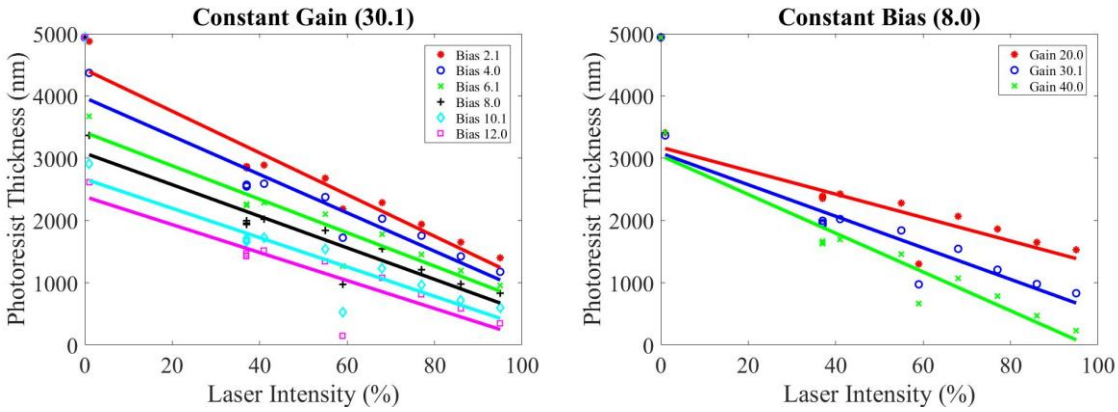

Figure A-1. Constant gain analysis at 30.1 (left) and constant bias analysis at 8.0 (right).

Remaining gain and bias settings tested on the same wafer included gains of 54.6, 49.9, and 33.2 with bias of 0.0, 4.7, and 8.2, respectively. The results in Figure A-2 confirm the control of thickness by bias at low intensities and gain at high intensities.

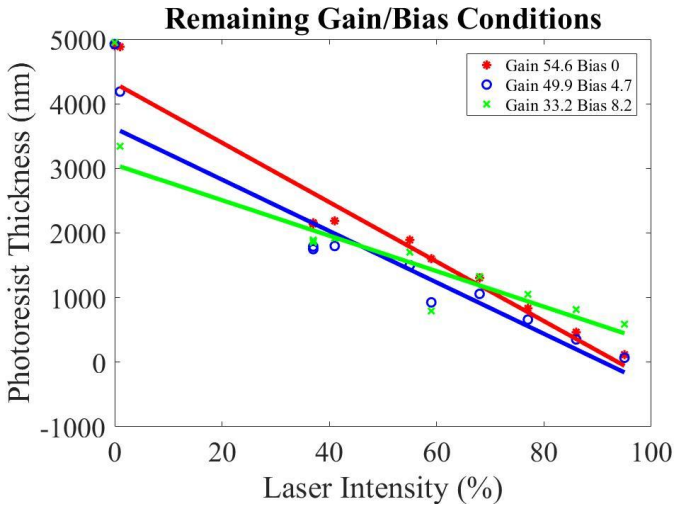

Figure A-2. Varying gain and bias together from high difference (red) to lower difference (green).

8-Bit Greyscale Range

The decision was also made to investigate 256 different levels of exposure over an 8-bit greyscale range for 53.6 gain and 0.0 bias. Therefore, each channel corresponded to a 0.39% increase in UV-exposure over the 0 to 100% exposure range. Three repeats were performed under these conditions with photoresist thicknesses measured for each of the 256 channels. In each repeat, a 2.0% exposure intensity led to the initiation of the linear relationship between thickness and intensity. The average of the three repeats showed that the photoresist was completely removed from the wafer at 52.0 ± 2.8% exposure, as seen in **Figure A-3**.

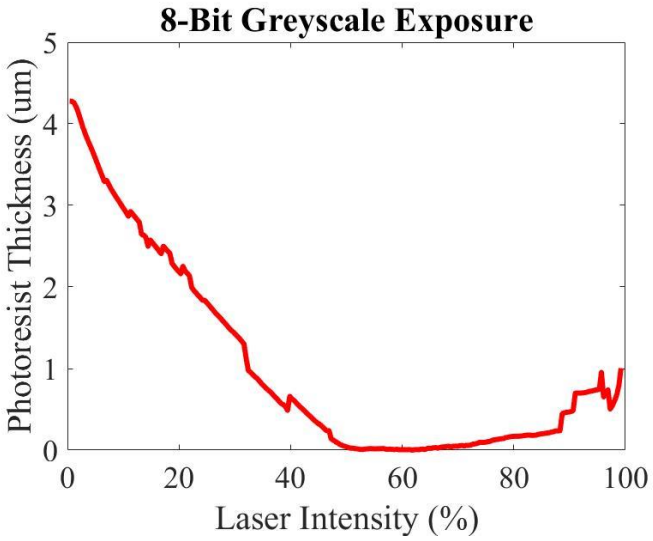

Figure A-3. Representative 8-bit greyscale exposure curve.

It is interesting that the three repeats showed this result, while the results from the previous investigation of varying gain, bias, and intensity found a more linear relationship across the entire spectra of laser intensities, regardless of gain or bias settings. However, the more complete analysis done in replicates across all 256 channels of greyscale shows an initial photoresist removal at low exposure settings that initiates the expected linear region until a specific value (in this case, around 50%). Afterward, all of the photoresist

has been removed from the wafer (with some noise in the profilometer measurement) at the end.

Narrowed Greyscale Range on Bosch Etch

An investigation on the full depth exposure was performed, where a baseline 2% laser intensity was utilized and the final laser intensity was varied from 5 to 50% over 11 different channels. The channel with 10% intensity (channel 10) had a defect in the photoresist and was therefore excluded in measurements. Roughness was calculated as the difference between the maximum and minimum measurements taken in the fully exposed region. A Bosch etch process with 208 cycles were utilized for an estimated depth target of 125 microns. From the profilometer data in **Table A-1**, this target was overshot and less cycles should have been utilized. Channels 1 and 2 were the only channels to have roughness values of 0.0 and reach the full depth upon etching. Therefore, for resist thicknesses in the range of 4.75 microns, a laser intensity of 47% and beyond is acceptable for full depth exposure. Pre-etch and post-etch channel profiles are displayed in **Figure A-4**.

Table A-1. Profilometer measurements of the post-etch channels.

Channel	Final Laser Intensity (%)	**Median Stenotic Depth (um)**	**Roughness (um)**	**Angle (deg)**
1	50	146.1	0.0	23.4
2	47	146.1	0.0	21.8
3	45	146.1	27.1	22.2
4	40	83.0	6.9	20.6
5	35	54.7	5.9	15.9
6	30	19.0	6.0	16.2
7	25	2.9	0.0	0.2
8	20	2.4	0.0	0.2
9	15	1.9	0.0	0.2
10	10	NA	NA	NA
11	5	0.2	0.0	0.0

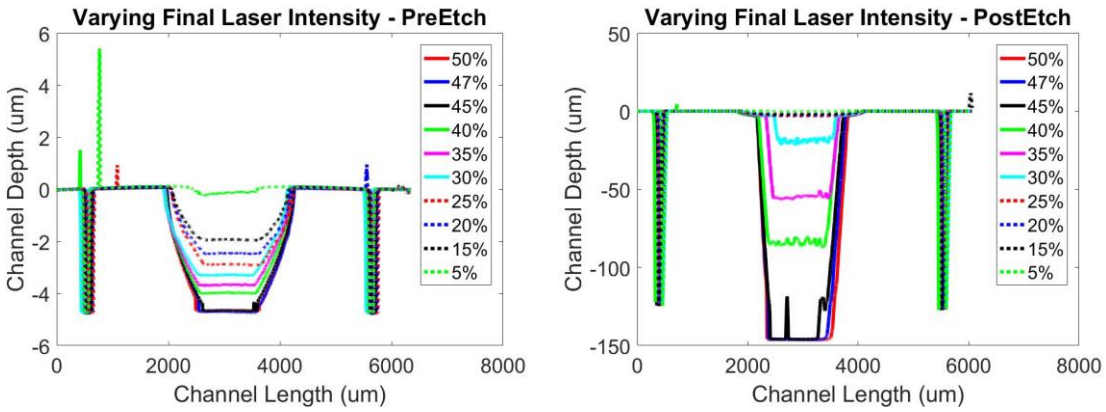

Figure A-4. Varying laser intensity effects on pre-etch (left) and post-etch (right) profiles.

Gradient Region Length and Convergence Angle

To further investigate the repeatability of the laser intensity at full exposure for fully clearing away photoresist in the test section of the channel, 4-channel devices were created on a wafer with photoresist thickness of 4.75 microns with the settings detailed in **Table A-2**. Final laser intensity was varied from 44 to 50%, while the length of the converging and diverging regions was varied for a few of the channels to assess its effect on reducing the final angle value. The assessment showed that intensities up to 49% still had variations in the depth greater than 1.0 micron, while all 50% intensity groups had SEM values below 0.6 microns. Therefore, a range of 2-50% laser intensity was selected as the nominal to full exposure values for this application.

In addition, the target angle for this application was 15.0 degrees. A length of 667 microns should have achieved this angle per Pythagorean theorem, but larger angles were observed. A length of 867 microns yielded an angle of 21.0 degrees. It was decided that final designs of the converging and diverging sections would be of length 1000 microns,

but no larger as to not create lengthy angled regions where step gradients from varying laser intensities would become more prominent.

Table A-2. Determination of laser intensity at full exposure and length of gradient to achieve target angle.

#	Full Exposure Laser Intensity (%)	Targeted Gradient Length (um)	Depth AVG (um)	Depth SEM	Angle AVG (deg)	Angle SEM
1	50	867	201.1	0.2	21.0	0.3
2	50	767	203.0	0.0	22.2	0.2
3	50	667	200.4	0.2	26.3	0.2
4	46	667	190.9	4.7	24.7	0.3
5	47	667	193.0	4.3	24.5	0.6
6	48	667	191.7	3.8	25.1	0.2
7	49	667	192.5	4.3	25.1	0.3
8	50	667	196.8	0.6	26.2	0.3
9	50	667	200.8	0.2	25.9	0.2
10	44	667	196.2	0.8	24.6	0.3
11	45	667	198.6	0.3	25.8	0.4

50% Intensity and 1000um Gradient Length

A length of 1000 microns was investigated in the converging and diverging regions in order to reduce the angle value. While this goal was achieved through yielding values below 20.0 degrees, only the devices in the center of the wafer (5, 6, and 7) did not have

defects in them after the etch process. The defects were assumed to be due to the thickness at the edges of the wafer being greater than desired, thus the resist was not fully exposed and cleared in these regions. A slightly higher RPM was selected on the next wafer to test the same settings again.

Table A-3. Profilometer measurements taken from wafer spun at 1500 rpm – thicker resist.

#	Laser Intensity (%)	Targeted Gradient Length (um)	Depth AVG (um)	Depth SEM	Angle AVG (deg)	Angle SEM
5	50	1000	181.8	0.3	18.4	0.1
6	50	1000	183.4	0.1	19.1	0.3
7	50	1000	181.3	0.2	20.0	0.3

After spinning photoresist on a wafer at 1750 rpm rather than 1500 rpm for 40 seconds, the wafer was exposed and etched following the previously described methods and parameters. The results in **Table A-4** show that repeatable measurements were obtained for devices using this method, particularly for devices in the center portion of the wafer (devices 5, 6, and 7).

Table A-4. Profilometer measurements taken from wafer spun at 1750 rpm – thinner resist.

Device	Laser Intensity %	Targeted Gradient Length (um)	Depth AVG (um)	Depth SEM
1	50	1000	221.7	0.3
2	50	1000	219.5	0.0
3	50	1000	219.8	0.3
4	50	1000	227.5	1.2
5	50	1000	219.6	0.0
6	50	1000	217.3	0.2
7	50	1000	217.8	0.0
8	50	1000	224.6	1.3
9	50	1000	223.2	0.3
10	50	1000	219.9	0.1
11	50	1000	222.2	0.5

Final Design with 3 Functional Devices

Utilizing the parameters detailed in the steps above, 11 devices were created on a 1mm thick silicon wafer. Photoresist was spun on the wafer at 1750 RPM. The laserwriter was utilized at 0 bias, 53.5 gain, 30% filter, lens 2, d-step 3, and intensity range from 2-50%. STS ICP BOSCH process was used at 200 cycles to a target stenotic depth of 180 microns. AZ6240 was then spray coated on the wafer to a thickness of approximately 10

microns, followed by a mask aligning process to align the overall device geometry on the wafer. STS ICP BOSCH process was used at 800 cycles to a target nominal depth of 250 microns (or stenotic height to 70 microns). From this process, three functional devices were created in the center of the wafer, with the edge devices having some sort of noticeable defect in the channels after the etch process. The profiles of the three functional devices are summarized in **Table A-5.**

Table A-5. Final device design measurements.

Device	Stenotic Height (um)	Stenotic Depth (um)	Angle (deg)
5	76.9 ± 0.3	180.5 ± 0.1	19.4 ± 0.3
6	73.7 ± 0.1	182.3 ± 0.1	20.0 ± 0.3
7	75.8 ± 0.4	180.4 ± 0.4	19.2 ± 0.7

Future work to minimize channel variability and creation of functional devices on the edges of the wafer could look to utilize spray coating at all coating steps rather than spin coating. Spray coating may allow for a more uniform thickness over the entire wafer, rather than thicker edge regions due to spin coating.

REFERENCES

1. Benjamin, E.J., et al., *Heart Disease and Stroke Statistics-2018 Update: A Report From the American Heart Association.* Circulation, 2018. **137**(12): p. e67-e492.

2. Casa, L.D., D.H. Deaton, and D.N. Ku, *Role of high shear rate in thrombosis.* J Vasc Surg, 2015. **61**(4): p. 1068-80.

3. Casa, L.D. and S.E. Gillespie, *Relative Contributions of von Willebrand Factor and Platelets in High Shear Thrombosis.* Journal of Hematology & Thromboembolic Diseases, 2016. **4**(4).

4. Schafer, A.I. and R.I. Handin, *The role of platelets in thrombotic and vascular disease.* Prog Cardiovasc Dis, 1979. **22**(1): p. 31-52.

5. Kumar, R.A., et al., *Kinetics of GPIbalpha-vWF-A1 tether bond under flow: effect of GPIbalpha mutations on the association and dissociation rates.* Biophys J, 2003. **85**(6): p. 4099-109.

6. Andrews, R.K., et al., *Glycoprotein Ib–IX–V.* The International Journal of Biochemistry & Cell Biology, 2003. **35**(8): p. 1170-1174.

7. Li, M., et al., *Microfluidic thrombosis under multiple shear rates and antiplatelet therapy doses.* PLoS One, 2014. **9**(1): p. e82493.

8. Whiteheart, S.W., *Platelet granules: surprise packages.* Blood, 2011. **118**(5): p. 1190-1.

9. Springer, T.A., *von Willebrand factor, Jedi knight of the bloodstream.* Blood, 2014. **124**(9): p. 1412-25.

10. Ruggeri, Z.M., *von Willebrand factor.* J Clin Invest, 1997. **100**(11 Suppl): p. S41-6.

11. Wellings, P.J. and D.N. Ku, *Mechanisms of Platelet Capture Under Very High Shear.* Cardiovascular Engineering and Technology, 2012. **3**(2): p. 161-170.

12. Mehrabadi, M., D.N. Ku, and C.K. Aidun, *A continuum model for platelet transport in flowing blood based on direct numerical simulations of cellular blood flow.* Ann Biomed Eng, 2015. **43**(6): p. 1410-21.

13. Schneider, S.W., et al., *Shear-induced unfolding triggers adhesion of von Willebrand factor fibers.* Proc Natl Acad Sci U S A, 2007. **104**(19): p. 7899-903.

14. Ruggeri, Z.M., et al., *Activation-independent platelet adhesion and aggregation under elevated shear stress.* Blood, 2006. **108**(6): p. 1903-10.

15. Miner, J. and A. Hoffhines, *The discovery of aspirin's antithrombotic effects.* Tex Heart Inst J, 2007. **34**(2): p. 179-86.

16. Hennekens, C.H., et al., *Aspirin and other antiplatelet agents in the secondary and primary prevention of cardiovascular disease.* Circulation, 1989. **80**(4): p. 749-56.

17. Craven, L.L., *Prevention of coronary and cerebral thrombosis.* Miss Valley Med J, 1956. **78**(5): p. 213-5.

18. Fernandes, A., J.W. McEvoy, and S. Halvorsen, *"Doctor, Should I Keep Taking an Aspirin a Day?".* N Engl J Med, 2019. **380**(20): p. 1967-1970.

19. McNeil, J.J., et al., *Effect of Aspirin on Disability-free Survival in the Healthy Elderly.* N Engl J Med, 2018. **379**(16): p. 1499-1508.

20. McNeil, J.J., et al., *Effect of Aspirin on Cardiovascular Events and Bleeding in the Healthy Elderly.* N Engl J Med, 2018. **379**(16): p. 1509-1518.

21. Gaziano, J.M., et al., *Use of aspirin to reduce risk of initial vascular events in patients at moderate risk of cardiovascular disease (ARRIVE): a randomised, double-blind, placebo-controlled trial.* Lancet, 2018. **392**(10152): p. 1036-1046.

22. Damman, P., et al., *P2Y12 platelet inhibition in clinical practice.* J Thromb Thrombolysis, 2012. **33**(2): p. 143-53.

23. Bhatt, D.L., et al., *Clopidogrel and aspirin versus aspirin alone for the prevention of atherothrombotic events.* N Engl J Med, 2006. **354**(16): p. 1706-17.

24. Goa, K.L. and S. Noble, *Eptifibatide: a review of its use in patients with acute coronary syndromes and/or undergoing percutaneous coronary intervention.* Drugs, 1999. **57**(3): p. 439-62.

25. Platelet Glycoprotein, I.I.i.U.A.R.S.U.I.T.T.I., *Inhibition of platelet glycoprotein IIb/IIIa with eptifibatide in patients with acute coronary syndromes.* N Engl J Med, 1998. **339**(7): p. 436-43.

26. Kandzari, D.E., et al., *Improved clinical outcomes with abciximab therapy in acute myocardial infarction: a systematic overview of randomized clinical trials.* Am Heart J, 2004. **147**(3): p. 457-62.

27. Born, G.V., *Aggregation of blood platelets by adenosine diphosphate and its reversal.* Nature, 1962. **194**: p. 927-9.

28. O'Brien J, R., *Platelet aggregation: Part I Some effects of the adenosine phosphates, thrombin, and cocaine upon platelet adhesiveness.* J Clin Pathol, 1962. **15**(5): p. 446-52.

29. Cattaneo, M., et al., *Recommendations for the Standardization of Light Transmission Aggregometry: A Consensus of the Working Party from the Platelet Physiology Subcommittee of SSC/ISTH.* J Thromb Haemost, 2013.

30. Hayward, C.P., et al., *Diagnostic utility of light transmission platelet aggregometry: results from a prospective study of individuals referred for bleeding disorder assessments.* J Thromb Haemost, 2009. **7**(4): p. 676-84.

31. Price, M.J., et al., *Standard- vs high-dose clopidogrel based on platelet function testing after percutaneous coronary intervention: the GRAVITAS randomized trial.* JAMA, 2011. **305**(11): p. 1097-105.

32. Marcucci, R., et al., *Cardiovascular death and nonfatal myocardial infarction in acute coronary syndrome patients receiving coronary stenting are predicted by residual platelet reactivity to ADP detected by a point-of-care assay: a 12-month follow-up.* Circulation, 2009. **119**(2): p. 237-42.

33. G., C., L. F., and C.E. Marcucci, *Point-of-Care Platelet Function Tests*, in *Peroperative Hemostasis*, M. C. and S. P., Editors. 2015, Springer, Berlin, Heidelberg.

34. Paniccia, R., et al., *Platelet function tests: a comparative review.* Vasc Health Risk Manag, 2015. **11**: p. 133-48.

35. Marcucci, R., et al., *Usefulness of aspirin resistance after percutaneous coronary intervention for acute myocardial infarction in predicting one-year major adverse coronary events.* Am J Cardiol, 2006. **98**(9): p. 1156-9.

36. Reny, J.L., et al., *Use of the PFA-100 closure time to predict cardiovascular events in aspirin-treated cardiovascular patients: a systematic review and meta-analysis.* J Thromb Haemost, 2008. **6**(3): p. 444-50.

37. Yamamoto, J., et al., *Global Thrombosis Test (GTT) can detect major determinants of haemostasis including platelet reactivity, endogenous fibrinolytic and thrombin generating potential.* Thromb Res, 2014. **133**(5): p. 919-26.

38. Saraf, S., et al., *Impaired endogenous thrombolysis in acute coronary syndrome patients predicts cardiovascular death and nonfatal myocardial infarction.* J Am Coll Cardiol, 2010. **55**(19): p. 2107-15.

39. Farag, M., et al., *Impaired endogenous fibrinolysis in ST-segment elevation myocardial infarction patients undergoing primary percutaneous coronary intervention is a predictor of recurrent cardiovascular events: the RISK PPCI study.* Eur Heart J, 2018.

40. Colace, T.V., et al., *Microfluidics and coagulation biology.* Annu Rev Biomed Eng, 2013. **15**: p. 283-303.

41. Casa, L.D. and D.N. Ku, *Geometric design of microfluidic chambers: platelet adhesion versus accumulation.* Biomed Microdevices, 2014. **16**(1): p. 115-26.

42. Hastings, S.M., M.T. Griffin, and D.N. Ku, *Hemodynamic studies of platelet thrombosis using microfluidics.* Platelets, 2017. **28**(5): p. 427-433.

43. Ku, D.N., L.D.C. Casa, and S.M. Hastings, *Choice of a hemodynamic model for occlusive thrombosis in arteries.* J Biomech, 2017. **50**: p. 110-113.

44. Li, R., T. Grosser, and S.L. Diamond, *Microfluidic whole blood testing of platelet response to pharmacological agents.* Platelets, 2017. **28**(5): p. 457-462.

45. Tovar-Lopez, F.J., et al., *A microfluidics device to monitor platelet aggregation dynamics in response to strain rate micro-gradients in flowing blood.* Lab Chip, 2010. **10**(3): p. 291-302.

46. Li, M., D.N. Ku, and C.R. Forest, *Microfluidic system for simultaneous optical measurement of platelet aggregation at multiple shear rates in whole blood.* Lab Chip, 2012. **12**(7): p. 1355-62.

47. Bark, D.L., Jr., A.N. Para, and D.N. Ku, *Correlation of thrombosis growth rate to pathological wall shear rate during platelet accumulation.* Biotechnol Bioeng, 2012. **109**(10): p. 2642-50.

48. Griffin, M.T., D. Kim, and D.N. Ku, *Shear-induced platelet aggregation: 3D-grayscale microfluidics for repeatable and localized occlusive thrombosis.* Biomicrofluidics, 2019. **13**(5).

49. *The Top 10 Causes of Death*. 2018, World Health Organization.

50. Shankaran, H., P. Alexandridis, and S. Neelamegham, *Aspects of hydrodynamic shear regulating shear-induced platelet activation and self-association of von Willebrand factor in suspension.* Blood, 2003. **101**(7): p. 2637-45.

51. Gorog, D.A. and V. Fuster, *Platelet function tests in clinical cardiology: unfulfilled expectations.* J Am Coll Cardiol, 2013. **61**(21): p. 2115-29.

52. Gorog, D.A. and Y.H. Jeong, *Platelet function tests: why they fail to guide personalized antithrombotic medication.* J Am Heart Assoc, 2015. **4**(5).

53. Branchford, B.R., et al., *Microfluidic technology as an emerging clinical tool to evaluate thrombosis and hemostasis.* Thromb Res, 2015. **136**(1): p. 13-9.

54. Ahn, S.G., et al., *Intra-individual variability of residual platelet reactivity assessed by the VerifyNow-P2Y12 assay in patients with clopidogrel resistance after percutaneous coronary intervention.* Platelets, 2011. **22**(4): p. 305-7.

55. Bender, M.T., et al., *Precision of VerifyNow P2Y12 Assessment of Clopidogrel Response in Patients Undergoing Cerebral Aneurysm Flow Diversion.* Neurosurgery, 2018.

56. Lepantalo, A., et al., *Variability in platelet responses to collagen--comparison between whole blood perfusions, traditional platelet function tests and PFA-100.* Thromb Res, 2001. **103**(2): p. 123-33.

57. Feuring, M., et al., *Circadian variation of platelet function measured with the PFA-100.* Platelets, 2009. **20**(7): p. 466-70.

58. Roest, M., et al., *Flow chamber-based assays to measure thrombus formation in vitro: requirements for standardization.* J Thromb Haemost, 2011. **9**(11): p. 2322-4.

59. Heemskerk, J.W.M., et al., *Collagen surfaces to measure thrombus formation under flow: possibilities for standardization.* Journal of Thrombosis and Haemostasis, 2011. **9**(4): p. 856-858.

60. Hansen, R.R., et al., *Characterization of collagen thin films for von Willebrand factor binding and platelet adhesion.* Langmuir, 2011. **27**(22): p. 13648-58.

61. Neeves, K.B., et al., *Sources of variability in platelet accumulation on type 1 fibrillar collagen in microfluidic flow assays.* PLoS One, 2013. **8**(1): p. e54680.

62. Farndale, R.W., et al., *The role of collagen in thrombosis and hemostasis.* J Thromb Haemost, 2004. **2**(4): p. 561-73.

63. Jaffe, R. and D. Deykin, *Evidence for a structural requirement for the aggregation of platelets by collagen.* J Clin Invest, 1974. **53**(3): p. 875-83.

64. de Witt, S.M., et al., *Identification of platelet function defects by multi-parameter assessment of thrombus formation.* Nat Commun, 2014. **5**: p. 4257.

65. Pugh, N., et al., *Synergism between platelet collagen receptors defined using receptor-specific collagen-mimetic peptide substrata in flowing blood.* Blood, 2010. **115**(24): p. 5069-79.

66. Pittens, C.A., et al., *Comparison between hirudin and citrate in monitoring the inhibitory effects of P2Y12 receptor antagonists with different platelet function tests.* J Thromb Haemost, 2009. **7**(11): p. 1929-32.

67. Paniccia, R., et al., *Assessment of platelet function: Laboratory and point-of-care methods.* World Journal of Translational Medicine, 2014. **3**(2).

68. Harrison, P., *Platelet function analysis.* Blood Rev, 2005. **19**(2): p. 111-23.

69. Cosemans, J.M., et al., *Multiple ways to switch platelet integrins on and off.* J Thromb Haemost, 2008. **6**(8): p. 1253-61.

70. Sakariassen, K.S., M. Ottenhof-Rovers, and J.J. Sixma, *Factor VIII-von Willebrand factor requires calcium for facilitation of platelet adherence.* Blood, 1984. **63**(5): p. 996-103.

71. Lehmann, M., et al., *On-chip recalcification of citrated whole blood using a microfluidic herringbone mixer.* Biomicrofluidics, 2015. **9**(6): p. 064106.

72. Tiryaki, F., et al., *Anticoagulation therapy for hospitalized patients: patterns of use, compliance with national guidelines, and performance on quality measures.* Am J Health Syst Pharm, 2011. **68**(13): p. 1239-44.

73. Chen, M. and J.G. Geng, *P-selectin mediates adhesion of leukocytes, platelets, and cancer cells in inflammation, thrombosis, and cancer growth and metastasis.* Arch Immunol Ther Exp (Warsz), 2006. **54**(2): p. 75-84.

74. Salzman, E.W., et al., *Effect of heparin and heparin fractions on platelet aggregation.* J Clin Invest, 1980. **65**(1): p. 64-73.

75. Jain, A., et al., *A shear gradient-activated microfluidic device for automated monitoring of whole blood haemostasis and platelet function.* Nat Commun, 2016. **7**: p. 10176.

76. Griffin, M.T., et al., *Inhibition of high shear arterial thrombosis by charged nanoparticles.* Biomicrofluidics, 2018. **12**(4): p. 042210.

77. Para, A., et al., *Rapid platelet accumulation leading to thrombotic occlusion.* Ann Biomed Eng, 2011. **39**(7): p. 1961-71.

78. Edelstein, A., et al., *Computer control of microscopes using microManager.* Curr Protoc Mol Biol, 2010. **Chapter 14**: p. Unit14 20.

79. Anderson, M.J., *Permutation tests for univariate or multivariate analysis of variance and regression.* Canadian Journal of Fisheries and Aquatic Sciences, 2001. **58**(3): p. 626-639.

80. Mehrabadi, M., et al., *A Predictive Model of High Shear Thrombus Growth.* Ann Biomed Eng, 2016. **44**(8): p. 2339-50.

81. Altman, R., et al., *The antithrombotic profile of aspirin. Aspirin resistance, or simply failure?* Thromb J, 2004. **2**(1): p. 1.

82. Jagroop, I.A., et al., *The effect of clopidogrel, aspirin and both antiplatelet drugs on platelet function in patients with peripheral arterial disease.* Platelets, 2004. **15**(2): p. 117-25.

83. Lordkipanidze, M., et al., *A comparison of six major platelet function tests to determine the prevalence of aspirin resistance in patients with stable coronary artery disease.* Eur Heart J, 2007. **28**(14): p. 1702-8.

84. Gum, P.A., et al., *A prospective, blinded determination of the natural history of aspirin resistance among stable patients with cardiovascular disease.* J Am Coll Cardiol, 2003. **41**(6): p. 961-5.

85. Hovens, M.M., et al., *Prevalence of persistent platelet reactivity despite use of aspirin: a systematic review.* Am Heart J, 2007. **153**(2): p. 175-81.

86. Michos, E.D., et al., *Aspirin and clopidogrel resistance.* Mayo Clin Proc, 2006. **81**(4): p. 518-26.

87. Hansen, M.L., et al., *Risk of bleeding with single, dual, or triple therapy with warfarin, aspirin, and clopidogrel in patients with atrial fibrillation.* Arch Intern Med, 2010. **170**(16): p. 1433-41.

88. Sadler, J.E., *Biochemistry and genetics of von Willebrand factor.* Annu Rev Biochem, 1998. **67**: p. 395-424.

89. Ikeda, Y., et al., *The role of von Willebrand factor and fibrinogen in platelet aggregation under varying shear stress.* J Clin Invest, 1991. **87**(4): p. 1234-40.

90. Spinthakis, N., et al., *Effect of P2Y12 inhibitors on thrombus stability and endogenous fibrinolysis.* Thromb Res, 2018. **173**: p. 102-108.

91. Santilli, F., et al., *Platelet cyclooxygenase inhibition by low-dose aspirin is not reflected consistently by platelet function assays: implications for aspirin "resistance".* J Am Coll Cardiol, 2009. **53**(8): p. 667-77.

92. Ghasemi, A. and S. Zahediasl, *Normality tests for statistical analysis: a guide for non-statisticians.* Int J Endocrinol Metab, 2012. **10**(2): p. 486-9.

93. Artusi, R., P. Verderio, and E. Marubini, *Bravais-Pearson and Spearman correlation coefficients: meaning, test of hypothesis and confidence interval.* Int J Biol Markers, 2002. **17**(2): p. 148-51.

94. Landis, J.R. and G.G. Koch, *The measurement of observer agreement for categorical data.* Biometrics, 1977. **33**(1): p. 159-74.

95. Chatterjee, M.S., et al., *Systems biology of coagulation initiation: kinetics of thrombin generation in resting and activated human blood.* PLoS Comput Biol, 2010. **6**(9).

96. Nielsen, H.L., et al., *Aspirin response evaluated by the VerifyNow Aspirin System and light transmission aggregometry.* Thromb Res, 2008. **123**(2): p. 267-73.

97. Singal, A.K. and G. Karthikeyan, *Aspirin for primary prevention: Is this the end of the road?* Indian Heart J, 2019. **71**(2): p. 113-117.

98. Brown, D.L., C.S. Fann, and C.J. Chang, *Meta-analysis of effectiveness and safety of abciximab versus eptifibatide or tirofiban in percutaneous coronary intervention.* Am J Cardiol, 2001. **87**(5): p. 537-41.

99. Tricoci, P., et al., *Thrombin-receptor antagonist vorapaxar in acute coronary syndromes.* N Engl J Med, 2012. **366**(1): p. 20-33.

100. *A randomised, blinded, trial of clopidogrel versus aspirin in patients at risk of ischaemic events (CAPRIE).* The Lancet, 1996. **348**(9038): p. 1329-1339.

101. Group, C.C., *Addition of clopidogrel to aspirin in 45 852 patients with acute myocardial infarction: randomised placebo-controlled trial.* The Lancet, 2005. **366**(9497): p. 1607-1621.

102. Doke, S.K. and S.C. Dhawale, *Alternatives to animal testing: A review.* Saudi Pharm J, 2015. **23**(3): p. 223-9.

103. Chapman, K.L., et al., *Pharmaceutical toxicology: designing studies to reduce animal use, while maximizing human translation.* Regul Toxicol Pharmacol, 2013. **66**(1): p. 88-103.

104. Mega, J.L., et al., *Cytochrome p-450 polymorphisms and response to clopidogrel.* N Engl J Med, 2009. **360**(4): p. 354-62.

105. Kaikita, K., et al., *Tailored Adjunctive Cilostazol Therapy Based on CYP2C19 Genotyping in Patients With Acute Myocardial Infarction- The CALDERA-GENE Study.* Circ J, 2018. **82**(6): p. 1517-1525.

106. Nemmar, A., et al., *Ultrafine particles affect experimental thrombosis in an in vivo hamster model.* Am J Respir Crit Care Med, 2002. **166**(7): p. 998-1004.

107. Lynch, I. and K.A. Dawson, *Protein-nanoparticle interactions.* Nano Today, 2008. **3**(1-2): p. 40-47.

108. Mahmoudi, M., et al., *Protein-nanoparticle interactions: opportunities and challenges.* Chem Rev, 2011. **111**(9): p. 5610-37.

109. Lundqvist, M., et al., *The nanoparticle protein corona formed in human blood or human blood fractions.* PLoS One, 2017. **12**(4): p. e0175871.

110. Boal, A.K., et al., *Self-assembly of nanoparticles into structured spherical and network aggregates.* Nature, 2000. **404**(6779): p. 746-8.

111. Loos, C., et al., *Functionalized polystyrene nanoparticles as a platform for studying bio-nano interactions.* Beilstein J Nanotechnol, 2014. **5**: p. 2403-12.

112. Jain, R.A., *The manufacturing techniques of various drug loaded biodegradable poly(lactide-co-glycolide) (PLGA) devices.* Biomaterials, 2000. **21**(23): p. 2475-90.

113. Jalil, R. and J.R. Nixon, *Biodegradable poly(lactic acid) and poly(lactide-co-glycolide) microcapsules: problems associated with preparative techniques and release properties.* J Microencapsul, 1990. **7**(3): p. 297-325.

114. Heller, J., *Biodegradable polymers in controlled drug delivery.* Crit Rev Ther Drug Carrier Syst, 1984. **1**(1): p. 39-90.

115. Heller, J., *Controlled release of biologically active compounds from bioerodible polymers.* Biomaterials, 1980. **1**(1): p. 51-7.

116. Kitchell, J.P. and D.L. Wise, *Poly(lactic/glycolic acid) biodegradable drug-polymer matrix systems.* Methods Enzymol, 1985. **112**: p. 436-48.

117. Bala, I., S. Hariharan, and M.N. Kumar, *PLGA nanoparticles in drug delivery: the state of the art.* Crit Rev Ther Drug Carrier Syst, 2004. **21**(5): p. 387-422.

118. Danhier, F., et al., *PLGA-based nanoparticles: an overview of biomedical applications.* J Control Release, 2012. **161**(2): p. 505-22.

119. Swider, E., et al., *Customizing poly(lactic-co-glycolic acid) particles for biomedical applications.* Acta Biomater, 2018. **73**: p. 38-51.

120. Avgoustakis, K., et al., *PLGA-mPEG nanoparticles of cisplatin: in vitro nanoparticle degradation, in vitro drug release and in vivo drug residence in blood properties.* J Control Release, 2002. **79**(1-3): p. 123-35.

121. Daniel, M.C. and D. Astruc, *Gold nanoparticles: assembly, supramolecular chemistry, quantum-size-related properties, and applications toward biology, catalysis, and nanotechnology.* Chem Rev, 2004. **104**(1): p. 293-346.

122. Moller, P. and J. Lykkesfeldt, *Positive charge, negative effect: the impact of cationic nanoparticles in the brain.* Nanomedicine (Lond), 2014. **9**(10): p. 1441-3.

123. Alric, C., et al., *The biodistribution of gold nanoparticles designed for renal clearance.* Nanoscale, 2013. **5**(13): p. 5930-9.

124. Lipka, J., et al., *Biodistribution of PEG-modified gold nanoparticles following intratracheal instillation and intravenous injection.* Biomaterials, 2010. **31**(25): p. 6574-81.

125. Sah, H., et al., *Concepts and practices used to develop functional PLGA-based nanoparticulate systems.* Int J Nanomedicine, 2013. **8**: p. 747-65.

126. Huang, W. and C. Zhang, *Tuning the Size of Poly(lactic-co-glycolic Acid) (PLGA) Nanoparticles Fabricated by Nanoprecipitation.* Biotechnol J, 2018. **13**(1).

127. Cho, Y.S., S. Ji, and Y.S. Kim, *Synthesis of Polymeric Nanoparticles by Emulsion Polymerization for Particle Self-Assembly Applications.* J Nanosci Nanotechnol, 2019. **19**(10): p. 6398-6407.

128. Mu, L. and S.S. Feng, *Fabrication, characterization and in vitro release of paclitaxel (Taxol) loaded poly (lactic-co-glycolic acid) microspheres prepared by spray drying technique with lipid/cholesterol emulsifiers.* J Control Release, 2001. **76**(3): p. 239-54.

129. Tshikhudo, T.R., Z. Wang, and M. Brust, *Biocompatible gold nanoparticles.* Materials Science and Technology, 2013. **20**(8): p. 980-984.

130. Pan, Y., et al., *Size-dependent cytotoxicity of gold nanoparticles.* Small, 2007. **3**(11): p. 1941-9.

131. Hirn, S., et al., *Particle size-dependent and surface charge-dependent biodistribution of gold nanoparticles after intravenous administration.* Eur J Pharm Biopharm, 2011. **77**(3): p. 407-16.

132. Platel, A., et al., *Influence of the surface charge of PLGA nanoparticles on their in vitro genotoxicity, cytotoxicity, ROS production and endocytosis.* J Appl Toxicol, 2016. **36**(3): p. 434-44.

133. Ratzinger, G.F., Christian; Kerleta, Vera; Wirth, Michael; Gabor, Franz, *The Role of Surface Functionalization in the Design of PLGA Micro- and Nanoparticles.* Critical Reviews in Therapeutic Drug Carrier Systems, 2010. **27**(1): p. 1-83.

134. Z Liu, Y.Z., RR Rao, JR Clausen, CK Aidun, *Simulating nanoscale suspension of particles and polymers using a coupled lattice-Boltzmann and Langevin-dynamics approach.* arXiv preprint, 2018. **1801.02299**.

135. Larson, R.G., *The rheology of dilute solutions of flexible polymers: Progress and problems.* Journal of Rheology, 2005. **49**(1): p. 1-70.

136. Ding, E.J. and C.K. Aidun, *The dynamics and scaling law for particles suspended in shear flow with inertia.* Journal of Fluid Mechanics, 2000. **423**: p. 317-344.

137. Ding, E.J. and C.K. Aidun, *Extension of the Lattice-Boltzmann method for direct simulation of suspended particles near contact.* Journal of Statistical Physics, 2003. **112**(3-4): p. 685-708.

138. Wu, J., et al., *Numerical investigation of the effects of channel geometry on platelet activation and blood damage.* Ann Biomed Eng, 2011. **39**(2): p. 897-910.

139. MacMeccan, R.M., et al., *Simulating deformable particle suspensions using a coupled lattice-Boltzmann and finite-element method.* Journal of Fluid Mechanics, 2009. **618**: p. 13-39.

140. Aidun, C.K. and D.W. Qi, *A new method for analysis of the fluid interaction with a deformable membrane.* Journal of Statistical Physics, 1998. **90**(1-2): p. 145-158.

141. Reasor, D.A., J.R. Clausen, and C.K. Aidun, *Coupling the lattice-Boltzmann and spectrin-link methods for the direct numerical simulation of cellular blood flow.* 2012: p. 767-781.

142. Z Liu, Y.Z., RR Rao, JR Clausen, CK Aidun, *Nanoparticle Transport in Cellular Blood Flow.* Computational Fluids, 2018.

143. Öttinger, H.C., *Gaussian approximation for Rouse chains with hydrodynamic interaction.* The Journal of Chemical Physics, 1989. **90**(1): p. 463.

144. Rotne, J. and S. Prager, *Variational Treatment of Hydrodynamic Interaction in Polymers.* Journal of Chemical Physics, 1969. **50**(11): p. 4831-&.

145. Yamakawa, H., *Transport Properties of Polymer Chains in Dilute Solution - Hydrodynamic Interaction.* Journal of Chemical Physics, 1970. **53**(1): p. 436-&.

146. Alexander-Katz, A., et al., *Shear-flow-induced unfolding of polymeric globules.* Phys Rev Lett, 2006. **97**(13): p. 138101.

147. Kremer, K. and G.S. Grest, *Dynamics of entangled linear polymer melts: A molecular-dynamics simulation.* The Journal of Chemical Physics, 1990. **92**(8): p. 5057-5086.

148. Sing, C.E. and A. Alexander-Katz, *Elongational flow induces the unfolding of von Willebrand factor at physiological flow rates.* Biophys J, 2010. **98**(9): p. L35-7.

149. Romijn, R.A., *Structural studies on the von Willebrand factor A1 and A3 domains*. 2003.

150. Kloet, S.K., et al., *Translocation of positively and negatively charged polystyrene nanoparticles in an in vitro placental model.* Toxicol In Vitro, 2015. **29**(7): p. 1701-10.

151. Wang, X., et al., *Detection of Circulating Tumor Cells in Human Peripheral Blood Using Surface-Enhanced Raman Scattering Nanoparticles.* Cancer Research, 2011. **71**(5): p. 1526-1532.

152. Manson, J., et al., *Polyethylene glycol functionalized gold nanoparticles: the influence of capping density on stability in various media.* Gold Bulletin, 2011. **44**(2): p. 99-105.

153. Mangin, P., et al., *Thrombin overcomes the thrombosis defect associated with platelet GPVI/FcRgamma deficiency.* Blood, 2006. **107**(11): p. 4346-53.

154. Martinez de Lizarrondo, S., et al., *Potent Thrombolytic Effect of N-Acetylcysteine on Arterial Thrombi.* Circulation, 2017. **136**(7): p. 646-660.

155. Day, S.M., et al., *Murine thrombosis models.* Thromb Haemost, 2004. **92**(3): p. 486-94.

156. Ciciliano, J.C., et al., *Resolving the multifaceted mechanisms of the ferric chloride thrombosis model using an interdisciplinary microfluidic approach.* Blood, 2015. **126**(6): p. 817-24.

157. Stockschlaeder, M., R. Schneppenheim, and U. Budde, *Update on von Willebrand factor multimers: focus on high-molecular-weight multimers and their role in hemostasis.* Blood Coagul Fibrinolysis, 2014. **25**(3): p. 206-16.

158. Springer, T.A., *Biology and physics of von Willebrand factor concatamers.* J Thromb Haemost, 2011. **9 Suppl 1**: p. 130-43.

159. Fu, H., et al., *Flow-induced elongation of von Willebrand factor precedes tension-dependent activation.* Nat Commun, 2017. **8**(1): p. 324.

160. Kulkarni, S.A. and S.S. Feng, *Effects of particle size and surface modification on cellular uptake and biodistribution of polymeric nanoparticles for drug delivery.* Pharm Res, 2013. **30**(10): p. 2512-22.

161. Hoshyar, N., et al., *The effect of nanoparticle size on in vivo pharmacokinetics and cellular interaction.* Nanomedicine (Lond), 2016. **11**(6): p. 673-92.

162. Investigators, P., *Comparative 30-day economic and clinical outcomes of platelet glycoprotein IIb/IIIa inhibitor use during elective percutaneous coronary intervention: Prairie ReoPro versus Integrilin Cost Evaluation (PRICE) Trial.* Am Heart J, 2001. **141**(3): p. 402-9.

163. Jiang, Y., et al., *Electrostatic Steering Enables Flow-Activated Von Willebrand Factor to Bind Platelet Glycoprotein, Revealed by Single-Molecule Stretching and Imaging.* J Mol Biol, 2019. **431**(7): p. 1380-1396.

164. Lundqvist, M., *Nanoparticles: Tracking protein corona over time.* Nat Nanotechnol, 2013. **8**(10): p. 701-2.

165. Lundqvist, M., et al., *Nanoparticle size and surface properties determine the protein corona with possible implications for biological impacts.* Proc Natl Acad Sci U S A, 2008. **105**(38): p. 14265-70.

166. Monopoli, M.P., et al., *Biomolecular coronas provide the biological identity of nanosized materials.* Nat Nanotechnol, 2012. **7**(12): p. 779-86.

167. Bahnak, B.R., et al., *Comparison of the primary structure of the functional domains of human and porcine von Willebrand factor that mediate platelet adhesion.* Biochem Biophys Res Commun, 1992. **182**(2): p. 561-8.

168. Korin, N., et al., *Targeted drug delivery to flow-obstructed blood vessels using mechanically activated nanotherapeutics.* JAMA Neurol, 2015. **72**(1): p. 119-22.